University Of Trento

Department of Cellular, Computational and Integrative Biology (CIBIO)

International PhD Program in Biomolecular Sciences

XXXV Cycle

Interfering with hnRNPA2B1:ExoRNA interaction to challenge the quality of secreted extracellular vesicles

Tutor

Prof. Vito Giuseppe D'Agostino

CIBIO – University of Trento

PhD thesis of

Jessica Corsi

CIBIO – University of Trento

Academic Year 2022 – 2023

Declaration of original authorship

I, Jessica Corsi, confirm that this is my own work and the use of all material from other sources have been properly and fully acknowledged.

Table of Contents

List of figures

Abstract

Amyotrophic lateral sclerosis (ALS) is a motor neuron disease. In ALS, RNA-binding proteins (RBPs) accumulate and/or misfold and eventually associate with stress granules, leading to proteotoxic damage and RNA toxicity, ultimately resulting in neurodegeneration. Extracellular vesicles (EVs) are released by most cells to the extracellular environment and are involved in cell-to-cell communication. In ALS, EVs have been proposed as a vehicle through which "meaningful signals" are delivered prompting the propagation of the disease. MicroRNA biomarkers are recently emerging as EVs cargo. To this extent, the activity of RBPs needs to be addressed in view of the enrichment of selected transcripts into EVs (EV-RNA). Among RBPs, the ALS-linked hnRNPA2B1 was discovered as a key player in the sorting of selected miRNA in exosomes (or small EVs). For these reasons, we proposed hnRNPA2B1 and its interaction with RNA as an interesting target for drug screening in ALS.

To study the mechanism of EV-RNA modulation, we optimized a proteomic approach and measured the EV-RNA upon modulation of hnRNPA2B1 in NSC-34 cells, finding that the protein effectively contributes to this regulation. Producing a human full-length hnRNPA2B1 protein and an RNA probe harboring the EXOmotif, previously known to be enriched in exosomal RNA, we performed a high-throughput drug screening with the aim to identify drugs able to interfere with hnRNPA2B1-RNA interaction. We screened a library of 2000 compounds, containing FDA-approved and natural scaffolds, and we identified 21 hits. We performed a counter screening using AlphaScreen and REMSA orthogonal techniques and we identified six active compounds able to interfere with protein:RNA interaction; RNA pull-down assay confirmed the compounds effects on endogenous Hnrnpa2b1 in NSC-34. To assess the interference with EV-RNA quality, we looked at miR-221-3p as a readout to measure vesicular hnRNP2AB1-regulated miRNAs. miR-221-3p levels resulted to be significant reduced, upon treatment, in NSC-34 and in NPC-derived motor neurons EVs. Therefore, we started some pilot experiments looking at the effects of these modulated EVs on recipient cells. miR-221-3p deprived-EVs, upon compound treatments, associated with hnRNPA2B1-mediated NF-κB activation in

recipient cells. Overall, we identified powerful compounds able to affect EV-RNA quality. This demonstrates the possibility to biochemically interfere with the EV-RNA cargo without altering the global particle release.

1. Introduction

1.1 Amyotrophic Lateral Sclerosis (ALS)

Amyotrophic Lateral Sclerosis (ALS) is a neurodegenerative disease characterized by the progressive degeneration of both upper motor neurons in the motor cortex and lower motor neurons in brainstem and spinal cord. The motor neuron degeneration has a focal start and then it diffuses to other parts of the CNS. Initial symptoms are weakness in the limb or bulbar muscles, leading at the end to the paralysis of the majority of skeletal muscles (Mead et al. 2023) (Hardiman et al. 2017). ALS is defined as an "orphan disease," since it has an incidence of about 2 out of 100,000 new cases per year and a prevalence of about 5 out of 100,000 total cases each year (O'Toole et al. 2008) in the United States (Armon 2007) and Europe (Alonso et al. 2009)(Johnston et al. 2006). The primary symptoms of ALS relate to motor dysfunction, but then up to 50% of patients develops cognitive and/or behavioral symptoms typical of frontotemporal dementia (FTD)(Hardiman et al. 2017).

The onset of the disease commonly occurs at 55 years of age. Fast progressor patients decease in 3-5 years after diagnosis, while slow progressors survive decades.

From the genetic point of view, ALS is divided in familial ALS (fALS), constituting about 10% of all cases showing Mendelian autosomal dominant pattern of inheritance, (Leblond et al. 2014), (Sreedharan, Brown, and Kingdom n.d.)(Peters, Ghasemi, and Brown 2015) or sporadic ALS (sALS), constituting all the remaining cases with no apparent family history; in this context, large, combined genome-wide association studies (GWAS) suggest the presence of rare variants that confer a certain risk (Als and Tables 2021). Nowadays, for the fALS, alteration in four genes is responsible for the disease in up to 70% of patients in European populations: C9orf72, SOD1, TARDBP and FUS. (Mead et al. 2023)

Cytosolic superoxide dismutase [Cu/Zn] (SOD1) was the first gene to be associated with the disease (Rosen et al. 1993) and is found mutated in 20% of fALS (Berdyński et al.

2022). It encodes for antioxidant enzyme Cu, Zn superoxide dismutase and is involved in response against reactive oxygen species (ROS). Mutation in the gene causes conformational and functional changes of SOD1 protein, possibly rendering the mutation a gain of function. In fact, misfolded SOD1 is responsible for excitotoxicity, oxidative stress, endoplasmic reticulum stress, mitochondrial disfunction, and prion-like propagation (Mead et al. 2023).

Mutations in TARDBP gene is present in 5% of fALS; it encodes for TDP-43 protein which is an RNA-binding protein (RBP) mainly localized in the nucleus where it is involved in splicing and RNA metabolism. However, in ALS, patients show both gain of toxic functions and loss of physiological activity that trigger neuronal death (Gagliardi et al. 2021). Aggregates of phosphorylated and ubiquitinated TDP-43 are present both in neurons and glial cells of ALS patients. They are present in more than 97% of all ALS subtypes and are recognized as a hallmark of the disease (Tamaki and Urushitani 2022).

Similarly to TDP-43, mutations in FUS gene are present both in familiar and sporadic ALS. Its mutations may cause protein cytoplasmic mislocalization with the subsequent sequestration of RNA transcripts and stress granules-like structure formation. Similarly to TDP-43 and SOD1, the inclusions in neuronal and glial cells of patients may cause neuronal toxicity and death (Mackenzie, Rademakers, and Neumann 2010)(Gagliardi et al. 2021).

Finally, mutations in C9orf72 gene are the most common in both fALS and sALS. It is a toxic gain of function in which the mutation affecting this gene is a hexanucleotide expansion (GGGGCC) in the non-coding region (Mejzini et al. 2019). Patients with alterations in this gene, not only present phosphorylated and ubiquitinated TDP-43 inclusions, but also dipeptide repeats (DPRs) derived from non-ATG repeat associated translation (RAN) (Wen et al. 2014). DPR-mediated toxicity is crucial for C9-ALS pathogenesis and is considered one of the major drivers of neuronal death (Gagliardi et al. 2021).

1.1.1 Pathological molecular mechanisms in ALS

Beside the four genes previously described, many other genes have been recently identified thanks to the evolving techniques for gene mapping and DNA. However, ALS

is the result of many different interacting mechanisms that culminate in larger network disruption. Among them, we find oxidative stress, mitochondrial dysfunction, impaired protein homeostasis, RNA processing, Nucleocytoplasmic and endosomal transport (NCT), DNA damage, excitotoxicity and neuroinflammation. (Mead et al. 2023) (Hardiman et al. 2017).

Oxidative stress (OS) resulting from the impairment in the natural defenses against reactive oxygen (ROS) or nitrogen chemical species, mediates protein injury, lipid peroxidation, and DNA and RNA oxidation, affecting the viability of CNS neurons (Singh et al. 2019). Moreover, OS has been found to increase TDP-43 insolubility, due to an enhancement of the post-translational modification (PTM) of the protein, like acetylation and phosphorylation (Tamaki and Urushitani 2022).

DNA damage response (DDR) has been found activated in ALS, as evident from the presence of yH2AX histone foci (marker of DNA repair) in C9orf72 spinal motor neurons (Mead et al. 2023).

Also, excitotoxicity has indirectly been associated to ALS (Hardiman et al. 2017). It is due to excessive stimulation of postsynaptic glutamate receptors with the result of an increasing intracellular calcium levels. ALS motor neurons have increased expression of calcium permeable AMPA receptor and a reduced mitochondrial calcium-buffering capacity (Nijssen, Comley, and Hedlund 2017). Moreover, the excitatory amino acid transporter 2 (EAAT2), that is the main synaptic glutamate reuptake transporter, is impaired in ALS models and patients (Hardiman et al. 2017).

Neuroinflammation has been linked to ALS in the context of the phenotype of microglia. M1 toxic phenotype has been observed in SOD1-transgenic mice but also in post-mortem brains (Hardiman et al. 2017).

Moreover, TDP-43 and FUS mutant proteins increase their presence and accumulation in the inner mitochondria membrane, leading to mitochondrial dysfunction. Also, mutations in SOD1 protein are reported to reduce the function of the electron transport chain in the mitochondria membrane (Tamaki and Urushitani 2022) (W. Wang et al. 2016).

Transport at the level of endocytosis, vesicle trafficking between different cellular compartments, NCT machinery and axonal transport are defective in ALS. They are

regulated by small Rab GTPases together with other proteins like exportin 1. Together, they regulate the rate of nuclear export across the nuclear pore complex (NPC). In G4C2 C9ORF72 expansions genetic variants but also in TDP-43 and sporadic models, the integrity of the NPC is compromised and the gradient of GTPases is altered (W. Wang et al. 2016)(Fallini et al. 2020).

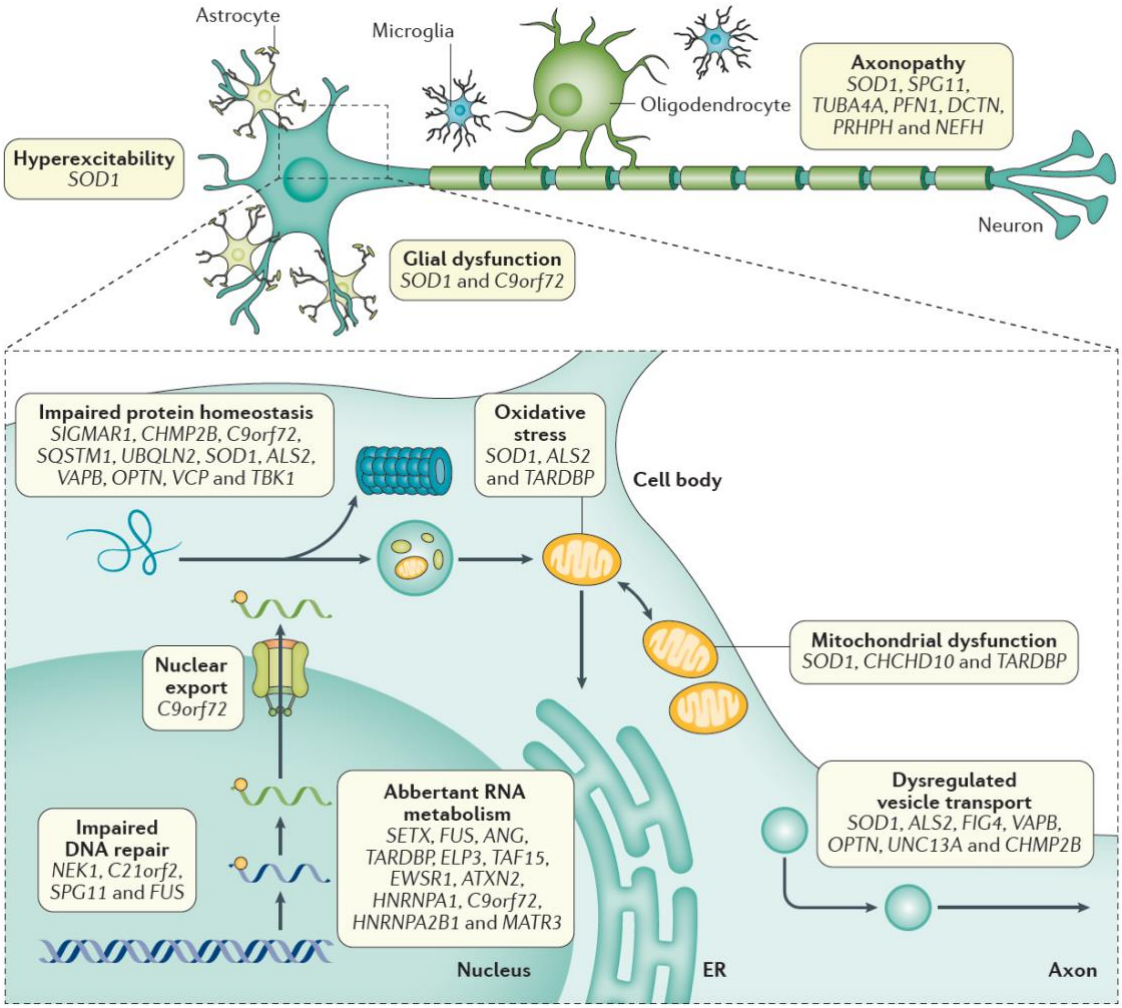

Figure 1.1. Pathophysiology of ALS. Cellular disruption and motor neuronal injury in ALS is the result of mutations in several genes which act through many pathophysiological mechanisms often interlinked that culminate in larger network disruption. SOD1 is the longest-studied gene and has been linked to the majority of pathophysiological mechanisms. Protein homeostasis and aberrant RNA metabolism are predominant factors linking multiple ALS causative genes to neuronal injury, since many ALS related proteins are RBPs as TDP-43, FUS and hnRNPA2B1. Mutant protein aggregates can generate mitochondrial dysfunction and oxidative stress, which in turns exacerbate stress on the already impaired protein homeostasis, further demonstrating the interconnection between the mechanisms. Other mechanisms like impaired nuclear export, impaired DNA repair and dysregulated vesicle transport and dysfunction of glial cells are implicated in ALS. Image adapted from Hardiman et al. (2017).

1.1.1.1 Focus on protein homeostasis and RNA metabolism: the role of RBPs

In the complex network of interacting mechanisms that culminate in the degeneration, RBPs have a central role. Mutations in genes encoding many RBPs, including TARDBP, FUS, hnRNPA1, hnRNPA2B1, TAF15, EWSR1, MATR3, ATXN2, and TIA-1 have been associated to ALS (Xue et al. 2020).

Impaired protein homeostasis is a common feature in ALS. The two main pathways responsible for the control of protein quality and maintain of cellular homeostasis, that are the ubiquitin-proteasome system (UPS) and the autophagy-lysosome pathway, are affected in ALS. Many of the proteins associated with the disease are substrate of these pathways (Fallini et al. 2020) like the full-length and cleaved TDP-43.
Many ALS related RBPs like TDP-43, FUS, EWSR1, TAF15, hnRNPA1 and hnRNPA2B1 have mutations in their low-complexity domain (LCD). Such prion-like domains increase the formation of phase separation inclusions and facilitate the co-aggregation of these proteins in stress induced membrane-less organelles termed stress granules (SGs). SGs are dynamic membraneless compartments composed of RBPs and RNA molecules that are transiently assembled in response to cellular stress. Their dynamics is perturbed by the misfolded RBPs present in the cytosol, making SGs to remain insoluble, further trapping wild-type RBPs leading to irreversible, toxic aggregates (Baradaran-Heravi, Van Broeckhoven, and van der Zee 2020). For example, the heterogeneous nuclear ribonucleoprotein particle proteins hnRNPA1 and hnRNPA2B1 are RBPs and binding partners of TDP-43 and are involved in RNA processing, including miRNA maturation, the nucleocytoplasmic transport of mRNA, and RNA metabolism (Purice and Taylor 2018)(Guil and Cáceres 2007). Mutations in the prion-like domains of hnRNPA2B1 and hnRNPA1 increase aggregation potential and the fibril formation as well their increased assembly into stress granules (K. Zhang et al. 2018)(Hong Joo Kim et al. 2013).

All the proteins cited above belong to the hnRNP family; they bind thousands of targets and regulate every stage of RNA metabolism. RNA trafficking, nuclear export, non-coding RNA biogenesis, ribosomal subunits synthesis as well as translation and RNAs degradation are the majority of involved pathways (Nedelsky and Taylor 2022). So, mutations in these proteins or perturbed functions due to SGs accumulation can lead to a vast scale impairment of RNA metabolism, which, in fact, is a key element in ALS (Tamaki and Urushitani 2022) (Taylor, Brown, and Cleveland 2016).

Nuclear RNA splicing and cytoplasmic RNA translation are the most observed ones. For example, nuclear depletion of TDP-43 results in the mRNA splicing aberrations of multiple RNA targets (Polymenidou et al. 2011), with the creation of cryptic exons (Brown et al. 2022). Similarly, also the depletion of FUS and hnRNPA1 resulted in altered RNA levels and splicing. Specifically, FUS depletion in adult nervous system resulted in the alteration of more than 950 mRNAs, mostly different from the TDP-43-dependent RNAs. Interestingly, in mouse brains, among the 45 mRNAs reduced upon depletion of TDP-43 or FUS, the majority encoded for proteins that are fundamental for neuronal functionality and some of them were also reduced in a similar model of stem cell-derived human neurons, suggesting a common pathway related to a loss-of-function mechanism (Lagier-Tourenne et al. 2012).

Moreover, C9ORF72 genetic variants have been associated with RNA foci, expanded RNA repeats retained in the nucleus, acting sequestering various RBPs and other RNA maturation factors (Tamaki and Urushitani 2022). In fact, the antisense RNA foci correlate with TDP-43 aggregation in the cytosol of C9orf72 motor neurons (Aladesuyi Arogundade et al. 2019). Moreover, these transcribed RNA repeats undergo RAN translation; this generates five different highly aggregation-prone DPRs that are poly-GP, GA, and GR (from the sense strand) and poly-PR, PA and GP (from the antisense strand) which can accumulate in SGs or in the nucleolus, altering in this way the ribosome biogenesis (Ash et al. 2013).

Putting everything together, it is actually probable that the main mechanism of ALS is dependent on the initial cause of disease, considering that many mechanisms are associated with a single mutation and are probably all interconnected. What is clear is

that at the end motor neurons cannot maintain their axonal projections, causing axonal retraction and denervation of the target cell.

Concluding, considering the many different mutations linked with ALS, a remarkable number of RBPs results to be involved in the pathogenesis of ALS leading to proteotoxic damage and dysregulation of RNA metabolism as key factor for neurodegeneration.

1.1.2 ALS as a non-cell autonomous disease

Motor neurons (MNs) loss is the main trait of the disease; so, much of the initial research focused on a neuron-centric view of ALS/FTLD (H. Chen et al. 2018). However, in the last twenty years non-neuronal cell types have been recognized to be involved in the pathogenesis of ALS, thanks to studies carried out on transgenic models (Weydt et al. 2004). These evidences gave rise to what is called non-cell autonomous disease hypothesis of ALS, according to which other non-neuronal cell types including astrocytes, oligodendrocytes, and microglia take part in the disease. Initial studies on transgenic mice revealed that non-neuronal cells expressing mSOD1 could lead to the formation of ubiquitin-positive protein aggregates in the surrounding MNs (Van Harten, Phatnani, and Przedborski 2021). Also, the simple deletion of mSOD1 in MNs only resulted in attenuation, but not abrogation, of the ALS-like phenotype, further supporting the role of non-MN cells in the degeneration of neighboring MNs in ALS (Boillée et al. 2006). Moreover, overexpression experiments of ALS related gene mutations in different cell types, especially the one targeting SOD1, were all showing that reducing mutant proteins per cell and having fewer cells expressing mutant proteins attenuated the ALS-like phenotype; further supporting the non-cell autonomous hypothesis (Van Harten, Phatnani, and Przedborski 2021). So, astrocytes, microglia, oligodendrocytes and peripheral blood cells affect MNs: In fact, TDP-43 inclusions were detected in both spinal MNs and oligodendrocytes in patients with sALS. In the same study, newly generated oligodendrocytes in spinal cords from transgenic mSOD1 mice could have myelination and metabolic defects due to a lower expression of myelin basic protein (MBP) and monocarboxylate transporter-1 (MCT1) (Philips et al. 2013). During disease progression, microglia can switch to an activated

neurodegenerative state (Weydt et al. 2004), or they can have a role in the initiation of the disease in hSOD1 G93A mouse model (Gerber et al. 2012). In a study exploiting SOD1 model, microglia carrying misfolded protein aggregates was demonstrated to create a pro-inflammatory environment by secreting soluble factors like ROS in the culture media (Xiao et al. 2007). Also, the analysis of post-mortem brain of ALS patients with C9orf72 expansion showed extensive microglial activation, which is correlated with neuronal and axonal loss, as well as with more rapid disease progression (Brettschneider et al. 2012). Astrocytes represent ~20–40% of glial cells in the CNS (Vahsen et al. 2021), and seem to play a key role in ALS. Similarly to microglia, astrocytes can switch to a neurotoxic phenotype. In mouse models, astrocyte-specific deletion of mSOD1 resulted in longer survival of the animals (Lijun Wang, Gutmann, and Roos 2011), indicating a gain-of-function, non-cell-autonomous neurotoxicity; even if also loss-of-function effects, including a reduction in homeostatic function have also been described in mSOD1-expressing astrocytes (Vahsen et al. 2021). A similar gain-of-function and loss-of-function neurotoxic mechanisms exist also from astrocytes in TDP-43 models exploiting TDP-43 mutant primary cultures and human induced pluripotent stem cells (iPSCs)-derived MNs and astrocytes co-cultures (Vahsen et al. 2021). It cannot be excluded that astrocytes neurotoxicity is exerted upon the interaction with other non-neuronal cell types such as microglia or non-glial immune cells.

Finally, numerous infiltrating monocytes, with pro-inflammatory profiles, were observed in the blood vessels in the brain in a TDP-43^{A315T} mouse model and in patients with TDP-43 pathology (Jara et al. 2019)(Vahsen et al. 2021).

Summarizing the studies done in animal models and postmortem brains, the damage in ALS is likely to initiate by the primary neurons, with a subsequent combination of a dysregulated and pro-inflammatory non-neuronal cell response to neuronal damage and a failure of the supportive roles of non-neuronal cells.

In this context, extracellular vesicles, as key player in intercellular communication among neurons and between neurons and glia or cells, are acquiring interest in the context of the altered intercellular communication in ALS, by which the MN-surrounding cell network affects the onset and progression of the disease.

1.2 Extracellular Vesicles (EVs) and ALS

1.2.1 EVs biogenesis and classification

Extracellular vesicles (EVs) are a heterogeneous group of cell-derived membranous structures composed of a lipid bilayer. They are released in biological fluids and are involved in multiple physiological and pathological processes. They can contain proteins, lipids, and nucleic acids with differences according to biogenesis, cell type, and physiologic conditions (Abels and Breakefield 2016). According to their origin, size, morphology, and cargo content, EVs are classified in two main categories: exosomes and microvesicles. They are formed at distinct regions in the cells, but they have common intracellular mechanisms and sorting machineries, limiting in this way a clear separation of the subpopulations.

Exosomes have a diameter ranging between 30–100 nm; they are generated as intraluminal vesicles (ILVs) in the lumen of endosomes during their maturation into multivesicular endosomes (MVEs). MVEs maturation and ILVs formation are driven by the endosomal sorting complex required for transport (ESCRT), involved in membrane shaping and scission. The ESCRT-0 and ESCRT-I subunits cluster cargoes on the membrane of MVEs and recruit, via ESCRT-II, the ESCRT-III subcomplexes that perform budding and fission. Accessories proteins like syntenin and the ESCRT accessory protein ALG-2 interacting protein X (ALIX) take part in the process supporting the intraluminal budding of endosomal membranes (Van Niel, D'Angelo, and Raposo 2018).

Exosomes can also be formed in an ESCRT-independent manner. In this mechanism, MVEs production requires the presence of ceramide, produced by the neutral type II sphingomyelinase, the enzyme responsible for the hydrolyses of sphingomyelin into ceramide. Ceramide allows the generation of membrane subdomains, imposing a spontaneous negative curvature on the membrane. Alternatively, ceramide could be metabolized to sphingosine 1-phospate to activate G-protein-coupled-sphingosine 1-phospate receptor, essential for cargo sorting into exosomal ILVs. Proteins of the tetraspanin family like CD63 but also CD81, CD92 and CD9 take part in the ESCRT-

independent mechanism and are directly involved in the sorting of various cargoes to exosomes (Teng and Fussenegger 2021) (Van Niel, D'Angelo, and Raposo 2018).

Once matured, MVEs can be targeted to lysosomes or autophagosomes for degradation or transported along microtubules to the plasma membrane. Targeting to lysosomes occurs by retrograde transport on microtubules; the RAB-GTPase RAB7 and its associated proteins promote the recruitment of the retrograde molecular motor dynein that targets MVE to lysosomes. RAB7 is also required for exosomes release together with RAB27A and RAB27B. SNARE proteins and synaptotagmin family members mediate the final step of exosome secretion controlling the fusion of MVEs with the plasma membrane with the subsequent release of ILVs as exosomes. (van Niel et al. 2022)

Microvesicles range approximately from 100-150 to 1000 nm. They are generated by the outward budding and fission of the plasma membrane and the subsequent release of vesicles into the extracellular space. The molecular mechanisms involved in their biogenesis are less characterized; Ca^{2+}-dependent enzymatic machineries like flippases and floppases rearrange in the membrane phospholipids to cause the physical bending of the membrane, favoring membrane budding and formation of microvesicles. Their release requires the interaction of actin and myosin with a subsequent ATP-dependent contraction. Moreover, the ESCRT machinery, small GTPase proteins or activation of acid sphingomyelinase (A-SMase), can also trigger the release of EVs (Van Niel, D'Angelo, and Raposo 2018) (Teng and Fussenegger 2021).

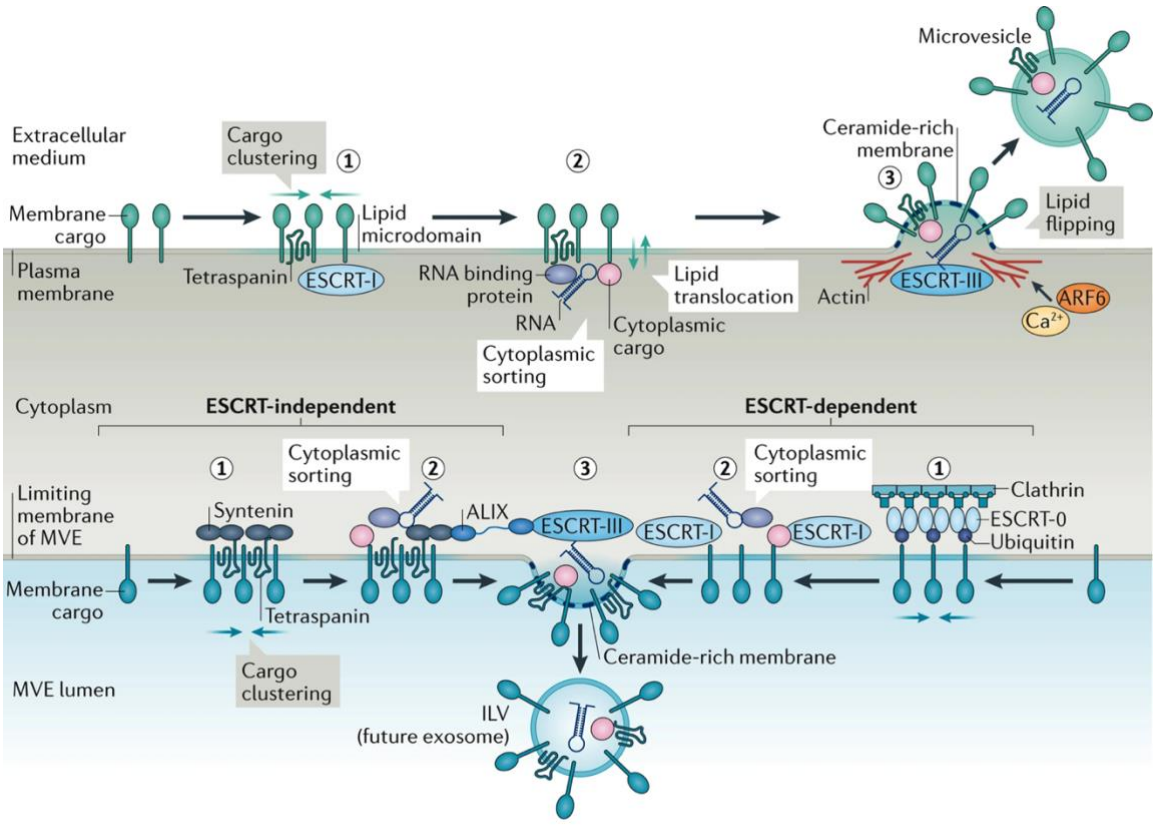

Figure 1.2. Biogenesis of Extracellular Vesicles (EVs): schematic representation of the steps and the machinery involved in the biogenesis processes. Microvesicles (top) originate from the clustering of lipids and membrane-associated proteins on membrane microdomains of the plasma membrane (1), followed by the recruitment of soluble components (2). Membrane budding and fission processes are the last steps (3) that allow the release of microvesicles. Exosomes (bottom) are formed from clustering of lipids and membrane-associated proteins on the MVE membrane (1), followed by recruitment of soluble components (2) and final membrane budding and fission with the formation of the ILVs (3). The molecular machineries that act at the different steps of extracellular vesicle biogenesis are partly common between exosomes and microvesicles. Image adapted from Van Niel, D'Angelo, and Raposo (2018).

Protein, lipids, and nucleic acids represent the main biomolecular content of EVs (Veziroglu and Mias 2020), that can be actively or passively loaded in EVs before secretion.

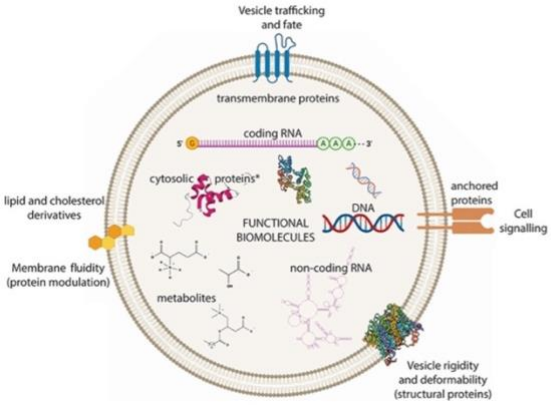

Figure 1.3. Extracellular vesicles composition: both DNA and RNA (coding and non-coding) are found in EVs. Proteins can be freely soluble, membrane associated, membrane anchored and trans-membrane. Also metabolites and other small molecules are found in EVs. Image modified from Veziroglu, E. M., & Mias, G. I. (2020).

Proteins in EVs can be present in the luminal part as soluble proteins, like heat shock proteins (HSP), cytoskeleton components and others (Yáñez-Mó et al. 2015); or as transmembrane insoluble proteins anchored to the lipids, like tetraspanins. A recent quantitative proteomic analysis carried out on 14 human cell lines derived EVs, allowed the identification of almost 1200 common ubiquitous proteins, representing the core proteome of exosomes. Among them, biogenesis-related proteins, such, ALIX, TSG101 and especially syntenin-1, are ubiquitous to exosomes from all of the cells evaluated and can be used as exosomes biomarkers, together with GTPases, ESCRT members, SNARE members. On the other hands, tetraspanins like CD9, CD63 and CD81 are heterogeneously expressed across the EVs, mirroring the expression pattern of the parental cells (Kugeratski et al. 2021).

RNA binding proteins represent one fourth of all the proteins contained in EVs; more details about their presence in EVs and their role in RNA sorting will be provided in the dedicated session in paragraph 1.4.

Lipids like phosphatidyl serine, sphingomyelin, cholesterol, and ceramide are enriched in EVs (Donoso-Quezada, Ayala-Mar, and González-Valdez 2021). Ceramide in particular is involved in the ESCRT-independent exosomes biogenesis and has a role in the RNA cargo segregation and proteolipid protein sorting (Horbay et al. 2022).

In general, EV-lipids are organized in detergent-resistant raft like structures, enhancing membrane stability (Donoso-Quezada, Ayala-Mar, and González-Valdez 2021) and forming lipid microdomains that are involved in EVs secretion and function (Ouweneel, Thomas, and Sorci-Thomas 2020).

Nucleic acids, and especially RNA, are one of the principal cargoes retrieved in EVs. A special section will be devoted to RNA population of EVs in the paragraph 1.3.1.

1.2.2 EVs role in ALS-associated proteins propagation

EVs are conceived to transport cargoes from donor to recipient cells representing vehicles of intercellular communication in short or long distance. In recent years, the biological role of EVs in the pathogenesis of neurodegenerative diseases started to be explored, in the hypothesis that these could mediate the spreading of "death signals" to neuronal and non-neuronal CNS districts. (Hill 2019) (Gagliardi et al. 2021).

In ALS, according to the prion-like hypothesis, misfolded proteins, which form ubiquitylated inclusions in the cytoplasm, can be transferred to healthy cells, induce their endogenous counterpart to misfold and lead to the amplification of these pathological seeds (Gagliardi et al. 2021). This is the case for example of TDP-43, C9ORF72-derived DPRs, FUS, SOD1 as summarized in the table below (Table 1). Several *in vitro* and *in vivo* experiments showed how EVs could carry full length form or fragments of mutant form of these proteins, that have a prion-like behavior, promoting the misfolding of normal protein in the recipient cells (Ferrara et al. 2018)(McAlary et al. 2019). Moreover, in fALS many genes are directly or indirectly involved in vesicular trafficking: C9ORF72, VAPB, FIG4, ALS2, CHMP2B, SPG11, SQSTM1, OPTN, UBQLN2, VCP, TBK1 have all been associated with alterations in either endo-lysosomal trafficking, autophagy, or EVs secretion itself. (McCluskey et al. 2022)

EVs have already been associated with the spreading of misfolded proteins on other prion-like diseases such as Alzheimer's, Parkinson's, or Creutzfeldt-Jakob disease; in which Amyloid b, a-synuclein or the transmissible spongiform-associated prion protein (PrPTSE) together with Tau oligomers are known to be carried by EVs (Gabrielli et al. 2022) (Lööv et al. 2016)(Saá et al. 2014)(Jackson, Guerrero-Muñoz, and Castillo-Carranza 2022).

In ALS, misfolded SOD1 was initially found in ALS patients cerebrospinal fluid (CSF) (Zetterström et al. 2011). In the work by Basso et al, it has been shown that exosome-dependent secretion of SOD1 by mutant astrocytes results in in a decreased viability of neurons (Basso et al. 2013). Recently, it has been shown misfolded SOD1 carried on the surface of SOD1 murine brain-derived extracellular vesicles and on human SOD1 fALS spinal cord specimens (Grad et al. 2014).

Protein	Extracellular vesicle	Sample/model	Main finding	Reference
SOD1	Exosomes	Mouse MN-like NSC-34 cells	Possible protective role of SOD1-containing exosomes against ROS	(Gomes et al. 2007)
SOD1	Exosomes	SOD1 overexpressing astrocytes	Astrocyte-derived exosomes contribute to neuronal toxicity	(Basso et al. 2013)
SOD1	Exosomes	Mouse MN-like NSC-34 cells	SOD1 is transmitted from cell to cell through exosomes and misfolding native SOD1 is efficiently perpetuated in naïve cells	(Grad et al. 2014)
SOD1	Exosomes	Rat microglia cells	Microglial cells release SOD1- containing exosomes and are toxic to neurons	(Massenzio et al. 2018)
SOD1	Exosomes and MVs	SOD1 transgenic mouse	SOD1 is secreted in vivo in EVs derived from astrocytes and neurons	(Silverman et al. 2019)
TDP-43	Exosomes	Human neuroblastoma cells	Phosphorylated TDP-43 aggregates can propagate from cell-to-cell via exosomes	(Nonaka et al. 2013)
TDP-43	Exosomes	U251 cells	TDP-43-containing exosomes from CSF from ALS/FTD patients has prion-like transmissible properties *in vitro*	(Ding et al. 2015)
TDP-43	Exosomes and MVs	HEK293 cells and primary mouse neurons	Intracellular transmission and seeding properties	(Feiler et al. 2015)
TDP-43	Exosomes	Neuro2a cells and TDP-43 transgenic mouse	Cytoplasmic TDP-43 localization *in vitro*; possible contribution in TDP-43 neuronal clearance in vivo	(Iguchi et al. 2016)

FUS	Exosomes	SH-SY5Y and N2A cells	FUS secretion in FUS-overexpressing cells	(Kamelgarn et al. 2016)
DPRs	Exosomes	iPSC-derived MNs from C9orf72-related ALS patients	Cell-to-cell DPR transmission	(Westergard et al. 2016)

Table 1| Proteins with relevance for ALS identified in extracellular vesicles from in vitro and in vivo models: Information taken from Gagliardi et al. (2021)

TDP-43 presence in EVs together with its role in the propagation of cellular inclusions in EV-receiving cells has been show by different studies (Feiler et al. 2015) (McCluskey et al. 2022), even if its permanent presence in EVs is still under discussion. Nevertheless, EVs, together with autophagy, could be relevant for TDP-43 clearance; as a result, a blockage of exosome biogenesis with GW4869 or by silencing RAB27A resulted in increased intracellular TDP-43 aggregation in mouse models (Iguchi et al. 2016).

FUS was also found secreted in EVs in cellular model overexpressing the protein.

Finally, C9-derived DPRs was found in EVs from NSC-34 transfected with DPRs and spinal motor neurons derived from induced pluripotent stem cells from C9orf72-ALS patients (Ferrara et al. 2018)

Beside the role of EVs protein cargo in ALS spreading, the nucleic acid content and specifically the RNA content of EVs is grabbing a lot of attention, since RNA and RBP dyshomeostasis is crucial in ALS.

1.3 The vesicular RNA

1.3.1 The RNA populations associated with EVs

The RNA sequencing approaches have demonstrated that EVs can transport many RNA biotypes (Dellar et al. 2022). Current data in Vesiclepedia database (http://microvesicles.org) show more than 27,000 entries for mRNAs and more than 10,000 entries for non-coding RNAs in EVs (Fabbiano et al. 2020). The different RNA classes in EVs include protein-coding intact or fragmented RNAs (mRNAs) and many types of non-coding RNAs, including microRNAs (miRNAs), long non-coding RNAs (lncRNAs), circular RNAs (circRNAs), small nuclear RNAs (snRNAs), small nucleolar RNAs

(snoRNAs), transfer RNAs (tRNAs), ribosomal RNAs (rRNAs), and piwi-interacting RNAs (piRNAs) (K. M. Kim et al. 2017).

Likely, the EV-RNA content reflects the type and the physiological/pathological state of the source cells, however it differs in the relative concentration of specific RNA sequences if compared with the intracellular content (O'Brien et al. 2020).

Messenger RNAs are found in EVs as fragmented or as full length form; many of them can be translated and can have a functional effect in the recipient cells in protein expression, as demonstrated by different studies exploiting glioblastoma cells, MC/9 cells (Valadi et al. 2007), and human central nervous system (CNS)-patrolling macrophages (Mitsuhashi et al. 2013)(K. M. Kim et al. 2017). MicroRNAs are one of the most abundant non-coding RNA specie in EVs. They are small (~22-nt) noncoding, highly conserved, single-stranded RNAs with a potential role in regulating gene expression in recipient cells. The brain has the highest expression of tissue-specific microRNAs and thus microRNAs in brain EVs are grabbing attention in the context of EVs role in neurodegenerative diseases propagation (K. M. Kim et al. 2017).

Long non-coding RNAs (>200 nt) and circular RNA have been found in EVs, however the extracellular functions of circRNAs via EVs are not known yet.

In the small non-coding RNAs category, Y-RNAs represent a family of sncRNAs with a length of 84-112 nt. In humans hY1, hY3, hY4, hY5 Y-RNA have been described (Billmeier et al. 2022). From our point of view, Y-RNA are interesting since they were detected in EVs deriving from multiple cell types isolated by different purification methods (Driedonks and Nolte-T'Hoen 2019) and the ratio of all of the subtypes has been proposed as a biomarker for immune-related diseases (Driedonks et al. 2020).

So, focusing on the effect of EV-RNAs in recipient cells, they can be categorized into three types: RNAs with an established functionality when carried by EVs (like intact mRNAs and miRNAs), intact RNAs with a predicted, but not definitively demonstrated functionality in intercellular communication (for example, piRNAs and vtRNAs); and fragments of RNAs (for example, fragments of mRNAs, rRNAs and tRNA), some of which could have a functional role, but others may be degradation products with no functions (O'Brien et al. 2020).

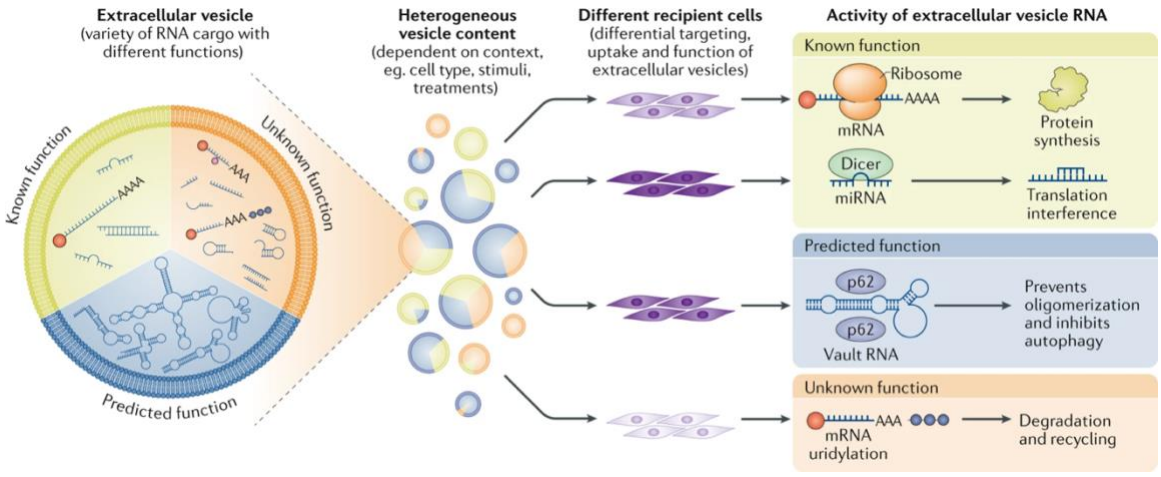

Figure 1.4. Principles of functional cell communication by extracellular vesicle RNA: schematic view representing the heterogeneity of RNA contained in EVs and the different roles of RNA cargo in the recipient cells. According to our knowledge, RNA in recipient cells can have a known, a predicted or an unknown function. Image taken from O'Brien, K., Breyne, K., Ughetto, S., Laurent, L. C., & Breakefield, X. O. (2020).

1.3.2 EV-RNA biology in ALS models

As mentioned before, EVs role in ALS has acquired interest in the context of disease spreading and the prion-like hypothesis, according to which misfolded proteins are transmitted to recipient cells causing the conversion of native protein into misfolded ones (Hill 2019).

Together with protein content, also EV-RNA has been linked to ALS. Nowadays a lot of efforts is directed both in the context of miRNAs in EVs from ALS patients' blood as potential biomarkers (Katsu et al. 2019)(Saucier et al. 2019)(Q. Xu et al. 2018), and in understanding the role of RNAs carried by EVs in modulating ALS phenotype and pathogenesis in recipient cells. Many studies exploit EV-RNA to find potential biomarkers. For example, a microarray analysis of neuron-derived EVs in plasma from patients with ALS and healthy control revealed a total of 30 miRNAs in the neuron-derived EVs that were differentially regulated in ALS relative to controls (Katsu et al. 2019). With a similar approach, 5 miRNAs (miR-146a-5p; miR-199a-3p; miR-151a-3p; miR-151a-5p; miR-199a-5p) were found up-regulated in ALS samples, while 3 miRNAs (miR-4454; miR-10b-5p; miR-29b-3p) were found to be downregulated in ALS compared to healthy controls. miR-199a-3p and miR-4454 were in common with the study of Saucier et al., conducted through a next-generation sequencing approach on EVs

extracted from plasma of patients with ALS and healthy controls (Saucier et al. 2019). All these studies focused on non-coding RNAs add information about disease-related genes and pathways, even if correlation with clinical parameter will be necessary. Beside the potential role as a biomarker, EV-RNA could modulate and interfere with the phenotype of recipient cells in ALS context, since RNA dyshomeostasis could be involved in the pathology (Gagliardi et al. 2021). An initial study on mSOD1 astrocytes showed how vesicles coming from mutant astrocytes were able to induce selective death of the WT motor neurons (Basso et al. 2013). Also, Grad et al. showed that exosome-dependent and independent mechanisms are involved in mSOD1 propagation; misfolded human WTSOD1 can be released from mouse motor neuron-like cells on exosomes and then taken up by neighboring cells (Grad et al. 2014). More recently, NSC-34 MNs wild type or transfected with mutant SOD1 were shown to transfer miRNA-enriched exosomes to N9 microglial cells, influencing their cell phagocytic ability and causing a persistent NF-κB activation (Pinto et al. 2017). Moreover, astrocytes derived from C9ORF72-ALS patients have impaired EVs formation and a downregulation of miR-494-3p, and this affects MN survival and the neurite network maintenance *in vitro* (Varcianna et al. 2019).

Interestingly, EVs coming from patients derived muscle cells (Mu) are shown to be toxic to healthy human iPSC-derived motor neurons, causing a greater cell death together with shorter neurites, with less branching. MuV showed an enrichment of RNA binding proteins, containing many known protein binding partners of TDP-43 and FUS and an upregulation of RNA-processing pathways. To test a possible involvement of RNA processing in ALS MuV toxicity, human iPSC-MNs derived from healthy subjects were treated with ALS MuVs, resulting in RNA accumulated in their nuclei, which has been reported to induce cell death (Le Gall et al. 2022).

Taken together, these results highlight the importance of EV-RNA cargo in the miscommunication process, pointing out the importance of RNA-processing and RBPs homeostasis in ALS.

1.4 RNA-binding proteins and RNA sorting into EVs

As mentioned before, the RNA cargo of EVs is packaged with different efficiencies (O'Brien et al. 2020). In this context, besides a passive loading of RNA in EVs due to its high abundance in the cytoplasm, or secondary configurations and differential affinity for membrane lipids (O'Brien et al. 2020), the selective incorporation of RNA in EVs mediated by RNA-binding proteins (RBPs) has been proposed as crucial determinant in diversifying the enrichment of selected transcripts into EVs (O'Brien et al. 2020)(Fabbiano et al. 2020). More than 500 RBPs are found in in mammalian cells, and they represent the 25% of the EV-protein content (Sork et al. 2018). RBPs can coalesce into large ribonucleoparticles and travel along the cytoskeleton carrying most RNAs from the nucleus to specific cellular locations (Di Liegro, Schiera, and Di Liegro 2014). Up to now, members of the hnRNP family (hnRNPA2B1, hnRNPC1, hnRNPG, hnRNPH1, hnRNPK, and hnRNPQ/SYNCRIP), as well as YBX1, AGO2, HuR, IGF2BP1, ALIX, MEX3C, ANXA2, LIN28, NCL, FUS, MVP, SRP9/14, QKI, and TERT RBPs have been found to be part of the EV biology (Fabbiano et al. 2020). They are associated with EVs at different levels: they can be secreted in EVs together with their target RNAs, or they can be secreted in EVs but their target RNAs are only deduced, or finally the transcripts in EVs contain sequences that are recognized by RBPs (Fabbiano et al. 2020).

The mechanisms implicated in the packaging rely on specific RNA sequences motifs, RNA secondary structures and also RBPs modifications, such as ubiquitylation, SUMOylation, phosphorylation and uridylation (O'Brien et al. 2020).

Biochemical, cell-based, and computational approaches showed an enrichment of transcript sequences, defined "RNA motif", recurrently found in EV-RNA and bound by RBPs. A microarray analysis of activation-induced changes in the miRNA and mRNA profiles of primary T lymphoblasts and their exosomes allowed the identification of two over-represented motifs in miRNAs specifically sorted in exosomes (EXOmotifs) and three in miRNAs retained in the cells (CLmiRNAs) (Villarroya-Beltri et al. 2013). Moreover, the in silico sequence analysis of miRNAs enriched in exosomes isolated from the media of five mouse cell lines, allowed the identification of more EXOmotif for each cell type, necessary for the miRNA sorting in EVs (Garcia-Martin et al. 2022). These

studies allowed the identification of RBPs like hnRNPA2B1 (Villarroya-Beltri et al. 2013), FUS and SYNCRIP (PMID: (Garcia-Martin et al. 2022) as players in the sorting mechanisms.

In general, the mechanisms below the EV-RNA sorting still need to be investigated further. So far data qualitatively demonstrate a link between RBPs and vesicular trafficking. hnRNPs family proteins together with other RBPs, such as YBX1 and MEX3C interact with many complexes of the EVs biogenesis machinery, moreover their PTMs status has been shown to influence EV-RNA, further strengthening a mechanistic role of RBPs in EVs and EV-RNA trafficking. It is the case of SUMOylation of hnRNPA2B1 or phosphorylation of YBX1 with consequence secretion of proangiogenic factors in vivo. The EV-RNA consensus proposed to be recognized by different RBPs, such as the A/G-rich stretches by hnRNPA2B1, hnRNPH1, hnRNPQ, AGO2, and ANXA2, C-rich stretches by hnRNPG, hnRNPK, YBX1, and NCL, AU-rich elements by HuR and hnRNPC1; suggest a cooperation between RBPs or competitive binding to RNA motifs which could regulate miRNA sorting in EVs (Fabbiano et al. 2020).

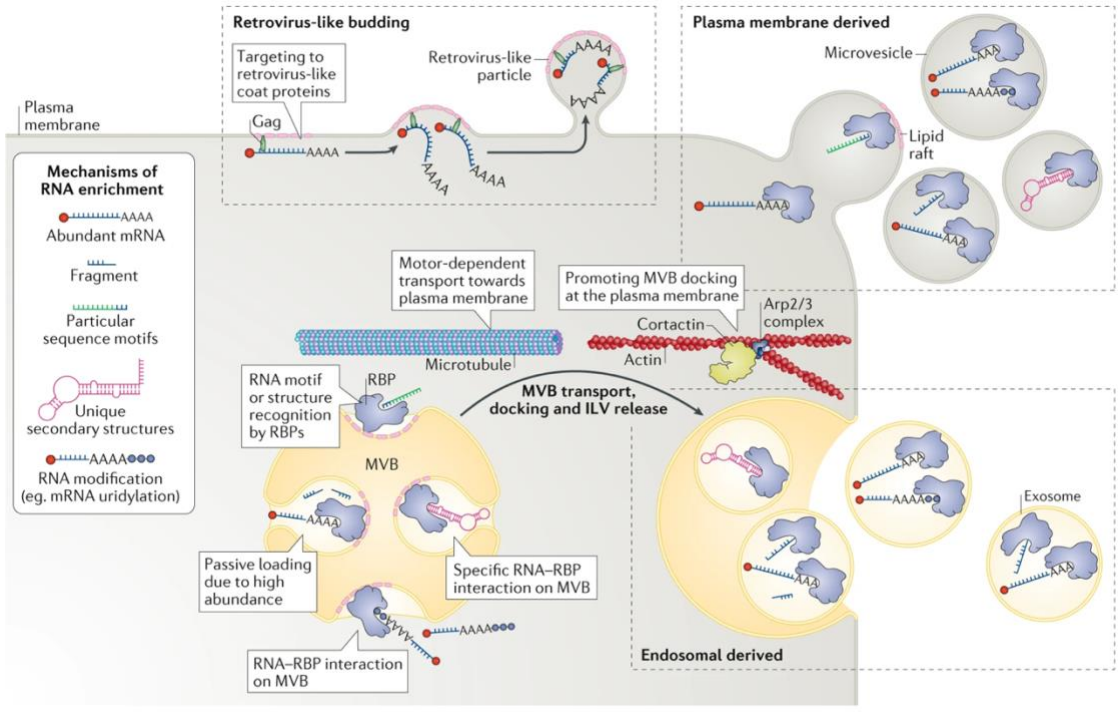

Figure 1.5. RNA packaging into extracellular vesicles and their release into the extracellular space: the variety of RNAs in EVs can be loaded with different modalities. It can be released in microvesicles when targeted to the plasma membrane, or in exosomes when targeted to the MVB, and so incorporated in the ILVs. RNA loading in EVs can occur passively (due to abundance of RNA in the cytosol), or by recognition of multiple RBPs which recognize particular sequence motifs or unique secondary structures in RNA. Image taken from O'Brien et al. (2020)

1.4.1 The function of hnRNPA2B1

Heterogeneous nuclear ribonucleoproteins (hnRNPs) constitute a family of 20 proteins in humans with specific RNA-binding capacities (Dreyfuss et al. 1993). Their structure is characterized by four unique RNA-binding domains (RBDs): the RNA recognition motif (RRM), the quasi-RRM (qRRM), a glycine-rich domain constituting an RGG box, and a KH domain (Geuens, Bouhy, and Timmerman 2016). Among the RBDs, the most common one is the RRM, while the glycine-, proline-, or acid-rich domains are responsible for homologous or heterologous interactions with other hnRNPs and are auxiliary structures (Geuens, Bouhy, and Timmerman 2016); not all the RBDs are present, and the RNA-recognition specificity is dependent flexible protein conformation and PTMs (Geuens, Bouhy, and Timmerman 2016).

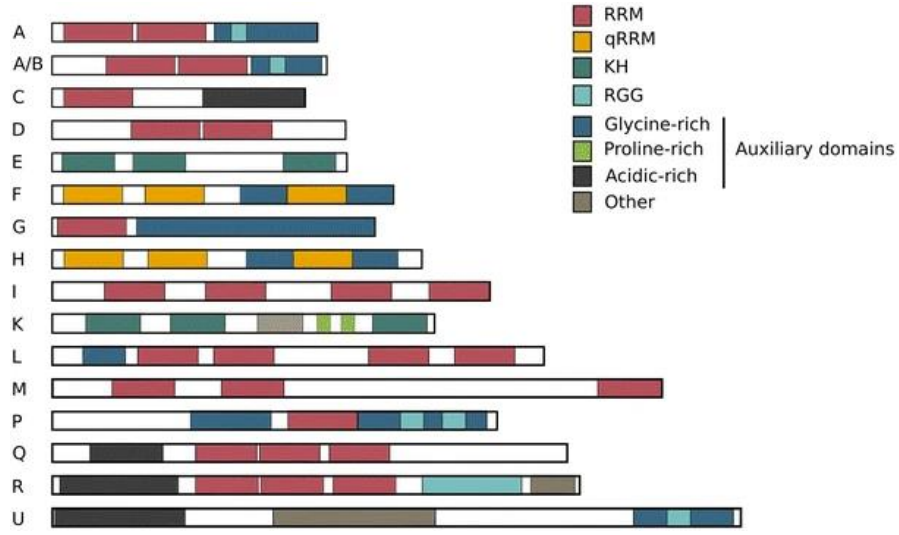

Figure 1.6. Structures of the hnRNPs family members: hnRNP proteins are characterized by four unique RNA-binding domains (RBDs): the RNA recognition motif (RRM), the quasi-RRM (qRRM), a glycine-rich domain constituting an RGG box, and a KH domain. Glycine, proline, and acid-rich domains are auxiliary domains responsible for homologous or heterologous interactions. Figure taken from Geuens, T., Bouhy, D., & Timmerman, V. (2016)

Among all the members of the family, hnRNPC1, hnRNPG, hnRNPH1, hnRNPK, hnRNPQ and hnRNPA2B1 emerged in association with EVs (Fabbiano et al. 2020).
They bind to specific RNA motifs and are involved in RNA loading in EVs, as summarized in the table below (Table 2).

Through MS/MS analysis hnRNPC1 was identified to possibly influence the loading of miR-30d in endometrial exosomes; moreover, in the same study the authors show its presence in exosomes through colocalization experiments with CD63 and FACS analyses (Balaguer et al. 2018).

hnRNPG, also known as RBMX, was found release by exosomes in the studies of de Jong et al, (de Jong et al. 2012) and Liang B et al (Liang et al. 2013). It is also associated to the exosome release of TNFR1 (Adamik et al. 2008), and it emerged to be one of the proteins having the highest number of predicted binding sites on lncRNAs in exosomes derived from four prostate cancer cell lines (Ahadi et al. 2016). Nevertheless, RBMX correlation with specific RNAs is only indirect.

hnRNPH1 mRNA and protein were both identified in exosomes (H. Xu et al. 2018)(Statello et al. 2018). Its association with exosomes is related to the exosomes biogenesis and release (Datta et al. 2017). Its possible role in RNA cargo sorting is reported the work of Statello and colleagues, who identified hnRNPH1 able to interact with exo-RNAs (Statello et al. 2018).

hnRNPK was associated to the transfer of lncRNA 91H in the context of colorectal cancer (CRC) progression, since a physical interaction between the two was inferred through Mass spectrometry analysis (T. Gao et al. 2018).

hnRNPQ (SYNCRIP) presence in exosomes from hepatocellular condition was linked to the control of specific miRNAs, such asmiR-3470a and miR-194-2-3p (Santangelo et al. 2016). The authors identified an exosome-enriched GGCU consensus motif responsible for the packaging of the motif-containing miRNAs into the vesicles. Remarkably, the SYNCRIP-dependent RNA cargo does not overlap with the hnRNPA2B1-dependent one.

Of note, hnRNPA2B1 emerged as a key player in the specific sorting of miRNAs in EVs.

Villarroya et al. demonstrated the direct binding of hnNRPA2B1 to specific miRNAs harboring GGAG motif present in their 3'-end. The GGAG motif (EXOmotif) was found in the 3' half of the miRNA sequence in 75% of the miRNAs enriched in exosomes (EXOmiRNAs) and hnRNPA2B1 was identified as the most relevant protein involved in the binding of miRNAs (i.e., miR-198 and miR-601) through the EXOmotifs. Moreover, hnRNPA2B1 SUMOylation was found to increase the miRNA sorting in EVs (Villarroya-Beltri et al. 2013); also, O-GlcNacylation of hnRNPA2B1 due to the interaction with caveolin-1 showed increase miR-17 and -93 into MVs (Lee et al. 2019). Long non-coding

RNAs (lncRNAs) are also target of hnRNPA2B1, and their hnRNPA2B1-dependent accumulation within the exosomes has been studied. lncRNA H19 is secreted through hnRNPA2B1-mediated packaging into exosomes in NSCLC cells through the binding to GGAG motif at the 5'-end region of H19, which, when mutated, impairs the binding ability of hnRNPA2B1 (Lei et al. 2018). A similar result was obtained by Chen et al. (C. Chen et al. 2020), in which a direct interaction, through the EXO-motif GGAG, was shown between hnRNPA2B1 and lncRNA LNMAT2 in bladder cancer (BCa) cells.

The most linear model involves the protein and its bound RNA transcripts as incorporated into EVs; in fact, the protein has been previously detected in EVs (Villarroya-Beltri et al. 2013).

However, there are evidences showing that hnRNPA2B1 is not detected in EVs, so, as a consequence, a sorting mechanism not relying on its presence in EVs is also present (Zhou et al. 2020).

Together, these data suggest that hnRNPA2B1 has a central role in the selection of miRNAs and lncRNAs, emphasizing its function in correlation with the vesicular trafficking (Fabbiano et al. 2020).

Protein	EV isolation method	Main interactors	RNA motif	RNA loading in EVs	References
hnRNPA2B1	Differential ultracentrifugation; Polymer precipitation	PTBP1, HNRNPL, HNRNPH1, SRSF1, TRA2B, HNRNPC, HNRNPA1, HNRNPF, HNRNPK, SRSF3	A/G-rich motifs 5'-AGG 5'-UAG 5'-GGAG	Sorting of miRNAs containing GGAG motif	(Villarroya-Beltri et al. 2013); (Lee et al. 2019); (Lei et al. 2018)(C. Chen et al. 2020)
hnRNPC1	Differential ultracentrifugation	HNRNPA1, HNRNPA2B1, ALYREF, HNRNPL, HNRNPM, CDC5L, HNRNPK, ELAVL1, SRSF1, HNRNPH1	AU-rich elements (AREs)	miR-30d	(Balaguer et al. 2018)
hnRNPG	Differential ultracentrifugation	HNRNPK, CDC5L, HNRNPH1, TR2B, HNRNPA1, HNRNPL, PTBP1, HNRNPC, SRSF3, HNRNPR	5'-CC[A/C]-rich	Predicted loading of lncRNAs	(Ahadi et al. 2016)
hnRNPH1	Differential ultracentrifugation	HNRNPA1, HNRNPK, HNRNPA2B1, HNRNPM, HNRNPA0, SRSF1,	5'-GGGA	exo-RNAs binding	(Statello et al. 2018)

		HNRNPF, HNRNPC, TRA2B			
hnRNPK	Differential ultracentrifugation; Polymer precipitation	HNRNPM, HNRNPA1, HNRNPH1, PTBP1, RBMX, HNRNPL, HNRNPF, ELAVL1, HNRNPA2B1, HNRNPC	5′-$UC_{3-4}(U/A)_2$	lncRNA 91H	(T. Gao et al. 2018)
hnRNPQ	Differential ultracentrifugation; Polymer precipitation; Ultrafiltration	APOBEC1, A1CF, PAPC1, PAIP1, CSDE1, HNRNPD, HNRNPR, SMN, HABP4, DHX9, HNRNPU, IGF2BP1, YBX1, ELAVL1	5′-AYAAYY 5′-UAUYRR 5′-GGCU	miR-3470a and miR-194-2-3p	(Santangelo et al. 2016)

Table 2| Technical and biological indications about hnRNPs identified in EVs. Table adapted from (Fabbiano et al. 2020).

As anticipated in the previous paragraph, hnRNPA2B1 is a ubiquitously expressed member of hnRNP family and it is involved in maturation, transport, and metabolism of mRNAs (Dreyfuss, Kim, and Kataoka 2002) (He and Smith 2009). The hnRNPA2B1 gene encodes two protein isoforms, A2 and B1; with the last one having an insertion of 12 amino acids in the N-terminal (Burd et al. 1989); (Kozu, Henrich, and Schäfer 1995). Its structure (Figure 1.7) is similar to the one of the other proteins of the hnRNP family and is characterized by two CS-RNA binding domains (CS-RBD), RRM1 and RRM2, mediating RNA recognition, and a C-terminal glycine-rich region (Burd et al. 1989) which includes a prion-like domain (PrLD), an RGG box, and a PY-motif with a nuclear localization signal (PY-NLS) (B. Wu et al. 2018).

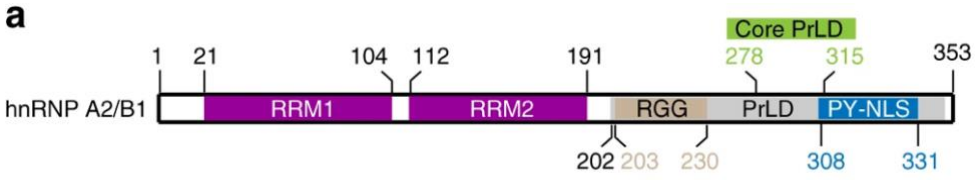

Figure 1.7. Schematic representation of the domain architecture of hnRNP A2B1. The protein is composed of an N-terminal region containing two RNA recognition motif (RRM1 and RRM2) and a C-terminal glycine-rich low-complexity region (LC) containing a prion-like domain (PrLD), a nuclear location signal (NLS) and a RGG arginine-glycine-glycine box. Figure taken from Wu et al. (2018).

hnRNPA2B1 binds to specific sequences of RNA and ssDNA molecules through the RNA binding domain (Y. Liu and Shi 2021), preferentially to A/G-rich sequences (Huelga et al. 2012) and mainly localizes in the nucleus but it shuttles between nucleus and cytoplasm

to perform its functions. It is involved in multiple stages of the intracellular processing of RNA, together with a variety of other functions, including, pre-mRNA alternative splicing (Martinez et al. 2016), transcriptional regulation, transport, mRNA stability (Goodarzi et al. 2012) or degradation, translation regulation, telomeres maintenance (Mckay and Cooke 1992) and miRNA sorting (Villarroya-Beltri et al. 2013). The protein recognizes A2RE, or A2RE-like response element sequences of some mRNAs in the cytoplasm of oligodendrocytes and neurons with elevated Ca2+ intracellular levels. (Munro et al. 1999)(Shan et al. 2003).

Besides mRNAs, hnRNPA2B1 also strongly interacts with primary miRNAs (pri-miRNAs). hnRNPA2/B1 may act as a “reader” of miRNA containing m6A modification, to promote m6A-dependent processing events of these primary-microRNAs (Alarcón et al. 2015). Alternatively, Wu B. et al proposed a mechanism by which m6A promotes accessibility of hnRNPA2B1 to different binding sites (B. Wu et al. 2018).

Given the multiple RNA target molecules, hnRNPA2B1 is one of the important regulatory proteins of RNA; so abnormal hnRNPA2B1 leads to a variety of diseases including cancers, autoimmune diseases and, of particular interest for us, also neurodegenerative (Y. Liu and Shi 2021).

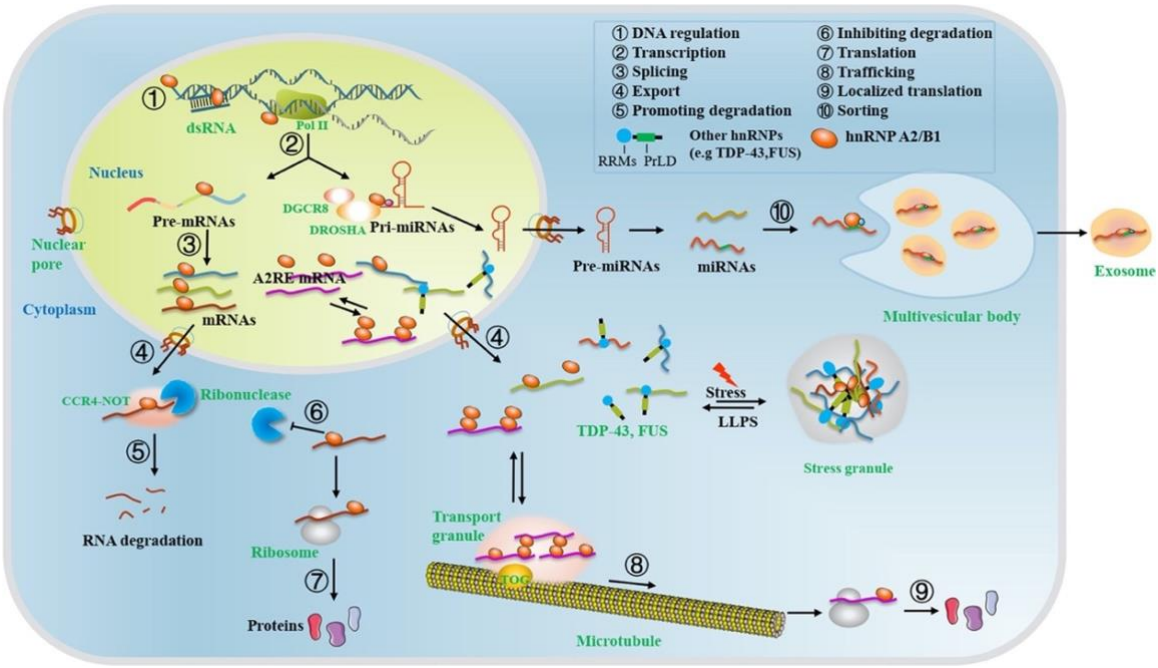

Figure 1.8. hnRNPA2B1 biological functions. Schematic representation of hnRNPA2B1 function in physiological situation and in disease. It is involved in DNA regulation by participating to DNA repair, telomere maintenance and recognition of viral DNA (1). Its main roles regard RNA synthesis and processing: In the nucleus it is involved in transcription (2), pre-mRNA splicing (2), polyadenylation site selection and nuclear transport (4), while in the cytoplasm it is involved in many processes like mRNA degradation regulation (5-6), localized translation (9) A2RE RNA granule assembly, transport, and exosome miRNA sorting 10). Under the stimulation of cellular stress, hnRNPA2/B1 protein binds RNA with other hnRNPs (such as TDP-43, FUS) and is recruited to stress granules. Figure taken from (Liu and Shi 2021).

1.4.2 hnRNPA2B1 in ALS: the mutation D290V

In ALS, many RBPs have been associated to the neurodegeneration, in fact mutations in TDP-43, FUS, but also hnRNPA1 and hnRNPA2B1 have been identified in association with ALS and/or FTD.

Their low complexity domain (LCD) also known as PrLD, is a key component that drives liquid–liquid phase separation (LLPS) and mediate stress granule (SG) formation. In fact, RBPs like TDP-43, FUS, EWSR1, TAF15, hnRNPA1, hnRNPA2B1, ATXN2 and TIA1 were identified to interfere with SG formation through mutation of their LCD (Baradaran-Heravi, Van Broeckhoven, and van der Zee 2020). These disordered structures tend to form fibrils, which are accelerated in presence of mutations In the PrLD.

Interestingly, altered dosage of hnRNPA2B1 has been associated to ALS. It has been reported that under the stimulation of cellular stress, WT hnRNPA2/B1 protein binds to RNA also interacting with other hnRNPs (such as TDP-43, FUS) and is recruited to stress granules (SGs) (Marcelo et al. 2021)(Baradaran-Heravi, Van Broeckhoven, and van der Zee 2020).

Recently, the mutation p.D290V/D302V in hnRNPA2B1 was identified in a family with dominantly inherited degeneration which affected bone, brain, muscle, and motor neurons (Hong Joo Kim et al. 2013). This mutation is located in the PrLD and cause the substitution of a highly conserved aspartate into a valine residue. CryoEM crystallization of the hexamer containing the mutation, revealed that the D290V mutation leads to a different conformation of the protein, inducing the formation of a thigh steric zipper structure. So, the reversible hnRNPA2 fibrils, normally formed by the protein, are converted into irreversible pathogenic aggregates (Lu et al. 2020).

These effects become biologically relevant if we consider abnormal alternative splicing events detected in induced pluripotent stem cells motor neurons (iPSC-MNs), associated

to an increased nuclear and insoluble hnRNPA2/B1 protein (Martinez et al. 2016) and a reduced survival in long-term culture. Moreover, the mutant protein forms cytoplasmic inclusions when expressed in Drosophila, and the D290V mutation accelerates aggregation *in vitro* (Paul et al. 2017).

1.4.3 The interaction between the RNA and hnRNPA2B1

hnRNPA2B1-RNA recognizes different RNA sequence motifs. Initial studies characterized the specific binding to UAGGG, GGUAGUAG, or AGGAUAGA sequences (Huelga et al. 2012)(Ray et al. 2013). Consistently, three independent *in vitro* and *in vivo* approaches confirmed the preference binding for UAG(G/A) motifs (Hutten and Dormann 2016)(Martinez et al. 2016) identified by a transcriptome-wide analysis of hnRNPA2B1 targets in the nervous system. Specifically, the UAG(G/A) motif identified the two *in vivo* approaches done on mouse spinal cord, through cross-linking and immunoprecipitation at individual nucleotide-resolution level (iCLIP) and on iPSC-derived human motor neurons), through enhanced CLIP (eCLIP), was confirmed by the *in vitro* approach, which exploited the recombinant hnRNPA2B1 RNA-binding domain to pull down interacting RNA sequences coming from a random RNA pool.

Moreover, recently it has been showed that hnRNPA2B1 recognizes a consensus motif containing UAASUUAU (in which S can be a G or a C) which is present in the 3' UTR of many mRNAs and helps the recruitment of the CCR4-NOT deadenylase complex (Geissler et al. 2016). The table below summarizes the binding motif identified for the protein and the related biological function of the protein upon the binding (Y. Liu and Shi 2021).

Motifs	**Functions**	**References**
A2RE/RTS	mRNA trafficking/translation	(Bériault et al. 2004); (Kwon, Barbarese, and Carson 1999)
TTAGGG	Telomere maintenance	(Mckay and Cooke 1992)

AU-rich motif (sRSM1 motifs)	mRNA stability	(Goodarzi et al. 2012)
(U)16 element	mRNA stability	(Fähling et al. 2006)
UAG(G/A) motifs	Alternative splicing	(Hutten and Dormann 2016), (Martinez et al. 2016)
EXO-motifs	Sorting of exosomal miRNAs	(Villarroya-Beltri et al. 2013)
UAGGG	Alternative splicing; mRNA stability	(Huelga et al. 2012); (Ray et al. 2013)
GGUAGUAG	Alternative splicing	(Huelga et al. 2012); (Ray et al. 2013)
AGGAUAGA	Alternative splicing	(Huelga et al. 2012); (Ray et al. 2013)
UAASUUAU (S = G or C)	mRNA decay	(Geissler and Grimson 2016); (Geissler et al. 2016)
RGAC	m6A-mediated A2/B1 binding	(Alarcón et al. 2015); (B. Wu et al. 2018)
Conditional GA-type motifs	Ca^{2+}-dependent trafficking	(Muslimov et al. 2014)
G-quadruplexes	HIV-1 transcription	(Scalabrin et al. 2017)
rCGG repeats	Neuronal degeneration	(Sofola et al. 2007)
GA-rich region (AGGGAGGA-GGGGAGGGAGGAGGAGG)	mRNA stability	(Kasim et al. 2014)

Table 3| Motifs recognized by hnRNPA2B1 and the related protein functions Table taken from Liu, Y., & Shi, S. L. (2021)

However, despite the bind to UUAGGG and UAG RNA motifs was already identified (Mckay and Cooke 1992)(Hutchison et al. 2002), all these studies do not provide the biochemical parameters for the binding specificities. In a recent work, Wu et al. aimed

to understand RNA-binding properties of hnRNPA2B1 at the molecular level. The authors obtained the crystal structure of the RRMs of the protein in complex with an 8mer RNA (5'-AGGACUGC-3'), a sequence derived from an iCLIP study (Martinez et al. 2016). The isothermal titration calorimetry (ITC) analysis, show binding of the 8mer RNA occurs at a 1:1 ratio with a Kd of 276.2 nM. (B. Wu et al. 2018). The 8mer RNA mainly interacts with the RRM1, which recognizes the AGG motif. They also design a 10mer RNA probe (5'-AAGGACUAGC-3') that includes the UAG motif, increasing the affinity for a recombinant protein only composed by the first two RRMs and lacking the PrLD (K_d= 114.7nM).

Finally, the specific recognition of the AG core motif by both RRM1 and RRM2 provides an explanation for how SUMOylated hnRNPA2B1 directs the loading of specific EXO-miRNAs into exosomes through the binding to the EXOmotif (GAGG).

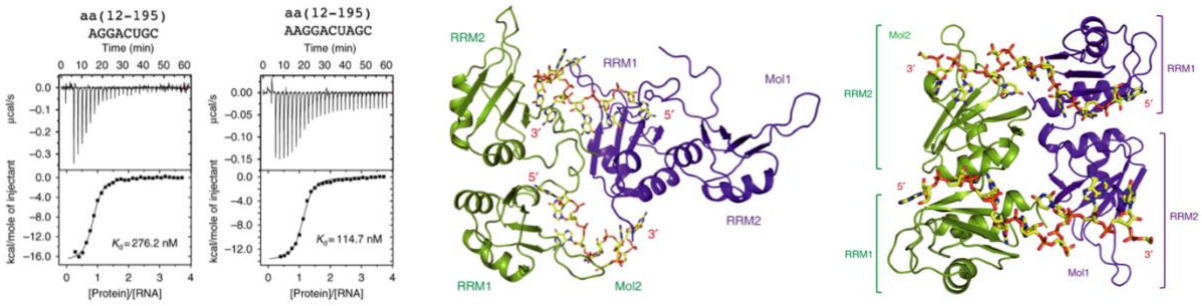

Figure 1.9. Overview of hnRNPA2B1 binding to the RNA probes. ITC results of hnRNPA2B1(12–195) with 8mer and 10mer RNA targets show greater affinity of the 10mer RNA (Kd=114.7) compared to the 8mer (Kd=276.2) (left). The hnRNPA2B1 structural recognition of 8mer RNA and 10mer RNA are shown. The molecules from two adjacent asymmetric units. The RNA backbones are colored in yellow shown by stick. Image modified from Wu et al. (2018).

1.4.4 Screening campaigns involving hnRNPA2B1

Up to now, there are no evidences of pharmacological screening directly targeting hnRNPA2B1. However, an indirect modulation of the protein has been assessed in different studies. For example, in the work of Cho KI and colleagues (Cho et al. 2015), the authors performed an *in silico* screening of 9 millions of small molecules (SM) to target cyclophilin domain of Ran-binding protein 2 (Ranbp2), with final aim to modulate hnRNPA2B1 proteostasis and nucleocytoplasmic shuttling. The experimental validation indicated compounds 11, (S)-N-(3-methyl-1-oxo-1-((pyridin-2-ylmethyl)amino)-butan-2-yl)-2-(1H-pyrrol-1-yl)benzodthiazole-6-carboxamide, and compound 13, 1-(2-

chlorophenyl)-5-cyclopropyl-N-[3-(2,5-dioxopyrrolidin-1-yl)propyl]-1H-1,2,4-triazole-3-carboxamide, as the only two molecules able to reduce the levels of hnRNPA2B1 in Hela cells.

Also, in a recent work, a high-throughput screening (HTS) allowed the identification of compound XI-011 as a molecule with a broad antitumor activity in cancer cell lines. From a pull down assay and a proteomic analysis performed using a biotin-conjugated XI-011, they identified hnRNPA2B1 as a binder to the compound. Also, binding affinity experiments showed a possible binding of the drug to the nucleotide-binding domain of hnRNPA2B1, specifically in the 19-glutamine (Gln), 22-lysine (Lys) and 66-phenylalanine (Phe) residues. Interestingly, the chemical disruption of hnRNPA2B1 recruitment to a specific transcription region resulted in a destabilization of the untranslated region of MDMX oncogene and in an inhibition in the promoter activity, as indicated from a ChIP assay (Hu et al. 2023).

Also, MO-460 compound (analog of (R)-(-)moracin-O) identified from a screening campaign, was shown to bind hnRNPA2B1 in its C-terminal glycine-rich domain, in this way inhibiting the binding of the protein to the 3'-untranslated region of HIF-1α mRNA (Soung et al. 2019).

In another work, daunorubicin, pyrvinium, and pararosaniline molecules, having planar aromatic moieties, efficiently altered the RNA-dependent recruitment to SGs of TDP-43, FUS, and hnRNPA2B1. This resulted in a reduced protein aggregates formation (Fang et al. 2019).

Overall, in these studies, hnRNPA2B1 emerged as a promising molecular target both in cancer and neurodegenerative context, suggesting the importance to perform a comprehensive pharmacological screening directly targeting the protein.

2. Aims of the project

Given the described role of EVs and EV-RNA and the role of hnRNPA2B1 in miRNA sorting, we hypothesized that it could be possible to interfere with EV-RNA sorting, thus influencing EV-RNA cargo.

We first performed experiments to exploit EV-RNA as a tool to investigate the intracellular dynamics of RBPs upon modulation of hnRNPA2B1. The experiments involved the development of a strategy to biotinylate EV-RNA from NSC-34 cells, and dedicated RNA pull-down and mass spectrometry analyses. With this approach we aimed to elucidate the contribution of the protein in the regulation of EV-RNA.

The primary aim of the project was to perform a pharmacological screening to find small molecules that could inhibit the interaction between hnRNPA2B1 and a specific RNA substrate. Also, we aimed to set up biochemical and EV-based strategies to validate the identified small molecules. Finally, we aimed to describe the paracrine effect of the modulated EV-RNA in ALS-relevant cellular models. In detail:

a. To address the first aim, we optimized an AlphaScreen assay using a human full-length GST-hnRNPA2B1 and an RNA probe harboring EXOmotifs (EXOmotif RNA) to characterize the binding kinetics and challenge the ligand interaction with a library of 2000 compounds. We exploited AlphaScreen and REMSA for the counter screening of top hit compounds.
b. In order to validate the molecules, we optimized pull-down assays at the equilibrium for the intracellular validation and a ddPCR assay on miR-221-3p to assess the EV-RNA quality upon compound treatments.
c. For the third aim, we set up pilot experiments to address the effects of the "treated" EVs on the recipient cells. We optimized a NF-κB-based inflammation assay and transwell co-colture assays on EV recipient cells using HEK293T cells and TDP-43 WT and Q331K mouse primary astrocytes.

3. Results

3.1 Proteomics confirms recognition of vesicular RNA by hnRNPA2B1

3.1.1 Overexpression of hnRNPA2B1 in NSC-34 and proteomics strategy set-up

To understand the contribution of hnRNPA2B1 in EV-RNA modulation, we optimized a proteomic approach in which we used biotinylated EV-RNA to perform a pull-down of cell lysates overexpressing the protein (Figure 3.1). With this approach we could have

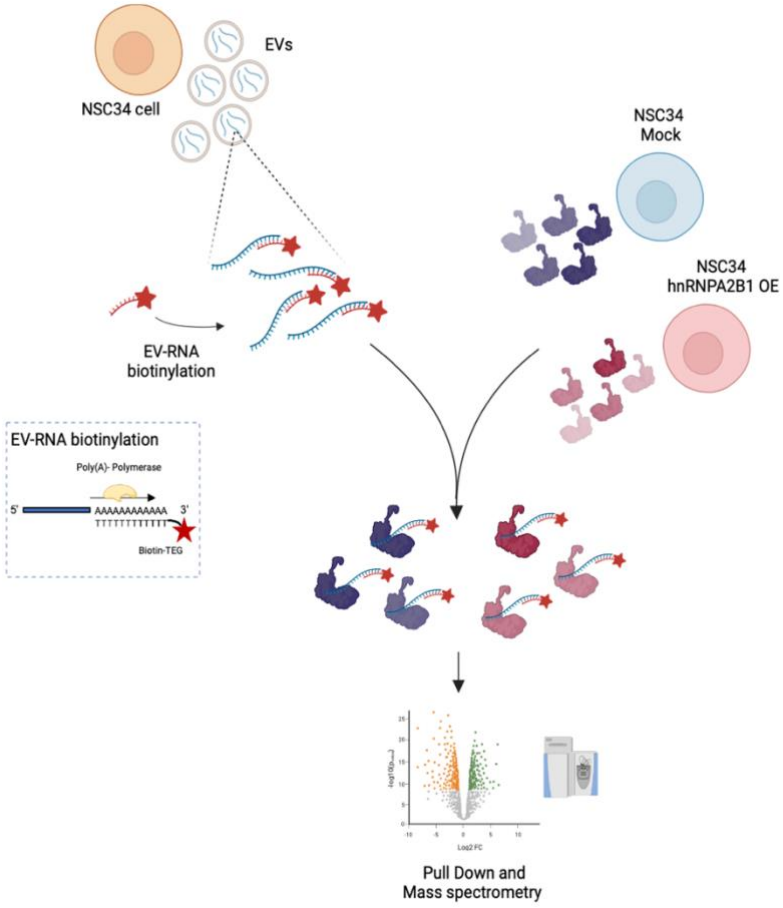

Figure 3.1. Workflow of the proteomic approach. EV-RNA was biotinylated exploiting a first polyadenylation reaction, followed by hybridization with a Biotin-Teg Oligo dT. Biotin-Teg EV-RNA was incubated with cell lysates overexpressing or not hnRNPA2B1. The pull-down with the streptavidin magnetic beads was subjected to MS/MS. Image created with BioRender.

an indication on the RBPs involved in EV-RNA binding and, interestingly, on the EV-RNA-binders upon hnRNPA2B1 overexpression in the cell.

We firstly characterized the overexpression model; we transfected NSC-34 cells with a plasmid encoding for the human hnRNPA2B1-Myc-DDK and we confirmed the overexpression of the recombinant protein by Western blotting (WB); the overexpressed protein corresponds to the band at the highest molecular weight, positive for the staining with anti-Myc antibody (Figure 3.2A). We also confirmed the presence of the protein in the EVs, as demonstrated by Villarroya-Beltri C at al. (Villarroya-Beltri et al. 2013). Specifically, we isolated the EVs with differential ultracentrifugation and NBI (Notarangelo et al. 2020) protocols from NSC-34 and HEK293T cells. As shown in the gel in Figure 3.2B, we detected the protein in the EVs deriving from both cell lines. Interestingly, in HEK293T-derived EVs we observed a band at a higher molecular weight in the 100K fraction which could correspond to the SUMOylated version of the protein, as reported (Villarroya-Beltri et al. 2013). Using differential ultracentrifugation, we could not retrieve the higher molecular weight band in NSC-34 cells, nor the 35 kDa band in none of the cell lines. This could be due to the different expression levels of the protein in the different cell lines which could result in a different detection in EVs. Moreover, we identified the 35 kDa protein in the EVs recovered through NBI method (Figure 3.2B). This could be explained by the fact that hnRNPA2B1 has been reported to be secreted in exosomes. In this context, NBI allows the purification of a heterogeneous population with an efficient recovery of small EVs, while ultracentrifugation can be less efficient in pelleting smaller particles (<150 nm) (Brennan et al. 2020). Probably, given the different protein expression levels between the different cell lines, increasing the starting material could allow the detection of the 35 kDa protein also by differential ultracentrifugation. By immunofluorescence we confirmed the main nuclear localization of both the endogenous and transfected hnRNPA2B1 (Figure 3.2C).

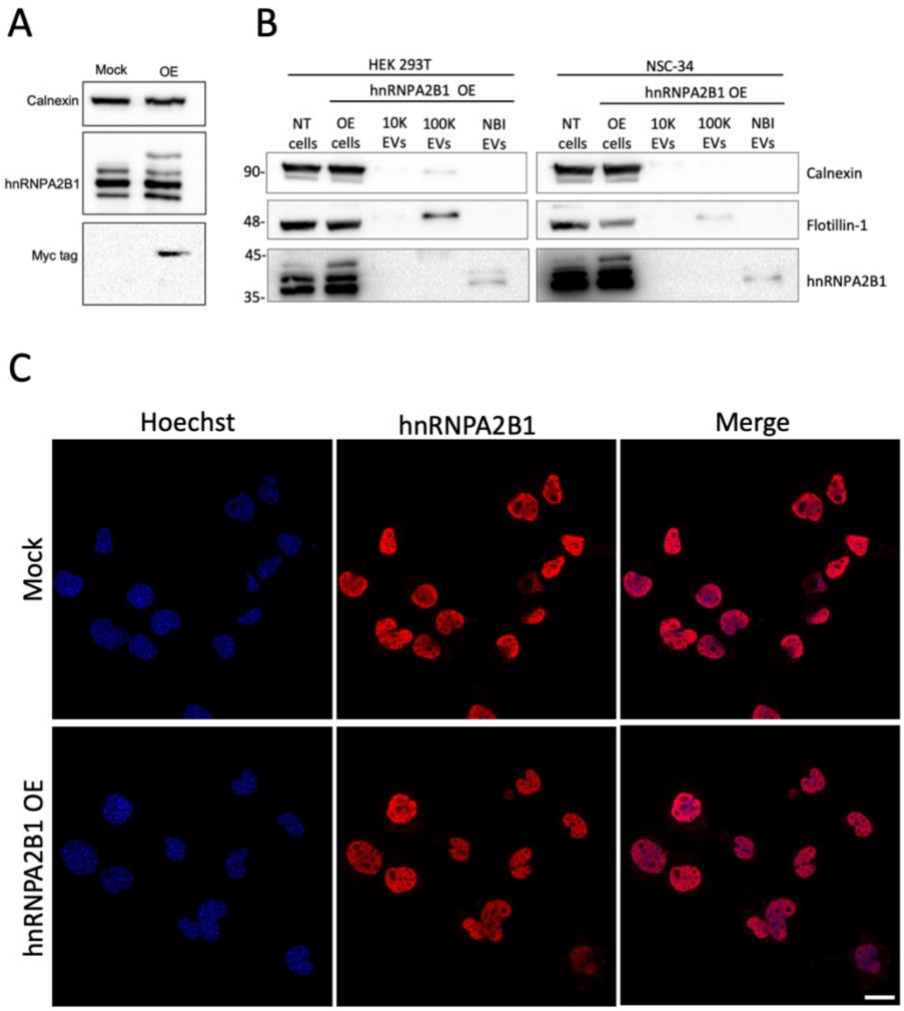

Figure 3.2. hnRNPA2B1 overexpression. A) Representative WB on NSC-34 cells. The endogenous protein presents different isoforms at different molecular weights; the transfected one is represented by the band at the higher molecular weight. B) hnRNPA2B1 in cells and EVs from HEK293T and NSC-34. "NT", non-transfected cells; "OE", hnRNPA2B1 overexpressing cells; "10K", 10,000g pellet; "100K", 100,000g pellet; "NBI", Nickel based isolation. C) Immunofluorescence representing the localization of hnRNPA2B1. Hoechst in blue, AlexaFluor 633 in red. Images were taken with Leica TCS SP8 confocal microscope with a HI-PLAN 63X objective. Scale bar= 20μm.

EV-RNA is composed of a pool of heterogeneous RNAs, in terms of both type and size. Therefore, in order to exploit it as a "probe", we tried different strategies to optimize a protocol which allowed to obtain a biotinylated EV-RNA. The optimized working strategy was based on a 3' biotinylation of EV-RNA, performed as follow: we extracted RNA from EVs (Paragraph 6.10) coming from steady state NSC-34 cells, and we quantified it reaching the maximum amount of 400ng of EV-RNA per condition. Then, thanks to the use of the Poly(A) reaction of TaqMan advanced miRNA cDNA synthesis kit, optimized for small amounts of RNA, we managed to efficiently polyadenylate EV-RNA. To confirm

the Polyadenylation of EV-RNA, we performed a retrotranscription of the Poly(A)-RNA through an oligo dT primer; with this reaction we expected to obtain an increased signal in the samples containing the polyadenylated RNA compared to control. As shown in Figure 3.3, a smear with higher intensity is visible in the retrotranscribed sample compared to control sample, represented by non-polyadenylated RNA. Since we are using a heterogeneous pool of RNA, it is expected to obtain a smear signal and not a single band. Also, since a part of EV-RNA is composed by full length and fragmented mRNA (Valadi et al. 2007), it is expected to detect a signal also in the retrotranscription of control sample, where the Poly(A) reaction did not occur.

Finally, we performed the biotinylation through the addition of a BiotinTeg-oligodT in order to obtain a hybrid RNA-DNA sequence biotinylated at 3'end as shown in the cartoon in Figure 3.1.

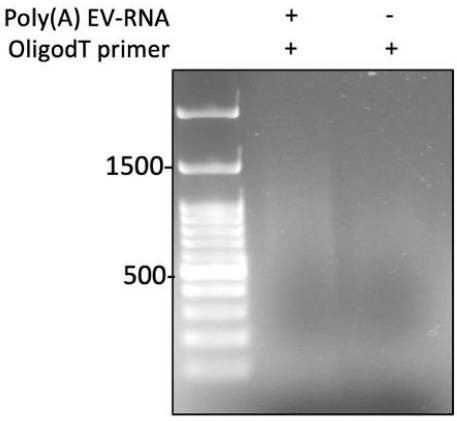

Figure 3.3. Polyadenylation reaction control. Agarose gel for the control of the correct polyadenylation of EV-RNA. The retrotranscription was performed using an oligo dT as a primer for elongation.

3.1.2 Proteomics reveals hnRNPA2B1-dependent rearrangement of RBPs recognizing the EV-RNA bait

The proteomic approach, used to understand the effect of hnRNPA2B1 modulation on the proteins able to interact with EV-RNA, allowed the identification of 495 significant differentially expressed proteins in hnRNPA2B1 overexpression (OE) lysate (Figure 3.4A) compared to mock. 337 proteins resulted to be upregulated upon hnRNPA2B1 OE, while 278 proteins resulted to be downregulated (Figure 3.4A). Interestingly, in the

upregulated list of proteins, 13 members of the Rab protein family, known to regulate vesicular trafficking and exosome formation (Blanc and Vidal 2018), resulted be significant upregulated, representing about a 4% of the total significantly upregulated proteins. In line with this observation, Gene Ontology (GO) analysis represented a significant abundance in proteins involved in GTPase activity in the overexpressed list, which was not the case for the downregulated ones. Moreover, both upregulated proteins and downregulated ones resulted to be significantly involved in RNA transport, underlying a reorganization of RBPs able to bind EV-RNA due to hnRNPA2B1 overexpression. Of notice, the KEGG pathway associated to proteasome resulted to be significantly downregulated upon hnRNPA2B1 overexpression; indeed, 26S proteasome subunits appeared in the list. Interestingly, proteasome dysfunction and assembly has been reported in ALS models (Kabashi et al. 2004), (Riemenschneider et al. 2022),(W. Zhang et al. 2021) (Figure 3.4B). Among the hnRNP family members, we identified Tdp43, Hnrnpd and hnrnpul2 to be significantly upregulated upon hnRNPA2B1 overexpression. TDP-43 is known to interact with hnRNPA2B1 (D'Ambrogio et al. 2009). Also, Immunoprecipitation (IP) followed by tandem mass spectrometry identified hnRNPA2B1 as a binding partner of hnRNPD (Kumar et al. 2015). The two proteins resulted to be functionally linked in the splicing of the 5'-splice site SD3632 of Human papillomavirus type 16 (HPV-16). They interact specifically with the AUAGUA motif of the HPV-16 splicing silencer, which is located upstream of late 5'-splice site SD3632 suppressing the 5'-splice site SD3632 (X. Li et al. 2013).

Overall, the results indicate how the modulation of hnRNPA2B1 changes the panel of RBPs involved in the EV-RNA binding and in the vesicular trafficking.

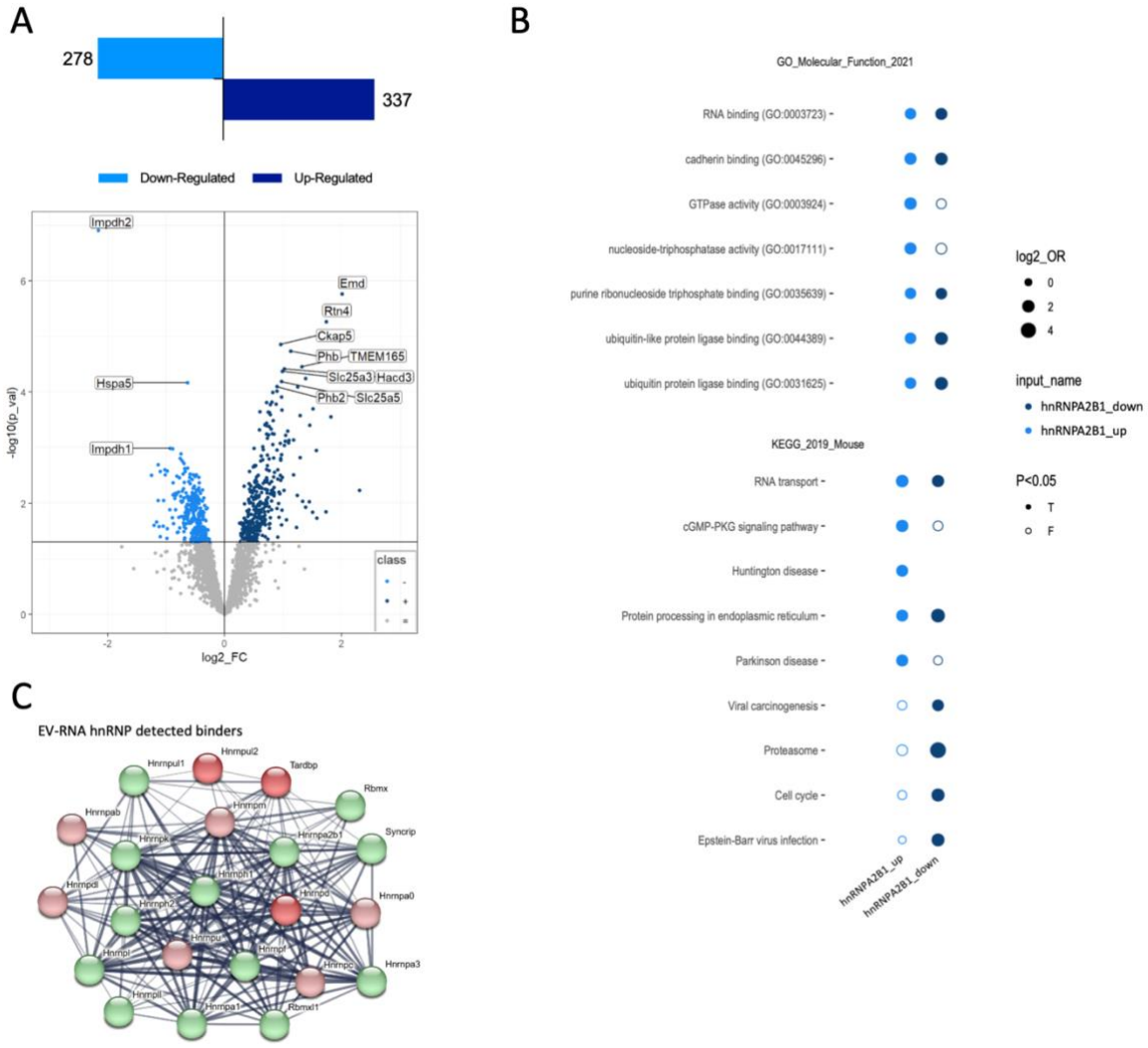

Figure 3.4. Proteomics and functional annotations. A) Number of significant differentially expressed proteins (DEPs) upon hnRNPA2B1 overexpression and relative Volcano plot. Class identifies the state of the peptides. "+" are the Up-regulated DEPs, "-" are the Down-regulated DEPs, "=" are the non-significative DEPs. B) Gene Ontology (GO) analysis. The graph visualizes only the significant enriched terms of the pre-selected data sets. The dimension of the point is given by the Odds Ratio in log2 scale. The filling is based on the significance of the adj.P. Value against the selected threshold. C) Interaction network of hnRNPs from proteomics. The graph represents the experimentally validated interaction from STRING database.

Moreover, with this approach, many members of the hnRNP family have been identified in the protein list, with Hnrnpd Hnrnpul2 and Tdp43 resulting significantly upregulated upon hnRNPA2B1 overexpression. Exploiting STRING database (von Mering et al. 2003), we selected and visualized the network of hnRNPs members detected by MS, considering only the experimentally validated interaction data (Figure 3.4C). Looking at the experimentally validated RNA sequences bound by these proteins, we identified enriched motifs per each protein using XSTREME software (Grant and Bailey 2021).

Among them, the GAAGGG motif appeared to be an enriched motif in common to all of them (Table 4).

Detected hnRNPs	Enriched RNA binding motifs	Common motifs
Hnrnpd	UGCAUUUAU GUACUC UUAUUUUAGUUAG	GAAGGG
Hnrnpc	AUAUUUUUAU	
Hnrnpa2b1	UAGUGCCC UGCAGAUGGUUAGUU GGAAUUAAG	
Hnrnph2	UGGGGA GGGAAGAGC	
Hnrnpl	GGAAAA ACCUAG	
Hnrnpa1	AGAAAUGGA UAGGGUUGU CUGACC	
Hnrnph1	GAAGGGGA AGAGCA	
Hnrnpf	AAGGGGAGGGG AGAGCAA	
Hnrnpk	UGUCAACCAG AAAGAGAAUAAAGA	

Table 4| Enriched RNA motifs bound by identified hnRNPs experimentally validated.

Also, we performed an independent experiment exploiting the same biotinylated EV-RNA with cells overexpressing TDP-43, another member of the hnRNP family. Also in this case, many members of the hnRNP family resulted differentially expressed upon TDP-43 overexpression, with Hnrnpul2, Hnrnpc, Hnrnpl and Hnrnpu resulting significantly upregulated and Hnrnpul1 significantly downregulated. Together these results show how overexpressing two members of the hnRNP family in two independent experiments, results in a similar fluctuation network of hnRNP proteins binding to EV-RNA, confirming their involvement in binding the EXOmotif, and so in the sorting of RNA in EVs.

For these reasons, we decided to use an RNA EXOmotif probe in our screening platform. This probe, previously designed in the lab, not only contains the EXOmotifs known to be bound by hnRNPA2B1 (Villarroya-Beltri et al. 2013) (Figure 3.5B), but it also represents the substrate of many RBPs effectively involved in the sorting of EV-RNA, as

demonstrated by the motifs identified (Table 4); thus recapitulating the EV-RNA probe we used in the proteomic approach.

We exploited a Biotin-Teg version of RNA EXOmotif and we set up an AlphaScreen based screening assay. This technique is ideal for our purpose as the ligands are normally used in low nanomolar range. As shown in Figure 3.5A, the assay is based on the usage of streptavidin donor beads recognizing the biotinylated RNA probe and Anti-Myc acceptor beads recognizing recombinant protein; only if the protein and RNA interact, the two beads are close enough to generate a signal measurable at 615nm. In this assay, the presence of interfering compounds, results in the loss of the interaction between the two ligands and thus a reduction in the Alpha signal.

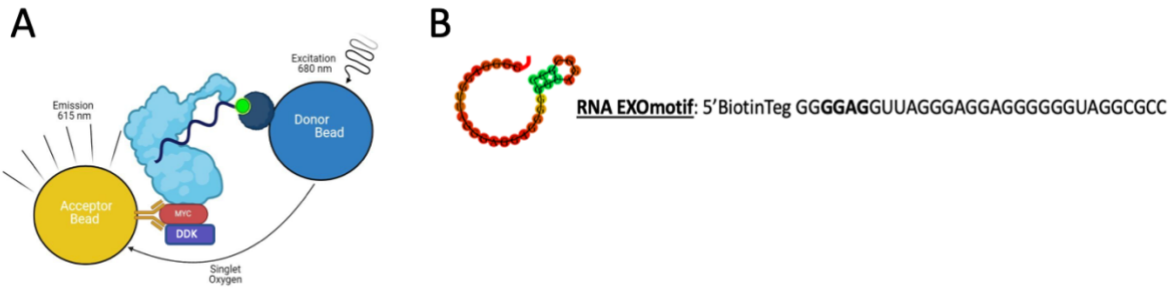

Figure 3.5. Schematic representation of AlphaScreen assay. A) Anti-Myc Acceptor beads recognize the Myc tag of the protein; Streptavidin Donor beads recognize the biotinylated RNA. When the two ligands interact, the beads are closed one to the other (max distance 200nm) and generate the signal. Image created with BioRender. B) Sequence and predicted structure of the RNA EXOmotif probe used in the High Throughput Screening.

3.2 Purification of a functional full length Human recombinant hnRNPA2B1

Despite its tendency of aggregation, we did not underestimate the importance of studying the full-length hnRNPA2B1, in order to increase not only the specificity for hnRNPA2B1 respect to other members of hnRNP family all containing RRMs, but also in view of downstream analyses to identify potential compounds able to interfere with the RNA-binding activity of the protein, rather than having the RRMs alone.

3.2.1 hnRNPA2B1-Myc-DDK and hnRNPA2B1-Myc-His purification attempts in HEK293T

In order to purify the full length hnRNPA2B1 we started from the same plasmid we used in the proteomics encoding for the protein fused with Myc-DDK tag (Origene) and we transfected HEK293T cells. We optimized a protocol for the protein purification based on the usage of anti-FLAG beads. As shown in the Figure 3.6, the usage of this protocol allowed the purification of the protein which we quantified with the Coomassie staining using BSA as a reference. Considering the band representing hnRNPA2B1 indicated by the arrows, we calculated a concentration of 100nM for EL1 and 80nM for EL2. We concentrated EL1 and EL2 reaching 500nM, as shown in the last lane of the gel (Figure 3.6A). The western blot in Figure 3.6B confirmed the effective purification of hnRNPA2B1. However, the densitometry, representing the quantification of the protein normalized over input, revealed a low efficient purification, resulting only in about 3% of the input protein in the eluted fraction (Figure 3.6C). Moreover, a high amount of the protein is retained in the pellet represented by the insoluble fraction retained after the cell lysis and centrifugation, probably contributing to the less efficient purification.

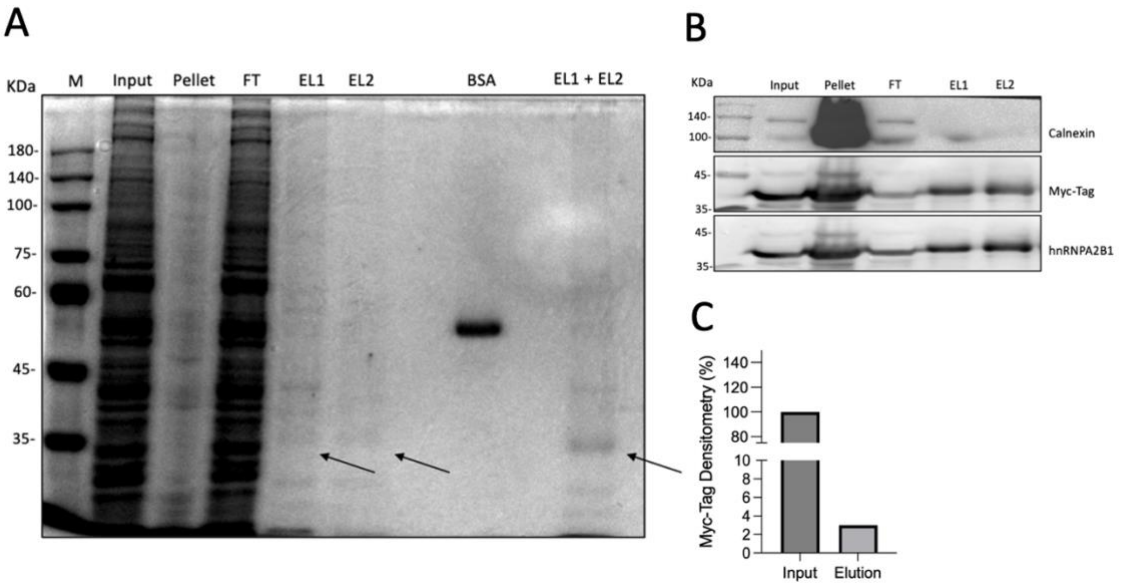

Figure 3.6. Purification of hnRNPA2B1-Myc-DDK. A) Coomassie representing the protein purification. Concentration was measured using 500ng of BSA as reference. EL1, elution 1; EL2 elution 2; EL1+EL2, concentrated protein. B) WB confirming the purification of the protein. C) Densitometry representing the quantification of the protein normalized over input.

Exploiting a protein purification from eukaryotic cells requires high amount of plasmid to be transfected. However, we found out that this plasmid cannot be amplified in the different bacterial strains we tried like DH5α, TOP10, STBL3 and BL21 using different protocols (data not shown). Thus, we cloned the ORF of hnRNPA2B1 in a pCMV6-AC-Myc-His vector (Origene) to produce the protein with Myc-His tag at the C-terminus (data not shown). Two colonies resulted to be positive (9 and 19) (Figure 3.7A) However, a larger bacterial culture resulted in a partial loss of the sequence as confirmed by control digestion of the midi sample (midi 9) (Figure 3.7A). The expression of the protein, checked by transfecting HEK293T with mini 9, mini 19 and the midi 9 (Figure 3.7B), confirmed the expression of the exogenous protein, with low amount in midi 9 sample, as expected. The exogenous protein is visible by the additional band present in the blot for hnNRPA2B1 at the expected MW and in the blot for His tag.

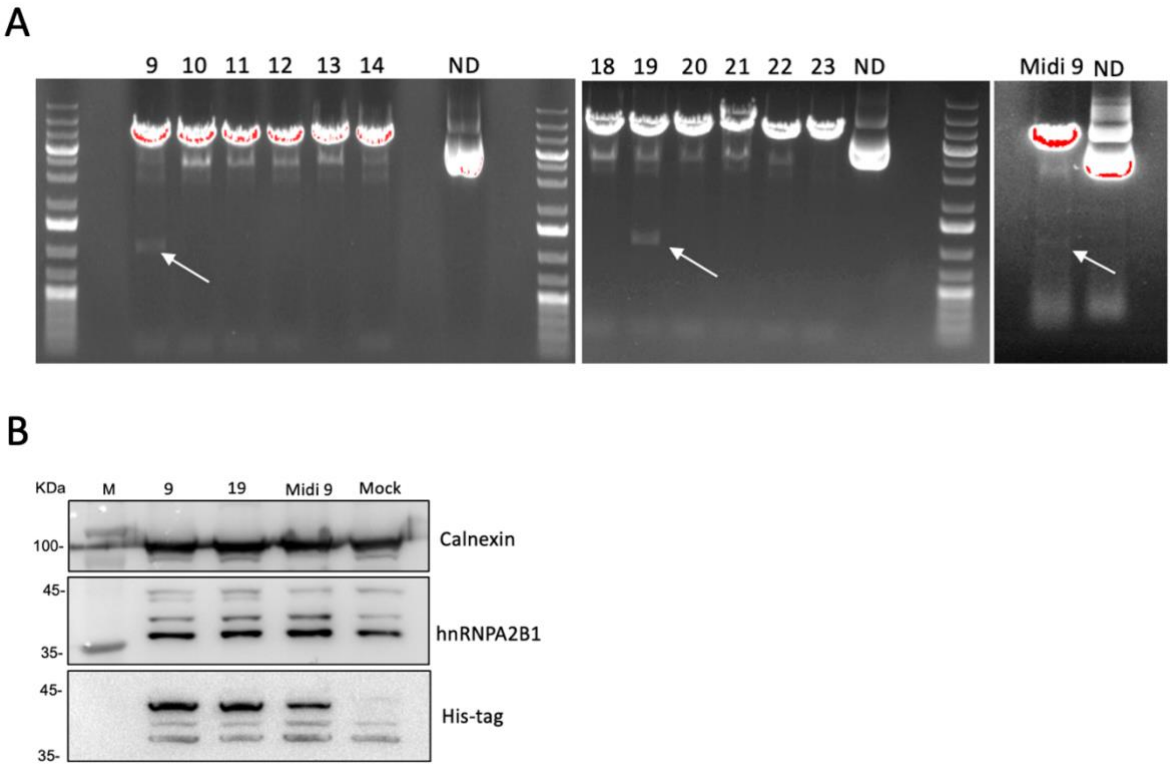

Figure 3.7. hnRNPA2B1 cloning and expression in HEK293T. A) Agarose gels representing the colonies selection. Colonies 9 and 19 confirm the presence of the insert. Midi amplification of colony 9 resulted in partial loss of the plasmid. B) WB showing the hnRNPA2B1-Myc-His expression in HEK293T.

Despite the presence of probably not pure mix of plasmids in midi 9, we used it to transfect HEK293T and we exploited the His Tag to optimize a Nickel-based protocol to

purify hnRNPA2B1-Myc-His. From a representative Coomassie showing the eluted protein (Figure 3.8A), we only appreciated a very faint band corresponding to the MW of the tagged hnRNPA2B1. We checked the purified protein through WB (Figure 3.8B). From the histogram representing the quantification of the three independent protein purifications, we observe that only about 0.5% of the input protein is found in the eluted fraction for all the purifications (Figure 3.8C). Moreover, as in the case of hnRNPA2B1-Myc-DDK, the majority of the protein is again found the pellet.

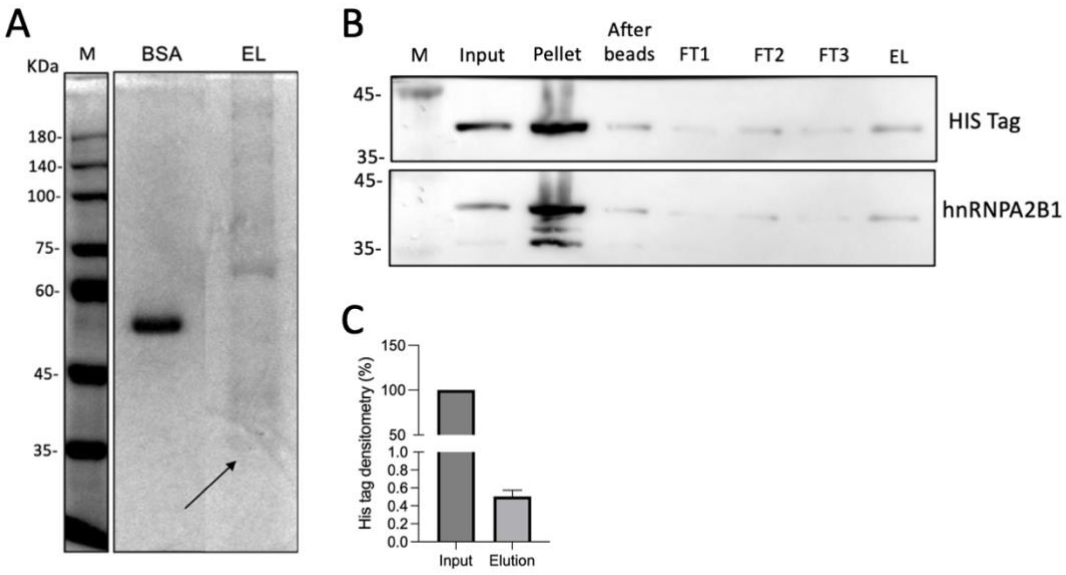

Figure 3.8. Purification of hnRNPA2B1-Myc-His. A) Coomassie representing the protein purification. EL represents the concentrated protein. Protein concentration was retrieved using 500ng of BSA as reference. B) WB showing the purification of the protein. C) Densitometry representing the quantification of the protein normalized over input. Standard deviations are relative to n=3 independent protein purifications. Mean ± SD.

Since the ligands in the AlphaScreen assay work in the low nanomolar range, we tested both versions of the produced hnRNPA2B1 in the assay. We first determined the RNA hooking point, corresponding to the RNA concentration at which the Alpha signal detected is maximum. Above the hooking point, the beads become progressively oversaturated resulting in a decrease signal. The hooking point of RNA EXOmotif resulted to be 25nM (data not shown).

Using 25nM of RNA EXOmotif, we tested different concentrations of the purified proteins based on the quantifications we retrieved form the Coomassie (Figure 3.6 and Figure 3.8). Upon increasing the concentration of the proteins, we did not observe an increase in the Alpha signal, as shown in Figures 3.9A and 3.9B. However, the proteins

resulted to bind the RNA EXOmotif, as shown by the REMSA assay (Figure 3.9C) in which we used a version of RNA EXOmotif harboring an infrared dye at the 5' end. This technique is based on the loading of the samples in a non-denaturing gel. Looking at the RNA migration, when the RNA is bound by the protein, a bigger complex is formed, which results in less migration in the gel, visible as a shift in the run in the gel. As shown in Figure 3.9C, by comparing the first lane representing the run of RNA EXOmotif alone, with the lanes containing both the protein and the RNA, a shift represented by the complex formation is observed for both the proteins.

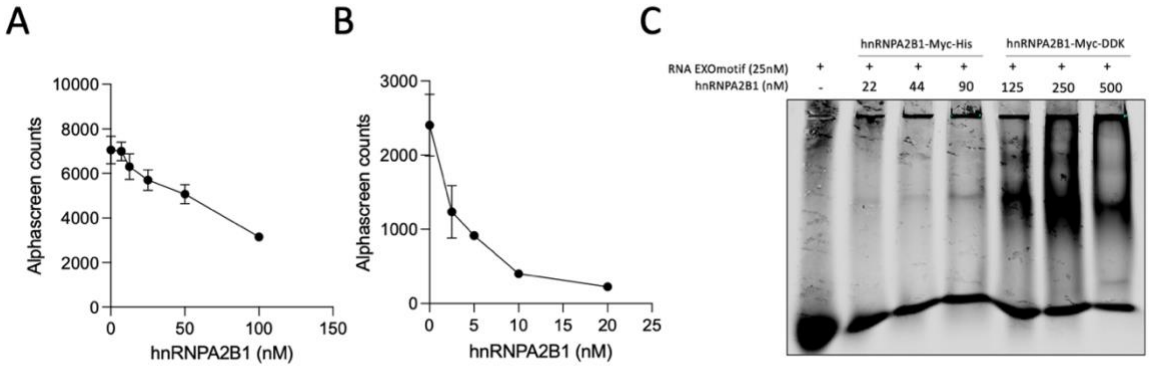

Figure 3.9. hnRNPA2B1-Myc-DDK and hnRNPA2B1-Myc-His test in AlphaScreen and REMSA. A) and B) Alpha Screen Assay using different concentration of the concentrated hnRNPA2B1-Myc-DDK and hnRNPA2B1-Myc-His proteins respectively. RNA EXOmotif was used at 25nM. C) REMSA Assay with both the proteins confirmed their ability to bind RNA EXOmotif.

Given the unsuccess in the AlphaScreen assay, we tested the platform exploiting a commercial version of the human full length protein harboring Myc-DDK tag at the C-terminus (Origene).

Both RNA EXOmotif and the two reference RNA probes RNA 114 and RNA 276 (Villarroya-Beltri et al. 2013) were able to bind commercial full length hnRNPA2B1, with RNA EXOmotif having the highest affinity compared to RNA 114 and 276 (Figure 3.10B). However, high amount of protein (300nM) was necessary to obtain a signal and to reach the optimal working amount (hooking point) (Figure 3.10A). We validated the hnRNPA2B1-RNA EXOmotif binding with RNA electrophoretic mobility shift assay (REMSA).

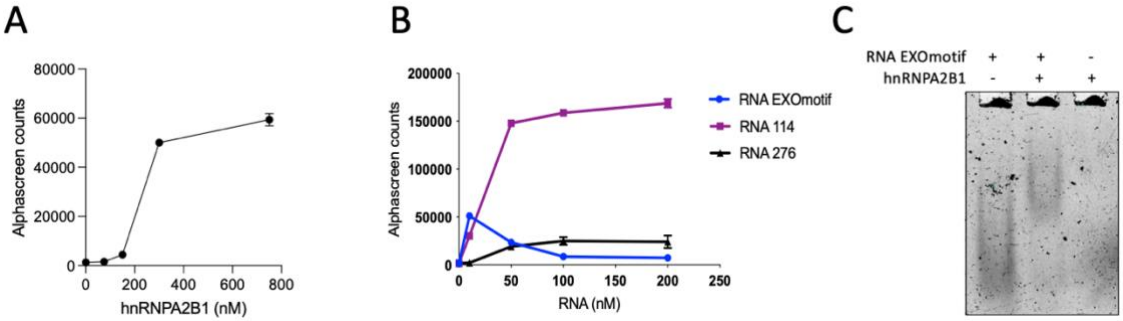

Figure 3.10. Commercial hnRNPA2B1-Myc-DDK in Alpha Screen and REMSA. A) Alpha Screen Assay using different concentration of hnRNPA2B1-Myc-DDK. RNA EXOmotif was used at 25nM. The hooking point is reached at 300nM B) AlphaScreen Assay using different concentration of. RNA EXOmotif, RNA 114 and RNA 276. hnRNPA2B1-Myc-DDK was used at 300nM. C) REMSA Assay confirmed commercial hnRNPA2B1 ability in binding RNA EXOmotif.

Overall, these results indicate that a huge amount of eukaryotic protein productions are needed to obtain a sufficient amount of hnRNPA2B1 in the soluble fraction to be used in the screening. This, in turn, requires the use of a big amount of plasmid in order to transfect the cells. However, given the bacterial toxicity mediated by both the plasmid tested, a eukaryotic protein production is not feasible for our purpose.

For these reasons we changed strategy, and we purified a version of the full-length protein harboring a GST tag at the N-terminus using bacteria expression and purification.

3.2.2 Purification of a functional GST-hnRNPA2B1 protein from bacteria

In order to purify hnRNPA2B1 from bacteria, we exploited the GST tag, and we optimized a protocol for purification based on the usage of anti-GST agarose beads (Jiang et al. 2021).

This method allowed the purification of a bigger amount of protein, reaching a concentration of about 2µM each purification, as seen in the Coomassie (Figure 3.11A). In order to verify that the 60kDa band corresponds to the protein fused to GST, we checked the elution fraction through WB. As shown in Figure 3.11C, the purification protocol allowed the efficient purification of the protein at the expected molecular weight. We then used REMSA assay to check the protein functionality. As seen in Figure 3.11B, we confirmed the functionality of hnRNPA2B1 protein in binding RNA,

represented in the third lane of the gel showing the complex formation. In fact, upon the addition of GST-hnRNPA2B1 a shift in the RNA EXOmotif migration is observed in the gel, compared to the migration of RNA EXOmotif alone. In the gel, two bands representing the complex formation are visible; this is probably due to the formation of complexes with different stoichiometry. Also, since different proteins are co-purified with GST-hnRNPA2B1, as shown in the Coomassie, additional bands could represent complexes formed by combination of hnRNPA2B1 and different proteins.

In the attempt to access the specificity of the binding, we also loaded an antibody against hnRNPA2B1. If the antibody binds to the protein, we expect to visualize a super shift in the gel, corresponding to the formation of a bigger complex made of protein, RNA and antibody. However, a super shift was not visible in the gel. This could be due to the steric hindrance of the GST tag, which may interfere in the recognition of the A2B1 by the antibody. Also, the interaction of the protein with itself or with other proteins could mask the recognition site for the antibody. To exclude a possible effect of the GST tag in the binding, we also loaded a biotinylated GST (Biotin-GST). As seen in the last lane of the gel, GST-tag alone is not able to bind our RNA probe, excluding a possible RNA binding mediated by the tag.

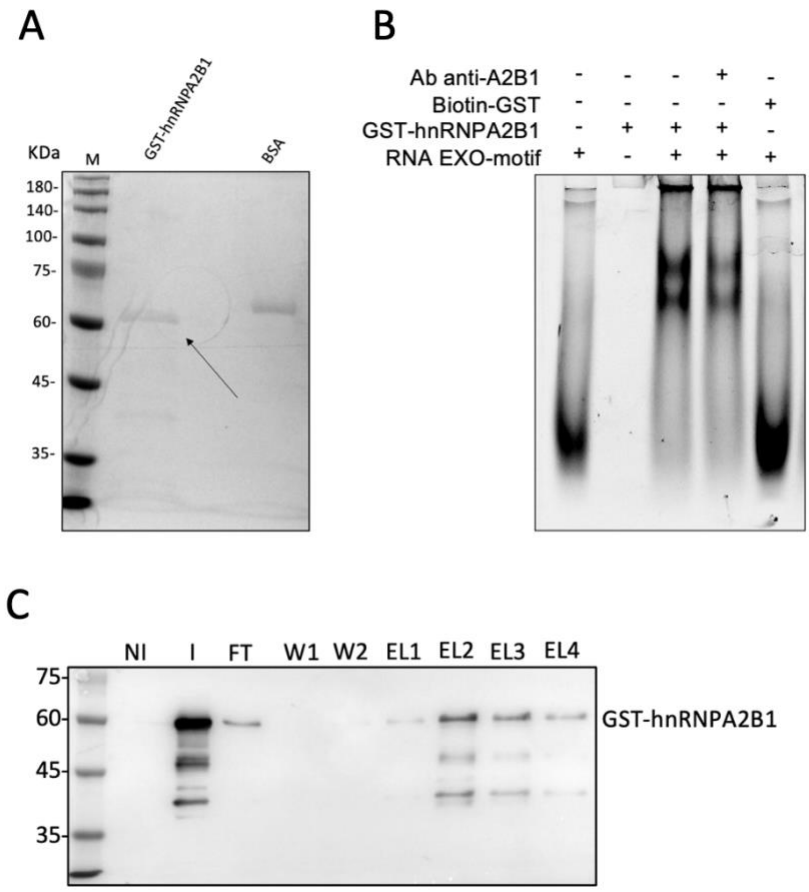

Figure 3.11. Purification of GST-hnRNPA2B1 and REMSA assay. A) Coomassie representing the concentrated GST-hnRNPA2B1. GST-hnRNPA2B1 concentration was retrieved using 1µg of BSA as reference. B) REMSA Assay confirmed the ability of the protein to bind RNA EXOmotif. The GST-Tag alone is not able to bind the RNA probe. C) WB showing the purification of the protein. "NI" non induced bacteria; "I", IPTG- induced bacteria, "W1, W2", Wash 1 and 2; "EL", elutions.

We then checked the functionality of the protein in AlphaScreen assay using GST-detection kit (Figure 3.12A). In this case, Acceptor beads recognize the GST tag, while Donor beads recognize the biotinylated RNA. Using the RNA probe at its hooking point of 25nM, we tested different concentrations of protein which could bind to the RNA EXOmotif (Figure 3.12B). Notably, the hooking point was reached at a concentration of 30nM, 10 times less compared to the eukaryotic counterpart (Figure 3.12B).

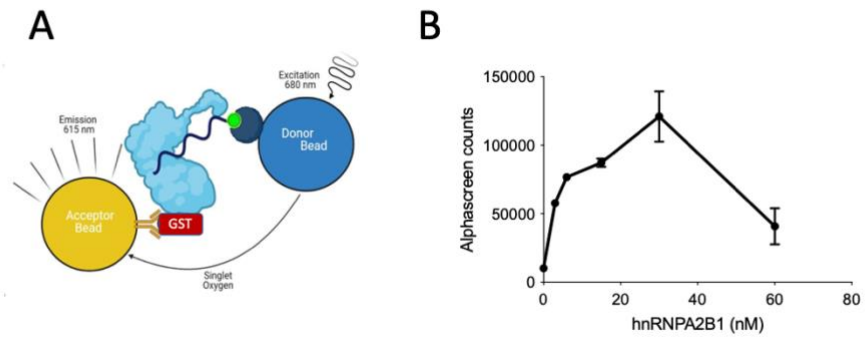

Figure 3.12. GST-hnRNPA2B1 in AlphaScreen. A) Schematic representation of AlphaScreen assay using Anti-GST detection Kit. B) Graph representing the hooking point of the protein (30nM).

This could be due either to the different post translational modifications characterizing the bacteria expression or to the presence of the bigger, high soluble GST tag at the N-terminus which could improve the solubility of the protein (Harper and Speicher 2011), (Schäfer et al. 2015), resulting in a reduced propensity of the protein to aggregate.

In order to set up the screening assay, we firstly measured the binding specificity including in the assay an AU-rich oligo (ARE), which is equivalent in size to RNA EXOmotif but working as negative control. Saturation binding experiments (Figure 3.13A) confirmed the binding specificity of the protein to the consensus sequence present on the probes compared to the ARE probe and confirmed the higher affinity of RNA EXOmotif compared to RNA 114. In order to calculate the binding affinity, we also performed kinetic experiments varying the concentration of the ligands in function of time. We calculated the equilibrium dissociation constant (Kd) as the ratio between k_{off} (rate constant of dissociation) and k_{on} (rate constant of association). So, the smaller the Kd value, the greater the binding affinity of the ligand for its target. Kd values from saturation binding experiments resulted to be 3.4 ±1.6 nM; from kinetic experiments we obtained a kon of 523664 and k_{off} of 0,02091, and a dissociation constant of 35±5 nM (Figure 3.13B). These differences are probably due to protein aggregation or to variability in the RNA folding. Higher number of experiments will be needed to have a more statistically significant result.

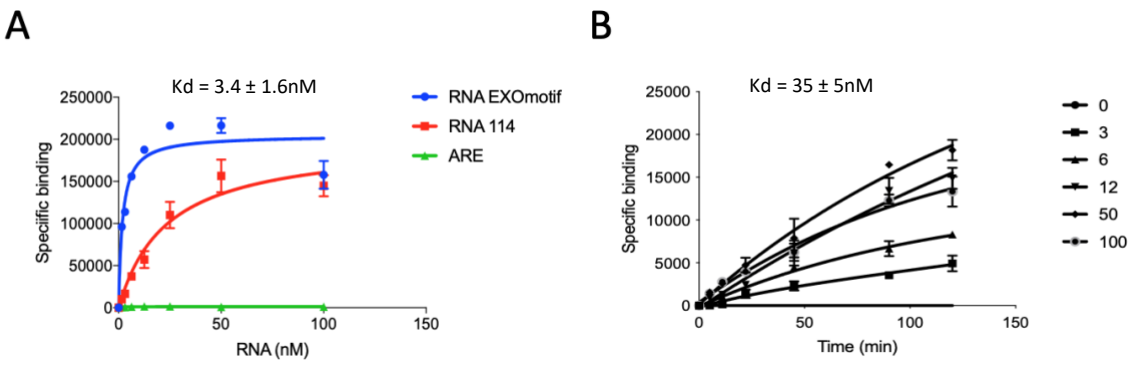

Figure 3.13. Characterization of the functional binding of GST-hnRNPA2B1 to the RNA substrates. A) Saturation binding experiment. Equilibrium dissociation constant (Kd) was determined from nonlinear regression using one site fitting model of GraphPad Prism 9. B) Kinetic experiments. The association (Kon) and dissociation (Koff) constants were determined from nonlinear regression using two phase association fitting model of GraphPad Prism 9. Kd was calculated from two independent experiments with two hnRNPA2B1 protein purifications.

3.3 High-Throughput drug screening and counter screening

In order to proceed with the screening, we firstly tested the quality of the Alpha assay and so its suitability for a high throughput screening. To do so, we calculated the Z-factor, a parameter measuring the global technical variability of the screening platform. It shows the separation between the distributions of the positive and negative controls and is calculated taking into account their mean and standard deviations (J. H. Zhang, Chung, and Oldenburg 1999). A good assay has a Z-factor comprised between 0.5 and 1. We obtained a Z-factor of 0.71 (Figure 3.14A), indicating a good suitability of the assay for the primary drug screening. We then tested a library of 2000 molecules, including 60% of FDA-approved compounds. In order to minimize the possible interference in the AlphaScreen, we used sub-optimal concentrations of ligands, staying below the hooking point, and we tested the compounds in the nanomolar concentrations, in order to select only the ones that strongly inhibited the binding. Excluding the positive control, we identified 21 hits which resulted to decrease the alpha signal below 120000 Alpha Counts (Figure 3.14B). To correct the plate-to-plate variability, we exploited the percent of control normalization (Malo et al. 2006), and we normalized the row measurements for each compound on the controls within the plate (figure 3.14C).

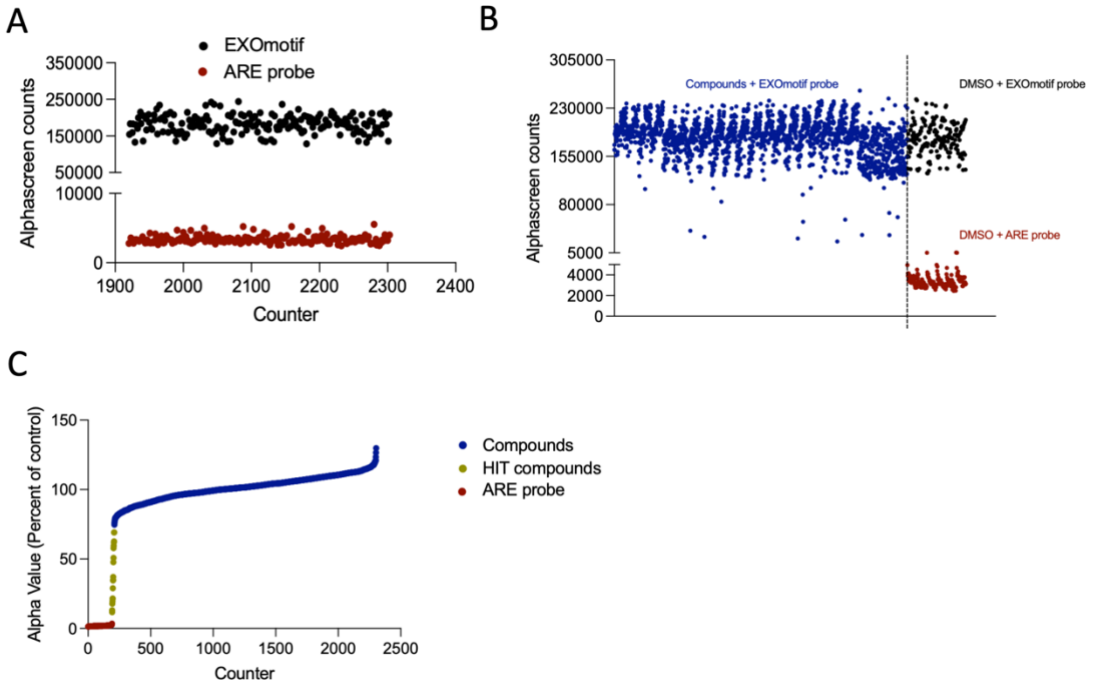

Figure 3.14. Robustness of the AlphaScreen assay and High Throughput drug Screening. A) hnRNPA2B1 and EXOmotif positive and ARE probe negative controls were tested at optimized nanomolar concentration in 20 µL final volume to calculate the Z-factor. B) Plot of the High Throughput Screening. 21 hits having alpha counts below 120000 were selected. C) Data plotted according to percent of control normalization.

We counter screened the 21 compounds through REMSA assay (Figure 3.15A) in order to select only the hits which confirmed the efficient inhibition also with an orthologous technique. Using this assay we expect a reduction in the RNA-protein complex formation in presence of the compound. So, if the compound works, the RNA in no longer bound by the protein; as a consequence, it is no more retained in the gel and its run is comparable to control, in which the protein is absent. As seen in the figure, six compounds, pointed by the arrows, were able to decrease the complex formation. Then, we also counter screened the selected six hits (Methacycline hydrochloride, Theaflavin Digallate, Hematein, Chrysarobin, Phenothrin, and Aurin tricarboxylic acid) through Alpha Screen using the two reference probes RNA 114 and 276. All the 6 hits confirmed the biochemical inhibition of GST-hnRNPA2B1 binding compared to DMSO (Figure 3.15B). We then calculated the IC_{50} of the 6 hits, representing a measure of the potency of the drug in inhibiting 50% of the detected binding according to the amount of ligands used. As shown by the dose response curves (Figure 3.15C), we could calculate the IC_{50} for compounds Methacycline hydrochloride, Theaflavin Digallate, Hematein, and Aurin

tricarboxylic acid; while higher dosage of Chrysarobin and Phenothrin would be needed to complete the curves and allow the software to calculate the IC_{50}. Of note, the IC_{50} is relative to each curve, so despite Methacycline hydrochloride and Hematein resulted to have the same IC_{50} and so they achieved 50% inhibition at the same compound concentration, Methacycline hydrochloride has limited maximal reduction showed a limited inhibition at higher compound concentration.

Overall, screening and counter screening experiments allowed the identification of six molecules which were able to inhibit the interaction between GST-hnRNPA2B1 and RNA EXOmotif probe.

We then proceeded with the validation of the molecules effect on the endogenous Hnrnpa2b1.

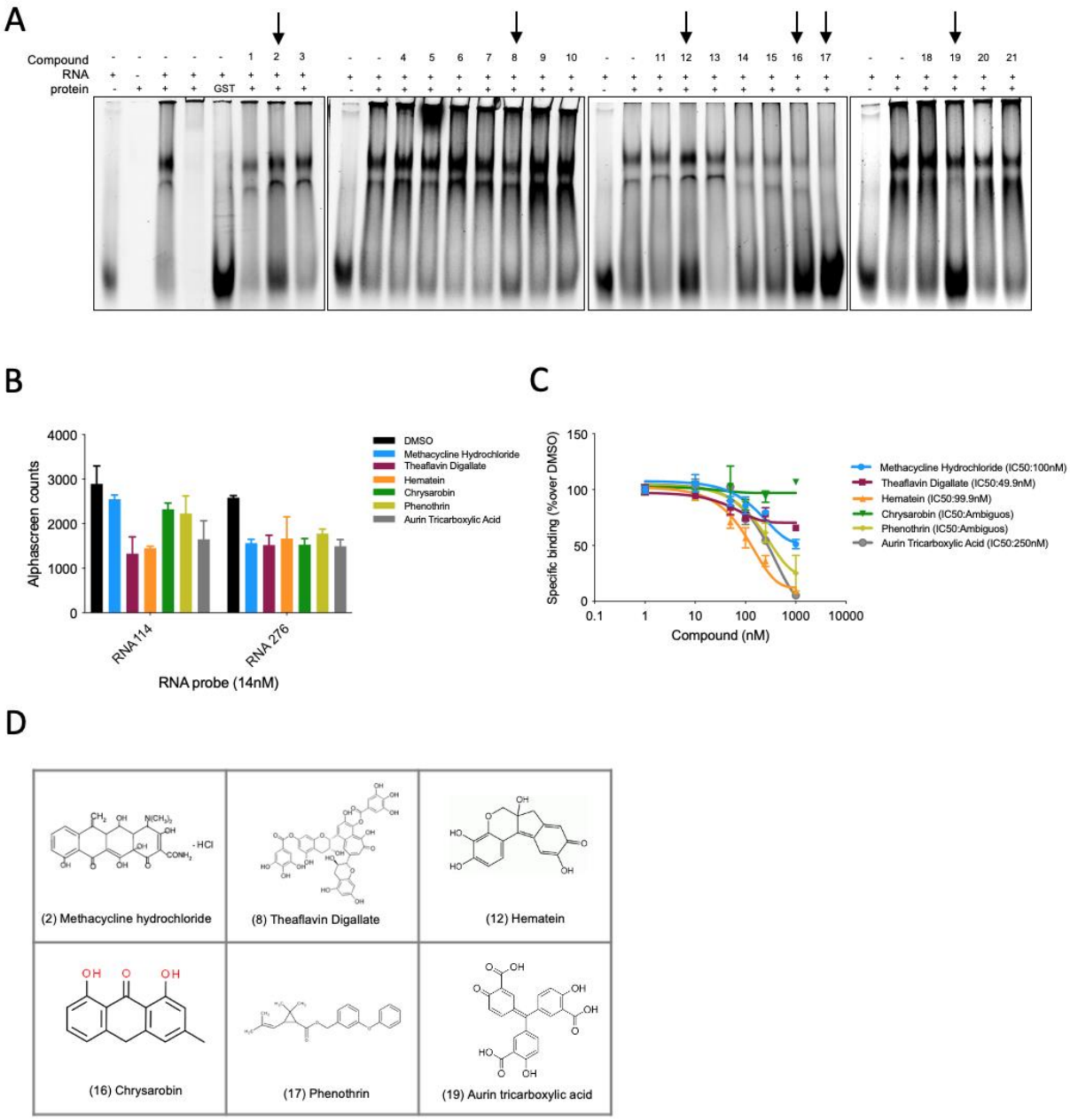

Figure 3.15. Counter screening of the 21 hits and IC_{50} calculation. A) Counter screening with REMSA assay representing the effects of the 21 hit compounds in interfering with hnRNPA2B1-RNA interaction. B) Counter screening with AlphaScreen using RNA 114 and RNA 276. C) Dose response curves. The IC_{50}. was determined from nonlinear regression using one site fitting model of GraphPad Prism 9. D) Table summarizing the chemical structure of the six selected compounds.

3.4 Functional validation: hit compounds affect the endogenous Hnrnpa2b1-RNA binding

In order to validate the molecules effects at the intracellular level, we used the three probes RNA EXOmotif, RNA 114 and 276 and we optimized a Pull-Down (PD) protocol without cross-linking and at the equilibrium. In this assay, the probes compete with the endogenous RNA for the binding with the protein. By optimizing RNA and lysate content, we managed to pull-down endogenous Hnrnpa2b1 with all the three probes compared to the negative control represented by a non-specific RNA sequence (ARE probe) (Figure 3.16A). Exploiting the same protocol, we treated NSC-34 cells with the drugs for 6 hours, a timeline already used to inhibit RBP-RNA binding (Julio and Backus 2021), (X. Wu et al. 2020). Then we subjected the cells to the PD using RNA EXOmotif. As shown in the WB (Figure 3.16C), all drugs except for compound Theaflavin Digallate resulted able to inhibit the binding of endogenous Hnrnpa2b1 to the RNA probe.

These results give an indication of the ability of the drugs to work not only in vitro, but also in cell-based assays.

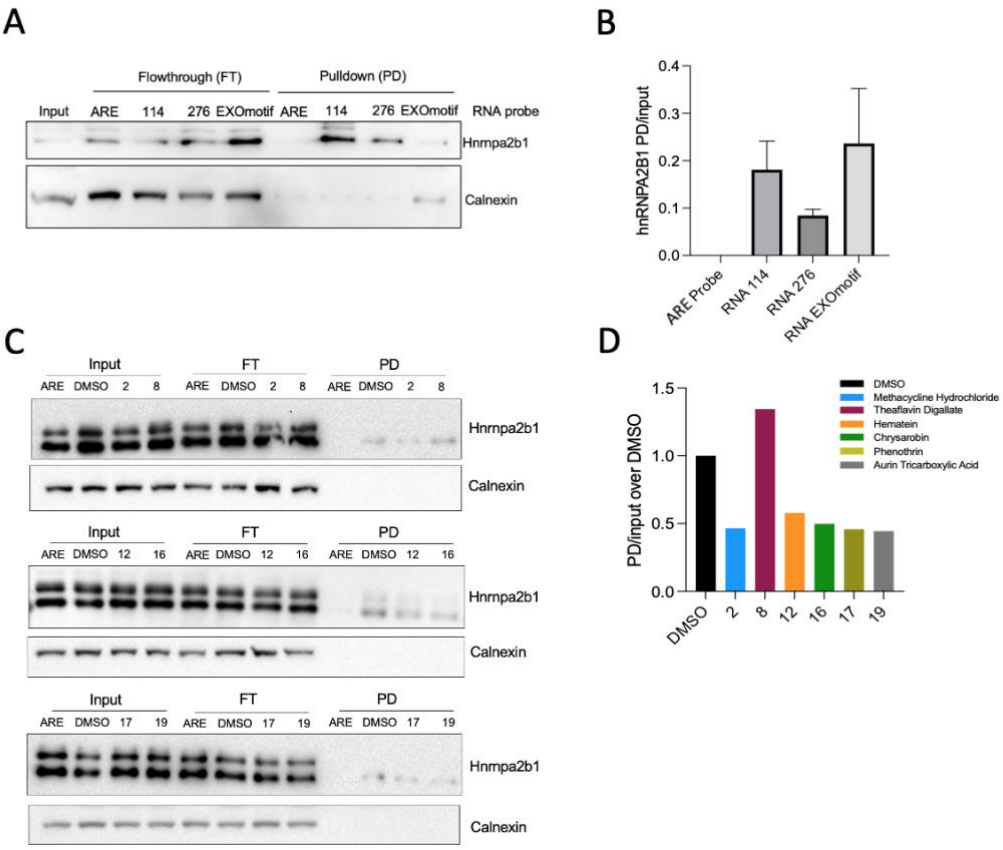

Figure 3.16. Compounds effects on endogenous Hnrnpa2b1. A) Representative image of the WB of the Pull-Down (PD) optimization with RNA EXOmotif, 114 and 276. B) Densitometry representing the quantification of the protein in the PD fraction normalized over input. Standard deviations are relative to n=3 independent biological replicates. mean ± SD. C) WB relative to the PD of Hnrnpa2b1 upon compounds treatment. D) Densitometry representing the quantification of the protein in the PD fraction normalized over input. Data are normalized on DMSO of each gel.

3.5 Functional validation: compounds modulate EV-RNA secretion

Given the effects of the drugs at intracellular level on the endogenous protein and since the protein is involved in miRNA sorting in EVs, we then wondered if the treatments with the compounds could have an effect on EVs release (number and size) and on EV-RNA abundance. To answer these questions, we treated NSC-34 cells with the compounds for 6 hours and we firstly look at the EVs release. As shown in Figure 3.17B, we did not observe a significant difference in the number of released EVs upon compounds treatment. Looking at the EVs profile retrieved from Nanoparticles Tracking

Analysis (NTA) and the relative quantifications, we also did not notice any significant difference in the EVs mean diameter and mode diameter (Figures 3.17A and 3.17B).

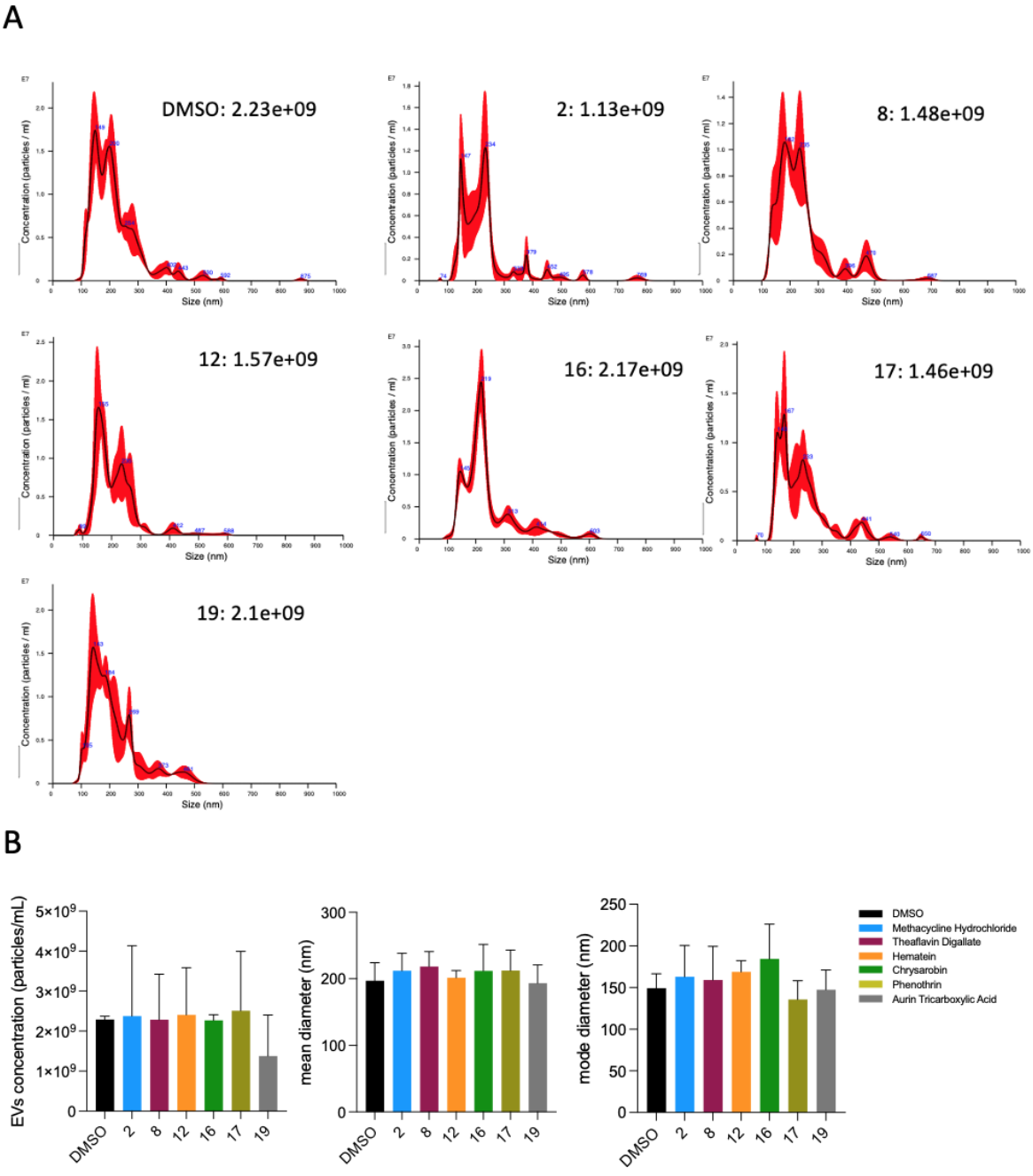

Figure 3.17. Effects of the compounds treatment on EVs. A) Representative NTA profiles of EVs retrieved after compounds treatments. B) Quantification of EVs number after compound treatment. Standard deviations are relative to two independent biological replicates. Mean ± SD. C) and D) Mean and Mode diameter of EVs retrieved after compound treatment. Standard deviations are relative to n=2 independent biological replicates. Mean ± SD.

We then moved to studying the RNA and we extracted and quantified the RNA from vesicles deriving from cells treated with the compounds. EVs mainly contain small RNAs, with a mean length of 200nt (O'Brien et al. 2020). Bioanalyzer profiles confirmed the typical EV-RNA size distribution, showing the main peak around 200nt (Figure 3.18A). We then normalized the amount of RNA to the amount of EVs released, in order to check a possible effect of the compound on the global RNA amount. As shown in Figure 3.18B, we did not observe a significant change in the abundance of global RNA released in EVs upon compound treatments except for compound Chrysarobin.

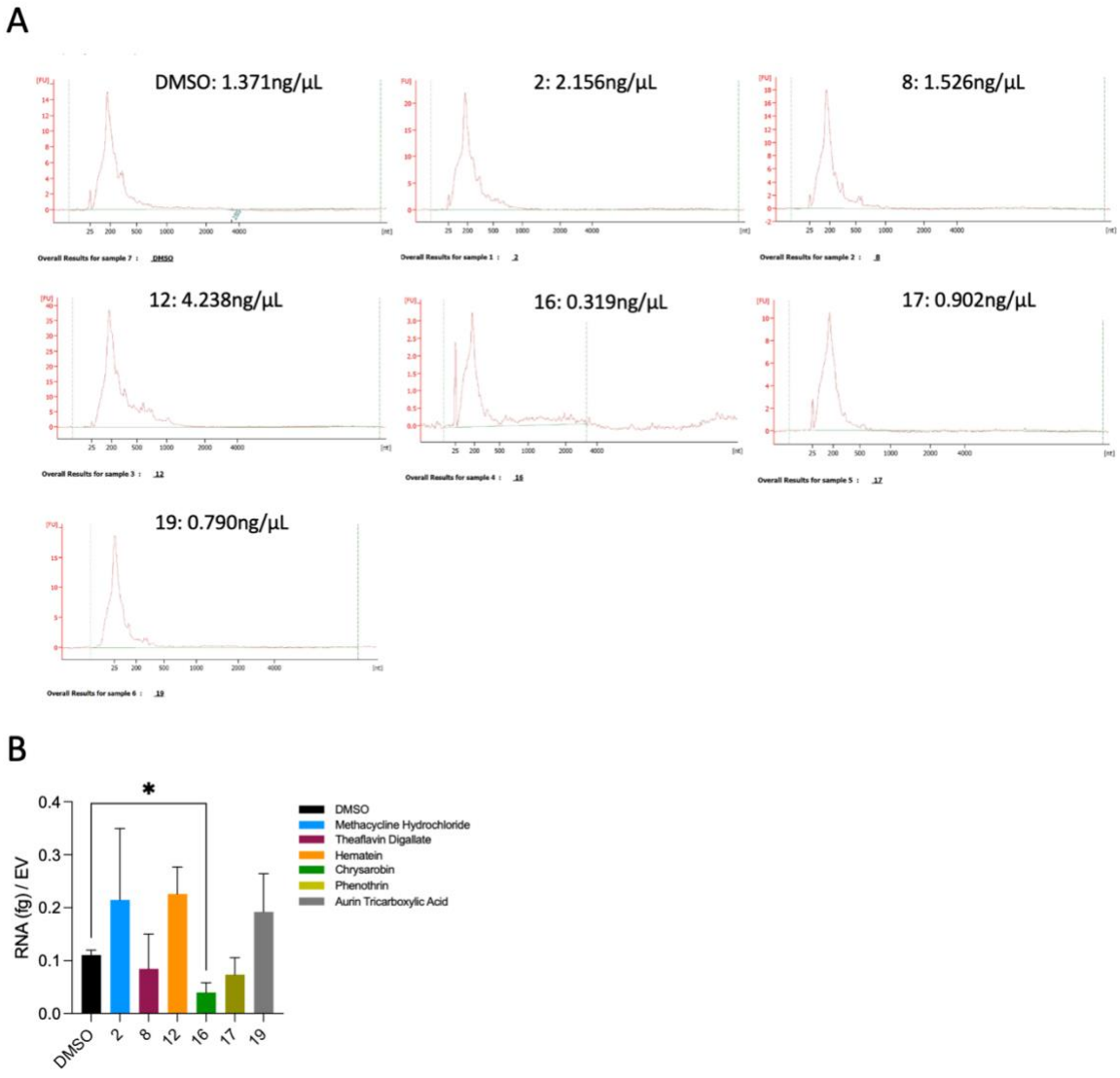

Figure 3.18. Effects of the compounds treatment on EV-RNA. A) Representative bioanalyzer profiles of EV-RNA after compounds treatment B) Quantifications of EV-RNA after compounds treatment. Standard deviations are relative to n=2 independent biological replicates. Mean ± SD. * P-value <0.05.

In order to understand whether the simple silencing of the protein could change the global EV-RNA, we silenced the protein in NSC-34 cells and quantified the global EV-RNA. The total RNA normalized on the number of EVs was not significantly altered upon silencing. However, despite the high variability, a trend of increase in RNA amount is observed upon silencing compared to scramble (Figure 3.19B).

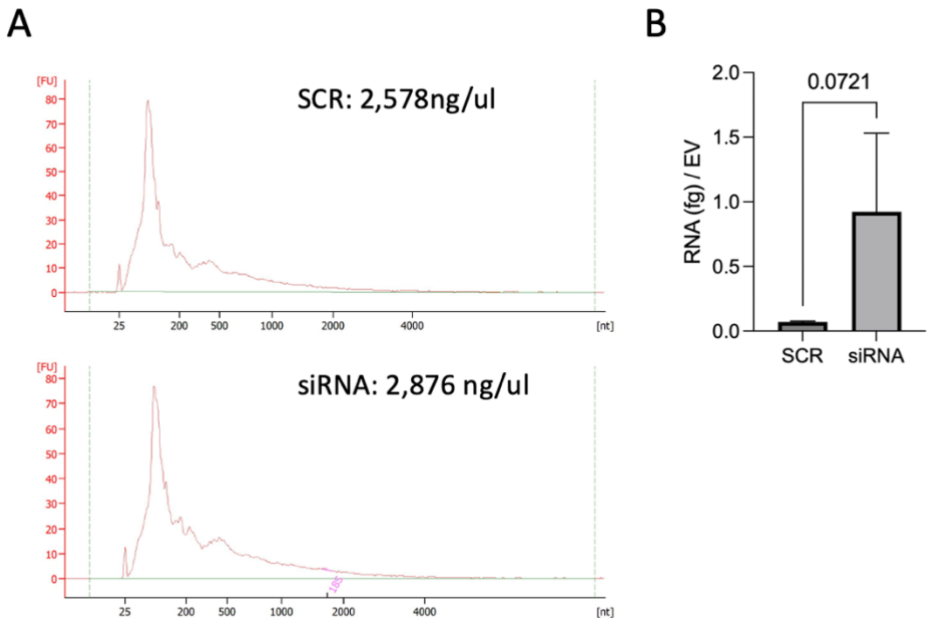

Figure 3.19. Effects of the Hnrnpa2b1 silencing on EV-RNA. A) Representative Bioanalyzer profiles of EVs retrieved after Hnrnpa2b1 silencing. B) Quantification of EV-RNA per vesicle. Standard deviations are relative to n=3 independent biological replicates. Mean ± SD.

Despite the not significant alteration in EV-RNA amount upon compound treatments, there could be differences in the RNA types secreted upon the treatment which may not be appreciable looking at the global RNA level. For this reason, we decided to check if the quality of RNA was changed upon treatment with compounds. We focused on the amount of a specific miRNA, miR-221-3p, which we chose as a redout for the following reasons: miR-221-3p has been found to be substrate of different hnRNP members (Thiele et al. 2004) and is among the targets correlating with hnRNPA2B1 dosage (Klinge et al. 2021). Also, it has been found to be upregulated in muscles of ALS patients (Pegoraro, Marozzo, and Angelini 2020) and is a target present in blood that positively correlated with sporadic ALS patients progression rate (Liguori et al. 2018). Also, looking at its sequence, it contains sequences present in many miRNAs known to be bound by hnRNPA2B1 (Mayeda et al. 1998), (Yin et al. 2021), (Guil and Cáceres 2007). For these

reasons it represents an interesting target to measure EV-RNA quality. So, we firstly checked the suitability of miR-221-3p for our purpose by extracting the RNA form EVs deriving form cells simply overexpressing hnRNPA2B1 or silenced for the protein. We synthesized the cDNA, and we checked miR-221-3p levels through ddPCR. As shown in Figure 3.20A, miR-221-3p levels were significantly increased upon silencing of the protein compared to scramble, indicating that the levels of miR-221-3p are influenced by Hnrnpa2b1 modulations. We normalized the level of miR-221-3p on the number of released EVs, confirming the result. This is in line with the trend of increased global RNA secretion upon silencing, indicating that the target amount fluctuates in line with the Hnrnpa2b1 levels. We did not observe an opposite trend upon hnRNPA2B1 overexpression, despite we obtained a stable overexpression of the protein (Figure 3.20B). This may be due to the aggregation prone behavior of the protein which could happen in the overexpression condition (Baradaran-Heravi, Van Broeckhoven, and van der Zee 2020), limiting the amount of hnRNPA2B1 available for RNA binding and sorting in EVs and perturbing the equilibrium of the other RBPs binding the EV-RNA, in line with the high variability we observed in the replicates.

Overall, these results indicate the suitability of this miRNA to check EV-RNA quality.

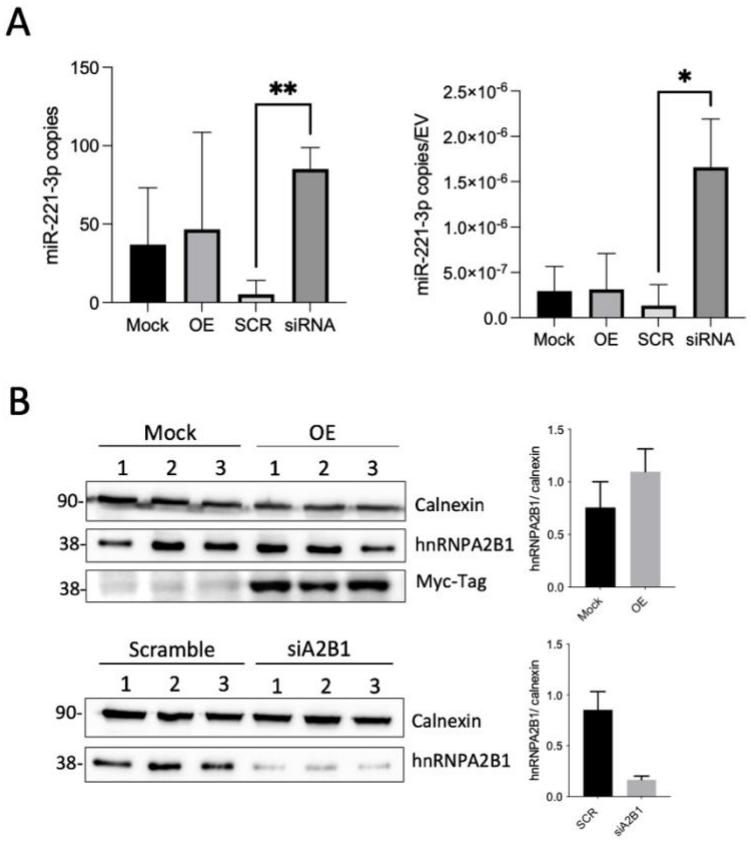

Figure 3.20. Effect of Hnrnpa2b1 silencing and hnRNPA2B1-Myc-DDK overexpression on miR-221-3p in EVs. A) miR-221-3p copies detected by ddPCR. Standard deviations are relative to n=3 independent biological replicates. Mean ± SD. * P-value <0.05; **P-value <0.01. B) WB and relative quantifications showing hnRNPA2B1 overexpression and silencing in the relative cells.

We then checked the effects of the compounds on miR-221-3p by performing the same experiments: we treated the cells for 6 hours with all the compounds except for Chrysarobin which was not commercially available for analytical purposes. Then, we purified the EVs and extracted the RNA. The ddPCR for miR-221-3p on the synthesized cDNA showed a significant reduction of the miRNA levels upon treatment with all the compounds respect to DMSO, except for Aurin Tricarboxylic Acid which resulted to have an opposite trend with high variability in the four biological replicates (Figure 3.21A). These data are in line with the usage of miR-221-3p as a redout of the compound treatment-induced reduction of EV-RNA secretion.

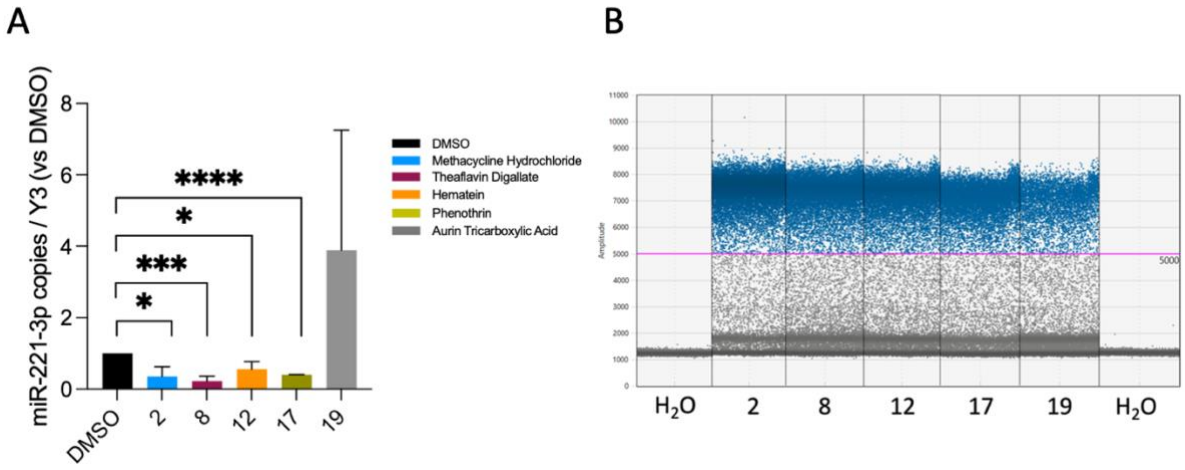

Figure 3.21. Effects of the compounds treatment on miR-221-3p in EVs. A) miR-221-3p copies, detected through ddPCR, in NSC-34-derived EVs upon compounds treatments. miR-221-3p copies are normalized on Y3 RNA detected through ddPCR after compounds treatment. Standard deviations are relative to n=3 independent biological replicates, each one normalized on its own DMSO. mean ± SD. * P-value <0.05; *** P-value <0.001; **** P-value <0.0001. B) Representative droplets relative to miR-221-3p in NSC-34-derived EVs after compounds treatment.

To strengthen this information, we decided to check the miR-221-3p levels in EVs released human neural precursor cells (NPC)-derived motor neurons. I moved to Lab of Translational Neurodegeneration Section "Albrecht Kossel" headed by Prof. Dr. Dr. Andreas Hermann in Rostock (Germany), where I differentiated the characterized NPCs model, genetically modified with FUS WT-GFP, into motor neurons (Naumann et al. 2018), (Naujock et al. 2016), (Figure 3.22B). At two weeks of maturation, I treated the cells with the compounds Methacycline hydrochloride, Theaflavin Digallate, Hematein, and Phenothrin acid for 6 hours. Given the high variability showed in NSC-34 cells we decided to exclude Aurin tricarboxylic acid from the experiments. 6h and 24h treatments showed no toxicity for the cells (Figure 3.22A). Looking at the intracellular distribution of the protein, we confirmed the main nuclear localization of endogenous hnRNPA2B1 also in this model; also, the treatment with the compounds did not alter its subcellular localization. Finally, both in DMSO conditions and in the treated ones the protein did not show any colocalization with FUS WT protein (Figure 3.22C).

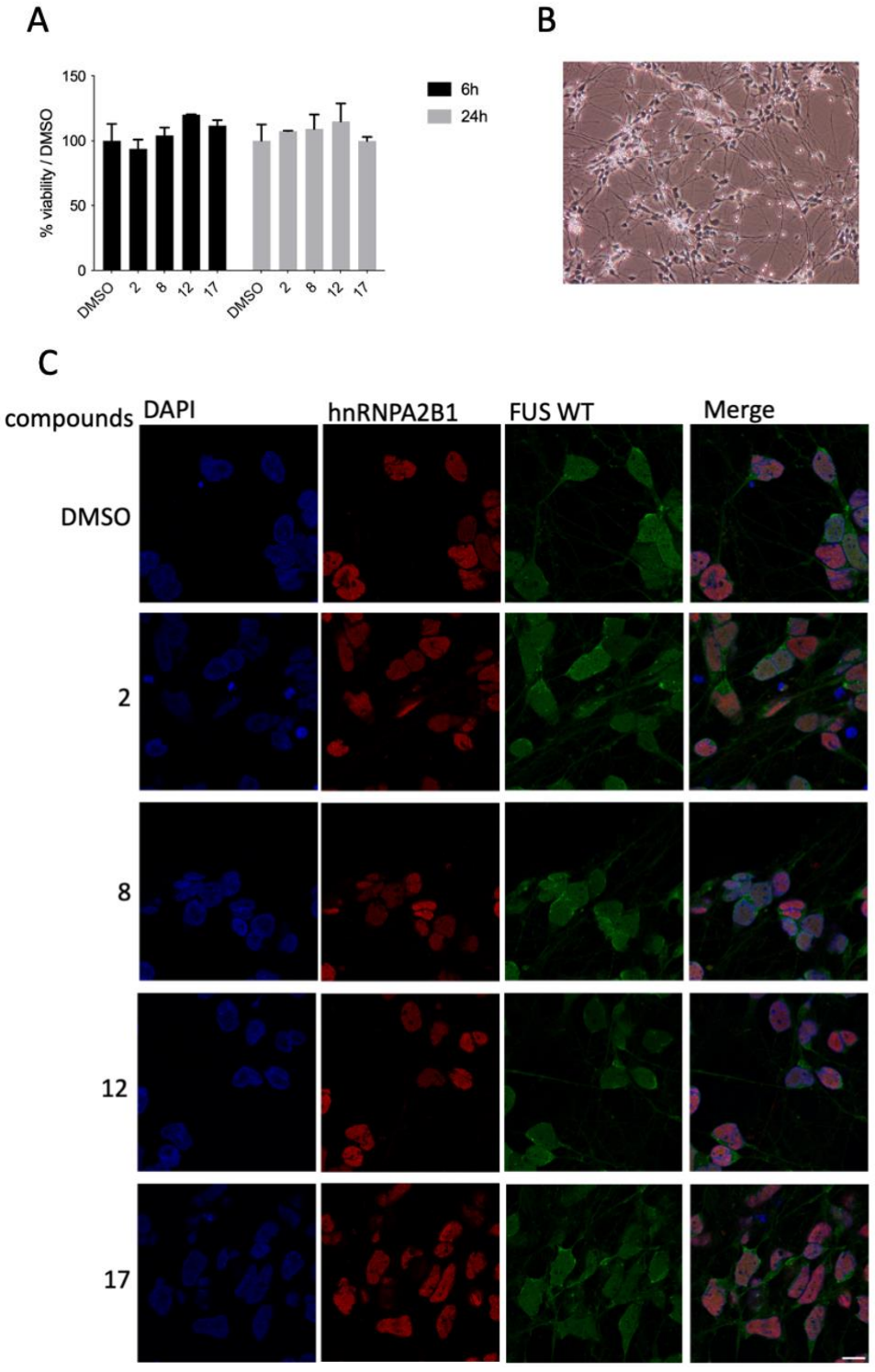

Figure 3.22. Effect of the compounds treatment on motor neurons. A) Viability of 2-weeks mature NPC-derived motor neurons after 6- and 24-hour treatment. B) Representative bright field image of 2-weeks motor neurons. C) hnRNPA2B1 localization in 2-weeks mature motor neurons. Images were taken with Zeiss LSM900 with AiryScan 2 super-resolution module. Scale bar= 10μm.

We proceeded with EVs purification, EV-RNA extraction, and cDNA synthesis. ddPCR on miR-221-3p from two weeks-motor neurons EVs revealed a significant reduction in this miRNA level upon treatment with Theaflavin Digallate and Phenothrin (Figure 3.23B).

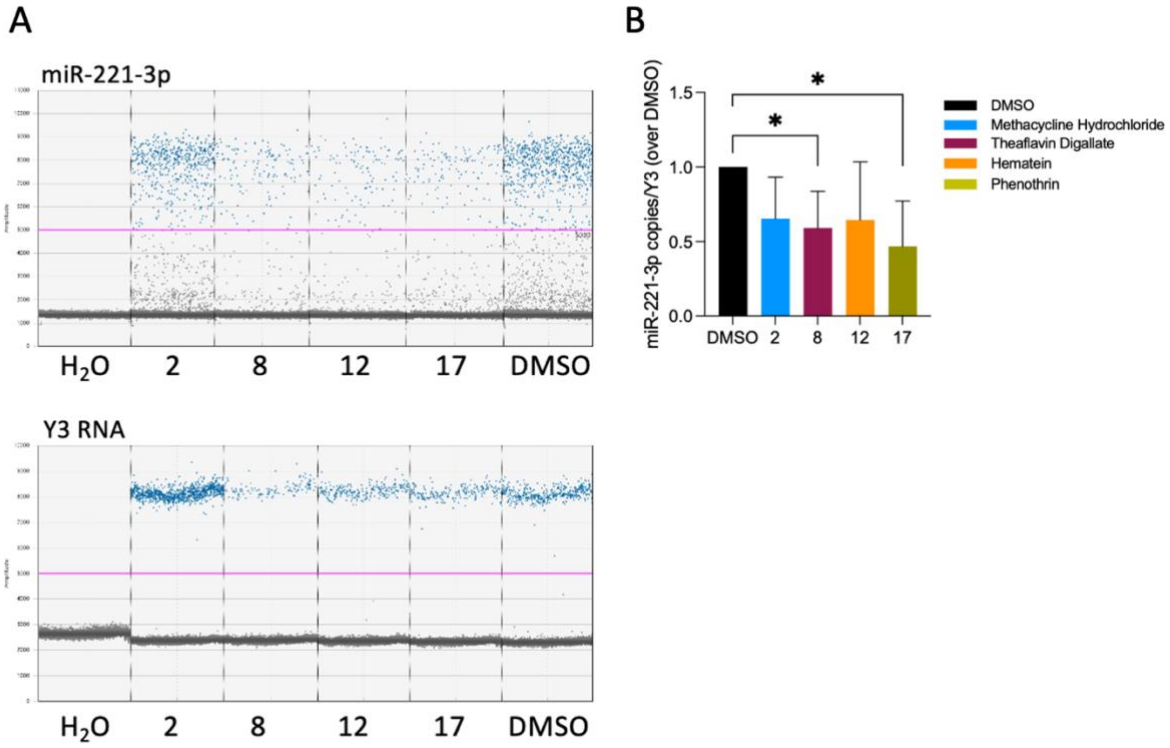

Figure 3.23. Effects of the compounds treatment on motor neurons derived EVs. A) Representative ddPCR droplets showing miR-221-3p and hY3 RNA amplifications. B) Histogram showing miR-221-3p copies normalized on hY3 RNA from motor neurons EVs detected through ddPCR after compounds treatment. Standard deviations are relative to n=3 independent biological replicates each one normalized over its own DMSO. Mean ± SD. * P-value <0.05.

Overall, these results confirm a role of the selected molecules in varying the RNA content of EVs in different cellular models.

Since we confirmed an effect of the molecules in changing mainly EV-RNA quality both in NSC-34 cells and in NPC-derived motor neurons, we wondered if the "modified" vesicles in terms of RNA content could have an effect on recipient cells. In our models, miR-221-3p levels resulted to be reduced upon compound treatments, and so, given the association of this miRNA to NF-κB activation and inflammation activation (Zhao et al. 2016), we started some pilot experiments focusing on NF-κB activation and viability in recipient cells.

3.6 Compounds influence EVs effects on recipient cells

To answer the above question, we firstly focused on NF-κB activation in recipient HEK293T. It is known that hnRNPA2B1 has a role in innate immune response activation; it translocates to the cytoplasm upon recognition of viral DNA and activates the TBK1–IRF3 pathway, upstream factors of NF-κB (Humphries and Fitzgerald 2019), (Lei Wang, Wen, and Cao 2019) and it also promotes m_6A modification, nucleocytoplasmic trafficking and translation of mRNAs activating IFN-α/β production (Lei Wang, Wen, and Cao 2019).

So, in order to measure NF-κB, we exploited a Luciferase assay: the recipient cells were co-transfected with two plasmids, one codifying for the control Renilla Luciferase, and the other codifying for the Firefly Luciferase under the control of NF-κB responsive element. In this setting, when NF-κB is activated, it binds to the responsive elements activating the transcription of Firefly Luciferase. Given the reported role of hnRNPA2B1 in activating NF-κB, we started testing NF-κB activation in recipient cells treated with EVs coming from HEK293T overexpressing hnRNPA2B1. In this experimental setting, we treated the co-transfected recipient HEK293T cells with 20'000 EVs per cell. We performed an acute EVs treatment which resulted in a 20% increase in NF-κB activation in cells exposed to "OE" EVs compared to controls from four independent biological replicates (Figure 3.24A). We then wondered if the effects of a chronic exposure could differently affect the secretome, so we performed a co-culture experiment exploiting the transwell system. In this setting, HEK293T cells were transfected for the overexpression of hnRNPA2B1, then, after medium change, they were put in contact with recipient HEK293T cells co-transfected with luciferase reporters for 6 hours. The usage of 0.4um pores-transwell allows the passage of the media and the secretome between the two seeded cells but not of the cells themselves. In this setting, despite we cannot ascribe the effects specifically on EVs, we obtained a bigger increase of NF-κB activation, reaching about 50% (Figure 3.24B). For this reason, we preferred the chronic exposure rather than the acute treatment with EVs to test the compounds effects.

As shown in figure 3.24C, Hematein treatment of HEK293T plated in the bottom part, was significantly able to reduce the activation of NF-κB in the above recipient cells compared to DMSO control. Despite the high variability in the three biological replicates, also Aurin Tricarboxylic Acid showed a trend of reduction.

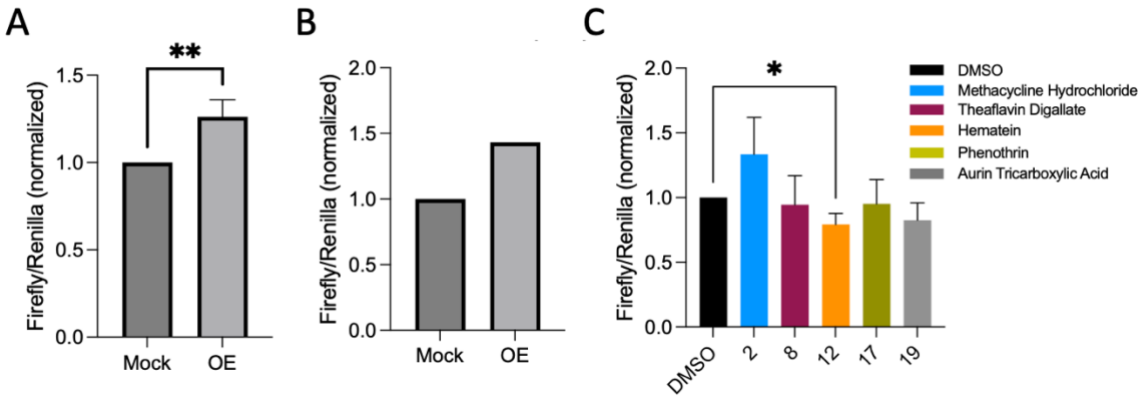

Figure 3.24. Effects of the compounds in NF-κB activation in recipient cells. A) NF-κB activation in HEK293T upon acute treatment. Cells were treated with EVs coming from cells Mock (Mock) or cells overexpressing hnRNPA2B1 (OE). Standard deviation is relative to four independent biological replicates each one normalized over its own Mock. Mean ± SD. **P-value <0.01. B) NF-κB activation in HEK293T upon chronic exposure (Transwell setting) to the secretome of cells mock or overexpressing hnRNPA2B1 (OE). C) NF-κB activation in HEK293T upon chronic exposure (Transwell setting) to the secretome of cells treated with the compounds. Standard deviations are relative to n=3 independent biological replicates, each one normalized over its own DMSO. Mean ± SD. *P-value <0.05.

Overall, these experiments showed an effect of the molecules in influencing the secretome of the treated cells, which in turns affect differently the recipient cells.

Given the effect of Hematein in counteracting NF-κB activation mediated by hnRNPA2B1 overexpression, we were curious to understand if the difference in the secretome upon compounds treatment could reveal a possible amelioration in the viability of the recipient cells.

To answer to this last question, we again exploited the same experimental setting mediated by the transwells and we took advantage of neonatal WT and TDP-43 Q331K mouse astrocytes kindly provided by the Laboratory of Transcriptional Neurobiology led by from Prof. Manuela Basso. This allowed us to have a more relevant disease model and also to compare the WT situation and the ALS-related setting. We treated the astrocytes with the hit compounds for 6 h and then we incubated the treated astrocytes with NSC-34 cells overexpressing hnRNPA2B1 for 24 hours. As shown in Figure 3.25A, NSC-34 exposed to mutant astrocytes treated with DMSO showed less viability

compared to WT astrocytes. These data are in line with the information retrieved in literature according to which the secretome of mutant astrocytes negatively impact on motor neurons (Basso et al. 2013), (Silverman et al. 2019). Looking at the effects of the compounds, we noticed a trend of improvement in NSC-34 cells exposed to treated astrocytes compared to DMSO control. Also in the WT astrocytes, the treatments with Phenothrin and Aurin Tricarboxylic Acid significantly increased the viability of NSC-34 cells (Figure 3.25B). A similar trend, despite not significant, is observed also in TDP-Q331K astrocytes (Figure 3.25C). Comparing the two graphs, that are relative to astrocytes coming from two WT and two mutant mice, in the mutant astrocytes the compounds seem to have a higher effect in counteracting hnRNPA2B1 overexpression, despite the high variability.

Together, these experiments, despite not giving a functional information about the role of EV-RNA in the process, provide an indication of a possible role of the compounds in influencing the secretome of the cells, in turn affecting the recipient cells.

Overall, we identified compounds able to interfere with EV-RNA cargo in different cellular models, with a mechanism of action which still needs to be elucidated. Also, from pilot functional experiments, we showed a possible function of the drugs in influencing the secretome of the treated cells, in turns affecting the recipient cells.

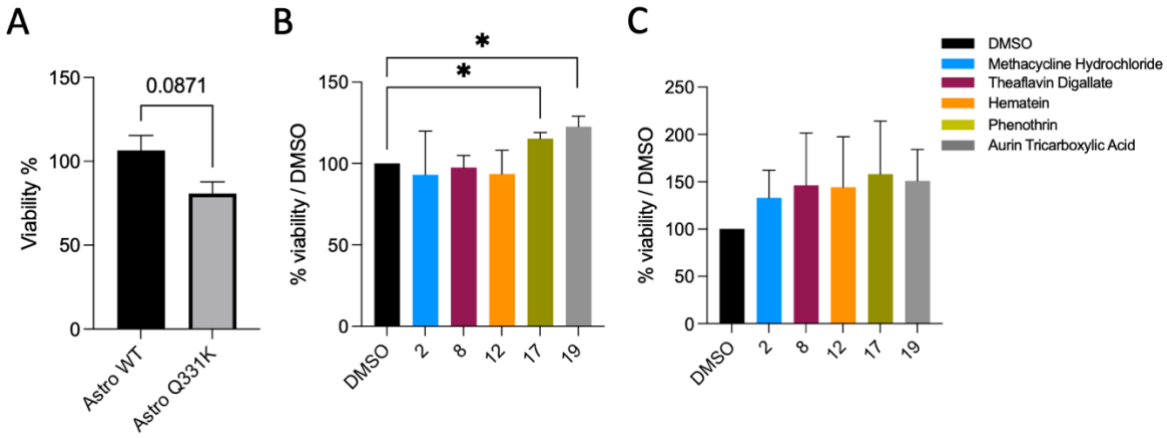

Figure 3.25. Effects of the compounds in the viability of recipient cells. A) % of viability of NSC-34 cells overexpressing hnRNPA2B1, exposed to the secretome of WT or TDP-43 Q331K astrocytes treated with DMSO. B) % of viability of NSC-34 cells exposed to the secretome of WT astrocytes treated with the compounds. C) % of viability of NSC-34 cells exposed to the secretome of TDP-43 Q331K astrocytes treated with the compounds. For all the experiments standard deviations are relative to n=2 biological replicates (Primary astrocytes derived from two transgenic TDP-43 Q331K mice and WT littermates). Each biological replicate has been normalized over its own DMSO. Mean ± SD. *P-value <0.05.

4. Discussion

In this thesis project we identified hnRNPA2B1 as good candidate to interfere with EV-RNA cargo. In the vision in which EVs could play a role in cell-to-cell communication, but also in disease spreading, it becomes extremely interesting to interfere with the EVs cargo, and especially with EV-RNA. In fact, as discussed in the paragraph 1.3.2 of introduction, RNA is emerging to be functionally involved in influencing the recipient cells and in the disease spreading.

4.1 Proteomic based approach confirms hnRNPA2B1 role in binding EV-RNA and in modulating the panel of RBPs binding to EV-RNA

Besides the data reported in the literature about the role of the protein in miRNA sorting in EVs, we proposed an innovative proteomic approach starting from biotinylated EV-RNA. By using steady state EV-RNA as a probe and modulating the cell lysate by overexpressing A2B1, we were able to retrieve information on the interplay of different RBPs in the EV-RNA binding, and on the effects of the overexpression of an EV-RNA binding protein on the other RBPs. In this setting, we performed a pull-down assay at the equilibrium without cross linking. Despite the absence of cross-linking could result in artifacts due to the pull-down of sticky proteins which can result as differentially expressed, this approach allowed us to identify not only the proteins which were more efficiently bound the EV-RNA at the equilibrium, but also the indirect interactors and complexes (as the 26S proteasome, Figure 3.4B) that can change upon RBPs modulation; an information that can be lost exploiting the cross-linking.

Of course, the usage of an heterogenous mixture of RNAs as a probe also present some limitations. We did not know the RNA sequences present in the EV sample nor the abundance of each sequence. This could lead to a biased result in terms of relative abundance of detected proteins, and therefore their quality, meaning that some

proteins could be lost due to low amount of a specific RNA target and not because they have a less efficient EV-RNA binding. Another thing to be considered is the efficiency of the polyadenylation of EV-RNA. In fact, the Poly(A) enzyme, widely used to sequence small RNAs, could have different propensity to work depending on the size of RNA, or have preferential binding for some type of RNA, or secondary structures, resulting in a fraction of EV-RNA that remains not polyadenylated. This, in turn, causes the loss of all the RBPs bound to that RNA which cannot be retained in the pull-down assay. However, despite the limitations, having all the EV-RNA at disposal allows to infer the dynamics of the interplay between RBPs binding EV-RNA which is limited when use a single RNA probe. Interestingly, as shown in Figure 3.4A, many proteins identified to be significantly upregulated or downregulated upon A2B1 overexpression are not reported to be RNA binder, indicating a possible role of them as indirect interactors.

The data retrieved from the proteomics, presented in the paragraph 3.1, confirmed a role of hnRNPA2B1 in modulating the panel of RBPs binding to EV-RNA, and this, in turn, demonstrates that hnRNPA2B1 modulation would results in different RNA cargo in the vesicles.

Moreover, looking at the lists of protein retrieved by this proteomic approach, many members of the hnRNP family are detected to fluctuate in response to hnRNPA2B1 OE. We checked the experimentally validated stretches of RNA bound by these proteins, identifying the enriched motifs (Table 4). Interestingly, the EXOmotif appeared to be in common between all the enriched motifs found. Also, an independent experiment performed using EV-RNA and TDP-43 overexpressing cells confirmed the different expression of hnRNP family members upon overexpression of TDP-43 (paragraph 3.1).

Together, the two experiments show that overexpressing two members of the hnRNP family in two independent experiments, results in a similar fluctuation network of hnRNP proteins binding to EV-RNA. This result, combined with the motif analysis, confirmed not only hnRNPs involvement in EV-RNA sorting, but also an EXOmotif-mediated binding to RNA.

For these reasons, the RNA EXOmotif probe we decided to use in the screening, not only contains the EXOmotifs for the binding to hnRNPA2B1 (Villarroya-Beltri et al. 2013), but

also represents the substrate of many RBPs effectively involved in the sorting of EV-RNA and, importantly, recapitulates the heterogenous EV-RNA sample.

4.2 Usage of a full length form of human hnRNPA2B1 protein in the High Throughput Screening

Given the effect of EV-RNA in ALS, hnRNPA2B1-RNA interaction represents a good candidate for the drug screening. As discussed in the paragraph 3.2, we underline the importance of the usage of a full-length version of the protein. In fact, its role in disease is mainly due to the presence of the LCD, or prion like domain (PrLD) (Hong Joo Kim et al. 2013), (Paul et al. 2017), which makes the protein to be recruited to the stress granules and take part in the liquid-liquid phase separation. Also, the LCD region and the folded domain have been demonstrated to interact through electrostatic interactions, allowing the stabilization of the phase behavior of the LCD region of hnRNPA2B1 (Martin et al. 2021); and so, the presence of the LCD could vary the RNA binding capacity of the protein (Van Lindt et al. 2022). For this reason, considering the protein in its full length allows us to better mimic the physiological condition and also allows the identification of compounds that can interfere with the protein despite its behavior.

Looking at the plasmids for the full-length protein expression, both pCMV6 plasmids coding for the full-length protein fused with Myc-DDK or Myc-His, caused high toxicity and plasmid recombination in bacteria, leading to impossibility of amplify the vectors nor the original form nor the sub-cloned one in our experimental settings. The presence of the highly repeated sequences of the PrLD of hnRNPA2B1 may contribute to pCMV6 plasmid recombination. After the many different trials we did for plasmid amplification and cloning, the producer company added a disclaimer about the impossibility of amplifying both the plasmids for unknown reasons. Thus, we exploited a N-Terminal GST tagged version of the protein, produced in bacteria exploiting PGEX-6-P1 vector.
Moreover, the usage of a GST tag allowed us to obtain a functional protein able to work both in REMSA and in Alpha in 10 time lower concentration compared to the eukaryotic

counterpart, maybe due to the contribution of the GST tag in increasing the protein solubility, as reported in the literature.

The High Throughput Screening was performed on a (Spectrum Collection, MicroSource Discovery, USA) library made of 2000 compounds containing 60% of FDA approved drugs, 25% of natural products and 15% of other bioactive compounds. The screening identified six molecules that were biochemically working: Methacycline hydrochloride, Theaflavin Digallate, Hematein, Chrysarobin, Phenothrin and Aurin tricarboxylic acid. Unfortunately, during the time of my PhD project, we couldn't do a biochemical characterization of the binding, which would be necessary to retrieve information about the mechanism of inhibition. In fact, the compounds could either bind to the protein or to the RNA probe.

4.3 Small molecules functional validation at intracellular and vesicular level

For the functional validation of the molecules at intracellular level on NSC-34 cells, we exploited a pull-down assay (Figure 3.16A) at the equilibrium without cross-linking and used the artificial RNA EXOmotif probe that we designed ad-hoc to contain the EXOmotifs for mimicking the binding site for hnRNPA2B1 (Paragraph 3.1). In this setting, we are using a competitive assay in which not only the protein competes with many different other RBPs in the lysate for the binding to the RNA probe, but also the compounds can recognize and bind many different targets in the cell lysate, resulting in less compound acting on endogenous hnRNPA2B1-RNA EXOmotif interaction. Nevertheless, in this complex setting, all the compounds, except for Theaflavin Digallate, resulted to be able to inhibit the interaction between RNA EXOmotif and endogenous hnRNPA2B1 in NSC-34 (Figure 3.16C) indicating that also in a physiological environment, the compounds are able to interfere with this interaction. This result is in line with the biochemical characterization of the molecules which showed a less efficient ability of compound Theaflavin Digallate in inhibiting the binding. Specifically, even if its IC_{50} resulted to be lower compared to other compounds, its maximum ability of inhibiting

the binding is only around 20%. Very different from the 100% inhibition achieved with Hematein (Figure 3.15C). Probably, when using the compound at intracellular level, the competition with other proteins further reduces the interference in hnRNPA2B1-RNA interaction, resulting in the loss of an appreciable signal in the western blot.

Given the capability of the compounds to work also in a physiological environment, we moved the attention at the EVs level. In fact, the final aim of the project is to interfere in the loading of RNA in the EVs mediated by A2B1, and influence in this way EV-RNA cargo. Up to now, we mimicked the EV-RNA using the artificial probe harboring the EXOmotifs. So, we decided to look what happened to the actual EV-RNA upon compounds treatment. As discussed in Paragraph 3.5, we took advantage of miRNAs and specifically on miR-221-3p which represented a good readout of the EV-RNA population influenced by A2B1 (Paragraph 3.5). In fact, the silencing of the protein significantly resulted in an increase of miR-221-3p presence in EVs compared to the scramble. Since hnRNPA2B1 is mainly located in the nucleus where is involved in different processes involving RNA, from splicing, transport, miRNA maturation etc., its absence could result in the impairment of miRNAs maturation in the nucleus resulting in not functional miRNAs that can be secreted outside as waste material. Also, the Taqman probe we use to measure miR-221-3p cannot discriminate between the pre-miRNA and the mature form; so, an increased presence of pre-miRNA due to the absence of the protein could be the cause for detecting increase miR-221-3p in EVs upon silencing. Moreover, the silencing of the protein could be counteracted, in terms of vesicular secretion, by other members of the hnRNP family known to be part of the RNA packaging machinery in EVs (Fabbiano et al. 2020). On the contrary, overexpressing the protein did not show the opposite trend, resulting in an increased variability, as anticipated in the Paragraph 3.5. hnRNPA2B1 OE could create a more complex system in which the protein could show both a gain or a loss of function. As reported in the literature hnNRPA2B1 is an aggregation prone protein found in stress granules. This could lead to a less protein available for the RNA binding. Interestingly, in our system, the overexpressed protein localizes mainly in the nucleus (Figure 3.2C), like the endogenous counterpart, this could result in more stabilization of the miRNA at nuclear

level, resulting in less secreted miRNA. These variables could render miR-221-3p less predictable and not dose-dependent.

Interestingly, all of the compounds except for Aurin tricarboxylic Acid resulted to be able to significantly inhibit the presence of miR-221-3p in EVs in NSC-34 (Figure 3.21A). Also, the two compounds showing the most significant effect (Theaflavin Digallate and Phenothrin) in NSC-34 EVs, confirmed their significant ability to reduce the miRNA level also in NPC-derived motor neurons EVs, further strengthening the result. Of note, as discussed before, despite its role on EV-RNA, Theaflavin Digallate did not show an efficient ability in inhibiting hnRNPA2B1-RNA interaction at intracellular level; so, the observed effects on EV-RNA could be mediated by different mechanisms involving the binding of the compound to different RBPs also targeting this miRNA, or direct binding of the compound to the miRNA itself.

Of note, the treatments with the compounds did not mimic hnRNPA2B1 silencing, resulting in a reduction of the miRNA in EVs rather than an upregulation. This is probably due to fact that these compounds do not target specifically A2B1 protein. The effect we see may be a combination of the interference of the compounds to the binding between different RBPs and miR-221-3p. As also demonstrated by the fact that this miRNA is target of other members of the hnRNP family (Y. Li et al. 2021). Therefore, the silencing itself may not be considered as a simple control of the compounds activity when considering the EV-RNA sorting.

In these experiments, we considered a 6 h window of treatments with the compounds. As reported in literature a time window comprised between 4 and 8 hours is necessary and sufficient to obtain an inhibition of RBP-RNA binding (Julio and Backus 2021), (X. Wu et al. 2020). However, 6h could be insufficient for all our compounds to exert the function. Also, more hydrophilic or lipophilic compounds can behave differently in the cells compared to the in vitro assay, increasing the variability. Specifically, the logP, which represent how much of a molecule dissolves in water versus an organic solvent, appeared to be relatively different among the compounds. A negative logP indicates high solubility in water, while logP higher than 1 represent increased solubility in organic solvent. According to CHEMBL, the logP for our compounds are: Methacycline

hydrochloride -0.44, Theaflavin Digallate 4.18, Hematein 1.33; Phenothrin 5.76; Aurin tricarboxylic acid 2.45.

4.4 EVs effects on recipient cells

The compounds we identified are able to interfere with hnRNPA2B1 *in vitro* and intracellularly, and can influence the content of EV-RNA. Given these information we explored some pilot experiments to check the effects of these "modified" EVs on recipient cells.

As already discussed in Paragraph 3.6, hnRNPA2B1 has been associated to inflammation. Specifically, through its translocation in the cytoplasm and interaction with FAM76B, it mediates NF-κB inflammatory pathway (D. Wang et al. 2022). Also, in Hepatocellular carcinoma model, hnRNPA2B1 is required for the regulation of cell migration mediated by miR503HG and for the NF-κB signaling pathway (H. Wang et al. 2018).

Interestingly, also miR-221-3p has been linked to NF-κB activation. Of note, its overexpression in macrophages led to significant increases in NF-κB and MAPK activation, associated with increased production of proinflammatory cytokines (Zhao et al. 2016). Its expression in human colorectal cancer cells forms a positive feedback loop which contributes to the constitutive activation of NF-κB and STAT3 (S. Liu et al. 2014). Also, in endothelial cells miR-221-3p was shown to repress AdipoR1 expression and activate NF-κB signaling (C.-F. Chen et al. 2015). So, given the role of miR-221-3p in NF-κB activation, measuring NF-κB activation in the recipient cells represent an interesting readout to understand a possible amelioration effect of our EV-RNA-manipulated EVs in recipient cells upon compounds treatment. In line with the hypothesis, vesicles coming from hnNRPA2B1 OE cells resulted in a significant 20% increase of NF-κB activation in the recipient cells. On the contrary, HEK293T cells exposed to the secretome of treated HEK293T, resulted in an overall trend of reduction in NF-κB activation upon treatments with compounds compared to control DMSO, with a significant reduction upon Hematein treatment. Of note, in this experimental setting we are exposing the cells to the whole secretome and not to EVs alone. For this reason, we cannot exclude an effect mediated by different component of the secretome. Another point to consider is that,

supposing an effect mediated by the EVs, we can't distinguish and so exclude an effect mediated by EV-Receptor binding, EVs internalization or EV-protein cargo, rather than EV-RNA cargo. However, despite not conclusive in terms of mechanism, these experiments give an indication of the effects of the compound-modulated secretome on recipient cells.

Given the decrease in the inflammation activation mediated by the compounds, we decided to explore the viability of the recipient cells through another pilot experiment. Also, we had the possibility to use ALS-related model represented by WT and TDP-43 Q331K primary astrocytes. In this way we had the possibility to check the possible role of the compounds in ameliorating the effect of the mutation, mediated by mutant astrocytes, in recipient cells. As discussed before (Paragraph 1.3.2 of introduction) EVs from mutant astrocytes are known to be toxic to motor neurons; in this context and in line with the effects of the compounds in reducing miR-221-3p in EVs and in reducing NF-κB activation in recipient cells, the treatment could counteract the effect of the mutant astrocytes on recipient cells.
Exploiting the same experimental setting, we exposed NSC-34 cells to the secretome of wt and mutant astrocytes treated with the compounds, in co-culture experiment. Treatment with Hematein and Aurin Trycarboxilic Acid resulted to significantly increase the viability of NSC-34 cells compared to DMSO. Also, despite the high variability, the mutant astrocytes seemed to be more susceptible to the compounds treatment, resulting in a higher window of increased variability in NSC-34 recipient cells.

Overall, I would consider Theaflavine Digallate and Phenothrin the most powerful compounds we identified, able to significantly reduce the miR-221-3p amount in EVs. Their mechanism of action needs to be studied, as also their potential other protein targets.
Theaflavin Digallate is an antioxidant natural phenol found in black tea studied in literature for its effect against tumorigenesis and tumor growth, due to the biological activities of its polyphenols (Sun et al. 2022), (Y. Gao et al. 2019), while Phenothrin is a synthetic pyrethroid used to kill adult fleas and ticks. It also used in humans to kill head

lice. It is a component of aerosol insecticides for domestic use and often used together with Methoprene, in order to interrupt the insect's biological lifecycle by killing the eggs. These compounds are not yet reported in literature as inhibitors of protein-RNA interactions.

Overall, the presented work provides a toolbox to challenge the content of RNA modulated in the cell to cause differential secretion. In the context of a neurodegenerative disorder such as ALS, our candidates necessitate further investigation. Nevertheless, given the demonstrated role of hnRNPA2B1 in vesicular trafficking and due to the interaction with other members of the hnRNP family (to be highlighted TDP-43 among others), we provided bona fide indications that interfering with the physiology of the protein could be instrumental for future therapeutic strategies in ALS.

5. Limits of the study and future perspectives

In this work we showed, for the first time, the possibility to perform a high throughput drug screening using the full-length form of hnRNPA2B1 and its interaction with RNA. Interestingly, we identified two molecules able to interfere between the binding and showing a significant reduction of the miR-221-3p in EVs in two different cellular models. We biochemically characterized the effect in the interaction exploiting AlphaScreen and REMSA assay. On this point, further biochemical characterizations are necessary at different levels. A first interesting information could be assessed on simple A2B1-RNA EXOmotif interaction. Specifically, the 31bp RNA EXOmotif we used for the screening is predicted to form a loop secondary structure from in silico predictions. For this reason, we cannot exclude a mechanism of binding mediated by the secondary structure. The usage of modified versions of the RNA probe, e.g. an RNA probe without the EXOmotif, a DNA version of the probe, or a probe having the EXOmotif but lacking parts of the sequence involved in the predicted secondary structure, could be informative on the mechanism of hnRNPA2B1-EXOmotif probe interaction, and would allow to understand a sequence or structure mediated interaction.

Moreover, as anticipated in the discussion session, we did not characterize the mechanism of inhibition of the compounds. The drugs could either bind to the RNA probe or to the protein. To answer to this question, we could use the same modified version of the probes in AlphaScreen. If the compounds exert the same inhibition across the different versions of the probe, we could possibly exclude an RNA binding of the compounds. However, an Isothermal calorimetry (ITC) approach could give a more relevant information on the binding partner of the compounds. After the proper optimization, by measuring the heat released or absorbed we could have an indication of the specificity of the compounds for the protein or the RNA.

Eventually, a crystal structure of the protein with the lead compound would be extremely informative to understand the binding pocket of the protein and would be necessary to create modified versions of the compounds to ameliorate the binding. Also, we could retrieve information about the region of the protein bound by the small molecule, and may have the possibility to have the crystal of the full-length form of the protein, not existing up to now.

Despite the biochemical characterization, our functional validation revealed an effect of the compounds in the sorting of the miR-221-3p in EVs, indicating an effect of the drugs in EV-RNA population. In this context, a transcriptomic analysis of the EV-RNA after compound treatment would allow the identification of probably more powerful targets modulated upon treatment which could give information about the global effects of the compounds on EV-RNA, and which could be used as readout in the functional experiments in the recipient cells.

In our pilot experiments, we exploited the miR-221-3p - depleted EVs for the functional tests in the recipient cells. As already discussed, this target has been associated to inflammation activation and NF-κB activation and, interestingly, the treatment with these modulated EVs resulted to affect the recipient cells. However, in our experimental setting, we cannot address the effect we observed on the recipient cells to the RNA. For these reasons, given the potential biological function of this target, it would be interesting to overexpress or express a mutant version of the miRNA on the donor cells and to check NF-κB and viability on recipient cells.

Finally, we set up an interesting proteomic approach exploiting EV-RNA which successfully gave us information on the reorganization of RBPs able to bind EV-RNA due to hnRNPA2B1 overexpression.
Validating the small molecules we identified on the RBPs identified from the proteomics could extend the drugs mechanism of action towards other RBPs involved in EV-RNA sorting.

6. Material and methods

6.1 Cell lines and growth conditions

Human embryo kidney HEK293T cell line and Mouse Motor Neuron-Like Hybrid Cell Line (NSC-34) were cultured in standard conditions using Dulbecco's modified Eagle's medium (DMEM), supplemented with 10% Fetal Bovine Serum, 1% L-glutamine, and 1% penicillin /streptomycin (Life Technologies, Carlsbad, CA, USA). Both were maintained at 37°C with 5% CO_2.

NPCs used derive from iPSCs produced and characterized in PMID: 29362359 and PMID: 26946488. In the project, NPCs were differentiated to produce 2-weeks-maturation motor neurons. In detail, a Matrigel coating composed of 1:100 Matrigel (Corning 354234) in KO-DMEM was prepared, added to the plates and incubated for 1h RT. The coating was removed before the plating. All the media were prepared in N2/SM1 base medium, made of 48.75% DMEM/F12, 48.75% Neurobasal, 1%Pen/strep/glut, 1% SM1 and 0.5% N2.

NPCs were seeded in 12-well plates and maintained in growth medium composed of N2/SM1 base medium supplemented with 3 mM CHIR99021, 150uM Ascorbic Acid and 0.5uM PMA. For the differentiation process to motor neurons, 1 million NPCs were plated on Matrigel coated 6-well-plates and fed with a patterning medium, composed of N2/SM1 base medium supplemented with 1uM PMA, 1ng/mL BDNF, 0.2mM Ascorbic Acid, 1uM Retinoic Acid and 1ng/mL GDNF. The cells were kept in patterning medium for 10 days, with a renewal of the medium very 2 days. The final step of differentiation was done on new plates coated with PLO and laminin. In details, 15% PLO (Merck/Sigma A-004-C) was added to 6-well plates in PBS and incubated at 37°C for 24h. The day after, PLO coating was removed and 1:100 mouse laminin (Biotechne 3400-010-02) in PBS was added to the plates and incubated for additional 24h. After 10 days in patterning medium, 1 million of cells were plates in the final PLO+laminin coated plates and maintained in a maturation medium for two weeks, with medium renewal very 2 days. The maturation medium was composed of N2/SM1 base medium supplemented with 5ng/mL Activin A (For the first day only), 0.1mM dBcAMP, 2ng/mL BDNF, 0.2mM

Ascorbic Acid, 1ng/mL TGFβ-3 and 2ng/mL GDNF. After two weeks of maturation, the NPC derived motor neurons were subjected to compounds treatment.

6.2 Overexpression and silencing

After 24 hours from seeding, NSC-34 and HEK293T cells were transfected with the plasmid codifying for the hnRNPA2B1 (NM_002137) Human Tagged ORF Clone (Origene, RC219318) using Lipofectamine™ 3000 Transfection Reagent (Invitrogen L3000001) and following the manufacturer instructions. The transfection mix was incubated for 48hours, then the cells were lysed and subjected to the different protocols.

hnRNPA2B1 silencing was performed on NSC34 and HEK293T cells. After 24 hours from seeding, cells were silenced using siRNAs targeting hnRNPA2B1 gene or scramble (SCR) siRNA as a control. (ON-TARGETplus Mouse Hnrnpa2b1 siRNA-L-040194-01-0005 were used for NSC-34, ON-TARGETplus Human HNRNPA2B1 siRNA- L-011690-01-0005 were used for HEK293T cells and control siRNA FE5D0018100305 - ON-TARGETplus Non-targeting siRNA #3 5 nmol for both). 25nM, 50nM and 100nM siRNA were incubated with INTERFERin® (Polyplus-101000036) transfection reagent, following the manufacturer instructions. The transfection mix was added to the cells and incubated with for 24, 48 or 96 hours.

6.3 Immunofluorescence

For immunostaining, coverslips (15 mm diameter) were inserted in 12 well plate and coated with poly-D-lysine (PDL) in PBS (P7280-5MG, Sigma – used 1:100) at 37°C for 1 hour. Then the solution was removed and 200’000 NSC34 cells were seeded on the slices. After 24h of growth in standard condition, NSC34 cells were transfected using the protocol described in the paragraph 3.1, or directly subjected to the fixation procedure. Specifically, the media was removed from the wells and 600 µl of 4% PFA (from 37% stock F875, Sigma) in PBS (previously heated at 37 °C) was added to cells and incubated for 10 min. Then, after three washes with cold PBS 5 min each, the cells were stored at 4°C or directedly subjected to immunostaining. For immunostaining procedure, firstly

cells were permeabilized with 500 µl of 0.1% Triton (BP151100) in PBS, for 5 min; then, after 3 washes with 500 µl of cold PBS for 5 min each, the blocking step was performed by adding 500 µl of 10% FBS + 0.05% Triton solution and incubated for 1 h at room temperature. The primary antibodies were prepared in in a 0.1% FBS + 0.05% Triton solution and incubated at 4 °C overnight. The day after, cells were washed three times with cold PBS and then 500 µl of secondary Ab prepared in a 0.1% FBS + 0.05% Triton solution was incubated for 1 hour. After 3 washes steps with cold PBS, the nuclei were stained adding 500 µl of Hoechst (62249, Thermo Fisher Scientific) solution (1:8000 in PBS) for 15 min. Finally, the slices were mounted with ProLong™ antifade mounting media (P36965, Thermo Fisher).

Samples were dried for at least 2 hours at RT. Images of NSC-34 samples were then the images taken with Leica TCS SP8 (Leica Microsystems, Wetzlar, Germany) confocal microscope with a HI-PLAN 63X objective. NPC-derived motor neurons images were taken with Zeiss LSM900 with AiryScan 2 super-resolution module.

Primary antibodies used: 1:200 Anti-hnRNPA2B1 (PA534939, Invitrogen)

Secondary antibodies used: Goat anti-Rabbit IgG (H+L) Alexa Fluor™ 633 (A21071, Thermofisher)

6.4 Immunoblotting

For western blotting experiments, NSC-34 and HEK293T cells were lysed in lysis buffer (50 mM Tris-HCl pH7.4, 150 mM NaCl, 1mM EDTA, 0.25%NP-40, 0.1% Triton X-100, 0.1% SDS, 1X protease inhibitor-ThermoFIsher,78429) and centrifuged at 14000g for 20 min at 4°C. The supernatant was then quantified using Pierce™ BCA Protein Assay Kit (23225).

40 mg of protein lysates were loaded on 10% acrylamide gel and run in Tris-Glycine buffer 1X. The proteins were then transferred in Glycine buffer 1X (with 20% methanol), on polyvinylidene difluoride (PVDF) membrane, activated with Methanol for 1 minute. Blocking was performed in 5% nonfat-dry milk in TBS-T (Tris-buffered saline, 0.1% Tween-20) for 1 hour. Primary antibodies were prepared in 3% % nonfat-dry milk in TBS-T and incubated overnight. After 1 hour incubation with the secondary antibody, the signal was signal was measured with Amersham ECL HRP-Conjugated Antibodies (Cytiva)

using Bio-Rad Chemidoc XRS+. Finally, the bands intensities were quantified using ImageJ software.

The following primary antibodies were used (1:1000): Anti-hnRNPA2B1 (PA534939, Invitrogen); Anti His-Tag (66005-1, Proteintech); Anti Myc-Tag (16286-1-AP, Proteintech); Anti-Flotillin-1 (610820, BDBiosciences); Anti Calnexin (Ab22595, Abcam).

The following secondary antibodies were used (1:10000): Goat Anti-Rabbit (Jackson ImmunoResearch Laboratories, Inc. 145804), Goat Anti Mouse (Jackson ImmunoResearch Laboratories, Inc. 150976).

6.5 Bacterial cells

DH5α, TOP10 and STBL3 bacterial cell lines were used for transformation, plasmid propagation and cloning experiments. BL21 strain was used to produce GST-hnRNPA2B1 protein. A glycerol stock made of LB with 20% glycerol was prepared and store at -80°C for long storage of GST-hnRNPA2B1 transformed BL21 cells usable for protein purification.

6.5.1 Plasmid amplification

25-50ng of plasmid were added on 90ul of competent cells and incubated 20min in ice. Then the heat shock was done at 42°C for 45 sec, followed by 2 min in ice. Subsequently, after the addition of 4 volumes of LB broth, bacteria cells were recovered for 60 min at 37°C at 200 RPM. finally, 200 µL of transformed bacteria were plated on LB-Agar dish supplemented with Ampicillin (50 µg/µL) or Kanamycin (25 µg/µL) according to the plasmid resistance.

6.5.2 Plasmid Cloning

The ORF of the hnRNPA2B1 (Origene RC219318), was cloned in the pCMV6-AC-Myc-His (Origene PS100006) backbone. Briefly, the ORF was amplified through PCR reaction using 15 ng of hnRNPA2B1 (Origene RC219318), 300nM of forward and reverse primers (FW: 5’ CTGCCGCCGCGATCGCCATGGAGAGA; RV: 5’GCGTACGCGTGTATCGGCTCCTCC) and 10 µL of Phusion Hot Start II High-Fidelity PCR Master Mix (Thermo Scientific), up to

20 µL final volume. PCR conditions are described in Table 5. The receiving vector was digested follow:

3 µg of pCMV6-AC-Myc-His (Origene PS100006) were reacted with 0,5 µL of Restriction Enzymes (FastDigest SfaAI and FastDigest MluI; Thermo Scientific) and 1 µL FastDigest Green Buffer (Thermo Scientific), up to 10 µL final volume. The reaction ran at 37°C for 30 min and then the enzymes were inactivated at 80°C for 20 min. Both PCR product and the digested vector we loaded on 1% Agarose gel stained with 1:10000 dilution of Xpert Green DNA stain.

Extraction from the gel was then performed using NucleoSpin Gel and PCR Clean-up Kit (Machery-Nagel). The cleaned PCR product was then digested exploited the same Restriction Enzymes and protocol mentioned above for the vector and subjected to an additional step of clean-up with the NucleoSpin Gel and PCR Clean-up Kit. The ligation was performed using 1:5 ratio for 1h at RT using 1U of T4 DNA Ligase Enzyme (T4 DNA Ligase, EL0011 Thermo Scientific) following the manufacturer's instructions. Half of the product was used to transform bacterial cells (paragraph 3.4.1). Positive colonies were let grow in LB medium supplemented with 100 µg/mL O/N, at 37°C and 200rpm rotation. Plasmid was extracted and purified using MINIprep NucleoSpin Plasmid kit (Macherey-Nagel) following manufacturer's instructions. The plasmid was used for additional bacterial transformation and growth in larger LB volume. Plasmid was extracted and purified using HiSpeed® Plasmid Midi Kit following manufacturer's instructions.

The plasmid obtained was used to express hnRNPA2B1 Myc-His tagged in HEK293T cells.

STEP	TEMP	TIME	CYCLES
Initial denaturation	96°C	1 min	1
Denaturation Annealing Extension	94°C T° gradient (60-62-64-66°C) 72°C	7 seconds 20 seconds 40 seconds	29
Final extension	72°C	5min	1
Hold	4°C		

Table 5| PCR conditions for hnRNPA2B1 ORF amplification

6.6 Recombinant proteins expression and purification

6.6.1 hnRNPA2B1-Myc-DDK

about 3*10^6 HEK293T cells seeded in 10cm dishes were transfected with 2 µg of hnRNPA2B1 plasmid tagged with Myc-DDK (Origene RC219318) using Lipofectamine™ 3000 Transfection Reagent (Paragraph 6.2) for 48h, to allow cell growth and protein expression. Then, after the medium removal and the PBS washing, the cells were lysed with 350 µL of Lysis Buffer (25 mM Hepes pH 8, 100 mM NaCl, 1 mM DTT, 0,2 mM EDTA, 0.1% Glycerol, Prot. Inhibitor 1,1x, Phosphatase Inh. 0,5x, In DEPC Water), scraped and collected. The samples were sonicated at 4°C in water bath at 45 amplitude, 7 sec ON, 30 sec OFF (5-7 cycle) and then centrifuged 4°C for 15 min at 12000 x g. the supernatant was then diluted 1:5 in Lysis Buffer and divided in low-binding Eppendorfs. 300µL of equilibrated Anti-DDK Agarose beads (Origene Anti-DDK Agarose Immunoprecipitation Kit) were added in each Eppendorf. After 1h 30 min incubation in rotation at 4°C, the samples were centrifuged at 2000 RPM for 2min, and the supernatant removed. The beads were washed twice with 1mL Lysis buffer and then resuspended in 120µL of Elution Buffer (25mM Hepes pH 8, 250 mM NaCl, 0,2 mM DTT, 250 µg/mL FLAG 3x peptide (Sigma-Aldrich)). The samples were incubated in rotor shaking for 30min at 4°C and then centrifuged at 2000 RPM; the supernatant was collected. The elution step was repeated twice. The protein was stored at -80°C or concentrated using Amicon Ultra – 0.5 mL Centrifugal Filters (Merck) according to the manufacturer's instructions. The protein concentration was measured through SDS-PAGE and Coomassie staining using BSA as reference. Band densitometry was calculated using Fiji/imageJ version 2.3.0/1.53n.

6.6.2 hnRNPA2B1 Myc-His

About 3*10^6 HEK293T cells seeded in 10cm dishes were transfected with 5 µg of Midi prep using Lipofectamine™ 3000 Transfection Reagent (Paragraph 6.2) for 48h, to allow cell growth and protein expression. Then the cells were lysed and sonicated in the same experimental conditions as described above (Paragraph 6.6.1). Then, 500 µL of previously equilibrated Ni-NTA Agarose resin (Qiagen) in equilibration buffer (20 mM

Tris-Cl pH 8.0, 100 mM NaCl, 20 mM Imidazole, 10 mM MgCl2) were added and the samples incubated at 4°C in rotation for 4-6h. Subsequently, the resin was centrifuged for 2min at 2000 RPM and the supernatant discarded. The following washing steps were done as follow: the resin wash resuspended in 1mL of Wash Buffer 1 (20 mM Tris-Cl pH 8.0, 150 mM NaCl, 50 mM Imidazole, 10 mM $MgCl_2$) in a low binding Eppendorf. After 5 min incubation at 4°C in rotor shaking and subsequent centrifugation, the supernatant was removed and the resin resuspended in Wash Buffer 2 (20 mM Tris-Cl pH 8.0, 150 mM NaCl, 100 mM Imidazole, 10 mM $MgCl_2$). After 5 min incubation at 4°C in rotor shaking and subsequent centrifugation, the supernatant was removed and the resin resuspended in Wash Buffer 3 (20 mM Tris-Cl pH 8.0, 300 mM NaCl, 100 mM Imidazole, 10 mM MgCl2) and incubated at 4°C in rotation for 10min. Then, after the centrifugation and supernatant removal, 400 µL of Elution Buffer (25 mM Hepes pH 8, 250 mM NaCl, 0,2 mM DTT, 500 mM Imidazole) were added to the samples. The vials were incubated at 4°C in rotor shaking for 30min and then centrifuged at 2000 RPM for 1 min at 4°C. the elution step was performed twice. The purified proteins were stored 80°C after the addition of 8% glycerol final concentration. The protein was concentrated using Amicon Ultra – 0.5 mL Centrifugal Filters (Merck) according to the manufacturer's instructions. The protein concentration was measured through SDS-PAGE and Coomassie staining using BSA as reference. Band densitometry was calculated using Fiji/imageJ version 2.3.0/1.53n.

6.6.3 GST-hnRNPA2B1

GST-hnRNPA2B1 was produced exploiting bacterial expression and purification. Specifically, BL21(DE3) bacteria competent cells were transformed with pGEX-6P-1-HNRNPA2B1 plasmid to express the protein with a N-terminal GST tag. A pre-inoculum of transformed BL21(DE3) was grown in LB broth (Sigma-Aldrich) supplemented with Ampicillin (50 µg/µL) O/N at 37°C at 220 rpm.

The day after, the pre-inoculum was put in 1L of LB supplemented with 50 µg/µL Ampicillin and the bacteria were cultured until the optical density measured at 600nm reached 0.7 (3-5h). Then, the protein expression was induced by adding 0.2 mM IPTG and incubating the inoculum for 13 hours at 25°C at 200 rpm. The day after, bacteria were centrifuged at 6371 × g for 15 min at 4°C and the pellet resuspended in 30 mL of

Lysis Buffer (50mM Tris HCl, pH 7.5, 2mM EDTA, 200 mM NaCl, 1:1000 Lysozyme (stock 25mg/ml), 1mM DTT, bacteria protease inhibitor cocktail). After 20 min incubation in ice, 0,1% tween was added to the lysate followed by additional 20 min incubation in ice. Samples were then sonicated for 7-8 cycles - 20" ON, 30" OFF and centrifuged at 13'000 g for 45 min at 4°C. The supernatant was then filtered with 0.45□m filters and incubated with 6mL of previously washed Pierce™ Glutathione Agarose beads (Pierce, 16101) for 2h at 4°C in rotation. The bacteria lysate incubated with the beads was then loaded on a closed column and the flowthrough (FT) was slowly collected. Then, the beads were washed twice with 25mL of high-salt wash buffer (50mM Tris HCl, pH 7.5, 500 mM NaCl). The elution was performed by adding 15mL of Elution Buffer (100mM NaCl, 50mM Tris HCl, pH 7.5, 0,1mM DTT, 300mM Glutathione) to the beads and collecting the eluted fractions slowly drop by drop. Finally, the protein was concentrated using Amicon Ultra-15 at 4000g (Merck Millipore) and stored at -80°C. The protein concentration was measured through SDS-PAGE and Coomassie staining using BSA as reference. Band densitometry was calculated using Fiji/imageJ version 2.3.0/1.53n.

6.7 AlphaScreen and High-Throughput drug Screening

AlphaScreen® assay is a bead-based assay used to study biomolecular interactions in a microplate format. Upon illumination at 680 nm, Donor beads converts ambient oxygen to an excited and reactive form of O2, singlet oxygen, due to phthalocyanine photosensitizer they contain. If an Acceptor bead is found within 200nm (singlet oxygen can diffuse approximately 200 nm in solution), the energy is transferred from the singlet oxygen to thioxene derivatives on the Acceptor bead, this cause light production at 520-620 nm. In this study this assay was used to access the interaction between hnRNA2B1 (recognized by acceptor beads) and different biotinylated single-stranded RNA probes: RNA EXOmotif (5'-Biotin-Teg- GGGGAGGUUAGGGAGGAGGGGGGUAGGCGCC) RNA 114 (5'- Biotin-Teg-AAGGACUAGC) and RNA 276 (5'-Biotin-Teg- AGGACUGC) that are recognized by Streptavidin donor beads.

The assays were performed in 20 μL final volume, using OptiPlate-384-well plates (PerkinElmer-6007299). The ligands were diluted in Alpha Buffer (25 mM HEPES pH 7.4, 100 mM NaCl, 0.01% BSA) and tested using the Detection Kits listed in Table 6.

Different concentrations of the RNA probes (0-100nM) and different concentrations of hnRNPA2B1 (0-600nM) were tested in presence of 20 μg/ml AlphaScreen® beads. The reactions were assembled as follow: 4 μL of the RNA probes were firstly added to the plate, then 16 μL of a mix containing all the other components was added. The plates were incυbated at room temperature for 1h and the signal measured using Enspire plate reader instrument (PerkinElmer; 2300-001A).

Interaction measured	AlphaScreen Kit
hnRNPA2B1-Myc-DDK – RNA EXOmotif	C-MYC detection kit (PerkinElmer ,6760611C)
hnRNPA2B1-Myc-His – RNA EXOmotif	C-MYC detection kit (PerkinElmer, 6760611C)
GST- hnRNPA2B1 – RNA EXOmotif	GST detection kit (PerkinElmer, 6760603C).

Table 6| AlphaScreen kits used to assess hnRNPA2B1:RNA interaction

The high-throughput drug screening was with the support of the HTS facility in CIBIO. A library of 2000 compounds was tested (MS Spectrum Collection, MicroSource) using GST detection kit (PerkinElmer, 6760603C). The assay was performed in 20□□l final volume OptiPlate-384-well plates. Specifically, 5nL of 1mM in DMSO (250nM final concentration) of compounds were dispensed in the plates using Echo 650 Liquid Handler (Beckman Coulter Life Sciences). Then 10 μL of a solution containing 60nM of GST-hnRNPA2B1 (30nM final concentration) were added using Biotek EL406 Washer Dispenser (Agilent) and the plates shook for 1min and incubated for 10 min. Subsequently, 25nL RNA EXOMotif (final concentration 17nM) were added to the plates using Echo 650 Liquid Handler. After 1h incubation at 70rpm shaking, fluorescence signal was measured using Enspire plate reader instrument (PerkinElmer; 2300-001A).

6.8 RNA Electromobility Shift Assay (REMSA)

REMSA assay was used to assess the functionality of the purified proteins in binding the RNA probes.

For the assays hnRNPA2B1-Myc-DDK, hnRNPA2B1-Myc-His and GST-hnRNPA2B1 were tested for the binding to IRD versions of the probes (DY-682-RNA EXOmotif, DY-682-RNA 114 and DY-682-RNA 276). The run was performed in a 4% native polyacrylamide gel (0,5 mL TBE 10x, 0,2 mL Glycerol 100%, 1,33 mL acrylamide 30%, 0,1 mL APS 10%, TEMED 15 μL and H_2O up to a 10 mL final volume).

Briefly, different concentrations of hnRNPA2B1 were incubated with 25nM of RNA probes in REMSA Buffer (20 mM HEPES pH 7.5, 50 mM KCl, 0.5 μg BSA, 0.25% Glycerol) to a final volume of 20 l (RNA EXOmotif was pre-treated with DTT (1mM) for 2min at 70°C, due to its G-rich sequence). Then the samples were incubated for 20min at RT. After the addition of 1.5 μL of 100% glycerol, each sample was load in the 4% Acrylamide gel and the run in 0.5X TBE at 4°C at 60V for the first 15min and at 80V for the remaining 60min. Signal was then measured using LiCor Odyssey infrared imaging system or Typhoon Instrument (Amersham™ Typhoon™ 5 - 29187191) using filters for infrared emission detection.

For the counter screening, 110nM of GST-hnRNPA2B1 were incubated with 1 μM of compounds in REMSA buffer at RT for 10 min. Then, 30nM of RNA EXOmotf was added in a final volume of 20 μL, and the samples incubated at RT for 50 min. The samples were then loaded on the 4% native polyacrylamide gel and run in 0.5X TBE buffer at 4°C at 60V for the first 15 min and at 80V for other 60min. the signal was then measured at Typhoon 5.

6.9 EVs isolation and characterization

6.9.1 Nickel-based Isolation (NBI)

NBI method has been applied on NSC34, HEK293T and NPC-derived motor neurons, since it allows polydisperse heterogenous EVs purification in a rapid and reproducible way (31047861) (33654737). The protocol has been carried out following the procedure described by Notarangelo et al (33654737). Briefly it is based on the usage of positively charged Ni Sepharose® High Performance beads (GE Healthcare, 17-5268-01) which are

re-functionalized using a 0.4 M NiSO4 (Sigma) solution in order to obtain 20 mg/ml in PBS beads having a specific positive charge on the matrix necessary to maximize the capture of negatively charged EVs. EVs isolation was performed on the serum-free media collected from NSC-34, HEK293T and NPCs-derived motor neurons after a first 2,800 g centrifugation aimed to eliminate cell debris. In brief, 25 µL of functionalized beads were added per ml of cell-conditioned media and incubated for 30 min at RT in orbital shaking. EV-bound beads were spun at 600g, and the supernatant was discarded. EVs were eluted from the bead pellet by adding EV elution buffer, composed of Solution A (16 mM EDTA, UltraPure pH 8.0, ThermoFisher) and Solution B (10 mM NaCl, 225 µM citric acid, Sigma) diluted 5 times in PBS and filtered with 0.2 µm filters. Specifically, 1X elution buffer was added to the beads in a volume equal to the volume of beads and then incubated 15 min at 28°C in a thermoshaker. After 1 min spin at 1,800g the eluted EVs were recovered in the supernatant.

6.9.2 Ultracentrifugation

Ultracentrifugation (UC)-based methods were used to purify EVs used for Western blot and EVs cell treatment. Briefly, after a first centrifugation step at 2,800g for 10 min, the cell-conditioned serum-free media was transferred to open-top Ultra-Clear centrifuge tubes (344058, Beckman Coulter) and subjected to 100,000g ultracentrifugation for 70 minutes at 4 °C under vacuum using a SW 32 Ti swinging bucket rotor in an Optima XPN-100 ultracentrifuge (Beckman Coulter, Brea, CA, USA). After ultracentrifugation, the supernatant was removed, and the EV-containing pellet was resuspended in a variable volume of 0.22 mm filtered PBS and used in further applications.

6.9.3 Nanoparticles Tracking Analysis (NTA)

NanoSight NS300 instrument (Malvern Panalytical Ltd., Malvern, UK) equipped with a 488 nm blue laser and a sCMOS camera was exploited to perform Nanoparticle Tracking Analysis (NTA). Accordingly, to the manufacturer's instructions, three washes with milliQ water were performed to the flow cell before the measurement of each sample. Samples were diluted in filtered PBS and measured with three individual consecutive 60 seconds videos, using 14 as camera level. A continuous flow of the suspension in the

chamber was maintained by setting the syringe pump at 30 a.u. The analysis was performed by adjusting the detection threshold between 3 and 5, according to individual signal noise of the different sample, in order to reach a ratio of at least 1:5 of particles valid/invalid. The analysis was performed using the built-in NanoSight Software NTA3.3.301 (Malvern). Downstream the processing we retrieved information about particles concentration, mean and mode diameter.

6.10 RNA extraction from cells and EVs

RNA from cells was isolated using TRI Reagent® (T9424, Sigma) according to the manufacturer's instruction. The cell pellets were homogenized using 300-1000 µL of reagent and incubated for 5 min at RT for the dissociation of nucleoprotein complexes. Then, 0.2 mL of Chloroform per 1 mL of TRI Reagent® were added to the tubes followed by vortexing. After 3 min incubation at RT, the samples were centrifuged at 12,000g for 15 minutes in a pre-chilled table centrifuge.

The upper aqueous phase was then carefully recovered without touching the interphase with the lower organic phase. 0.5 mL of isopropanol per 1 mL of TRI Reagent® were added to the aqueous phase and the samples incubated at -80 °C O/N in presence of RNase-free glycogen < 4 mg/mL, to allow RNA precipitation. The precipitates of RNA were then centrifuged for 10min at 12,000g and then washed with 75% ethanol. RNA pellets were let dry and then resuspended in RNase-free water. RNA samples were stored at -80°C. ThermoFisher Nanodrop 2000 Spectrophotometer was used for the quantification.

EV-RNA was extracted from NBI-recovered EVs using Single Cell RNA Isolation Kit (51800, Norgen Biotek Corp, Thorold, Canada) with no modifications. Briefly, 600 µL of RL buffer and 800 µL of ethanol were added to each EV-sample, mixed, and loaded on the pre-assembled columns. Samples were centrifuged at RT at 3.500g for 1 min and the flowthrough discarded. Then three washing steps were performed on the column by adding 400 mL of wash solution A (Norgen) and centrifuging the samples for 1min at 14000 g. An additional wash step of 2 min at 14000 g was performed without adding the wash reagent in order to dry the resin of the columns. Then RNA was eluted by adding

12-15 µL of RNase-free water and centrifuging the samples at 14000 g for 2 min. the EV-RNA samples were stored at -80°C.

1.5 µL aliquots were conserved and used for RNA profiling and quantification using Bioanalyzer RNA 6000 Pico Kit (Agilent Technologies) following the manufacturer's instructions.

6.11 EV-RNA biotinylation

EV-RNA biotinylation was performed by a first polyadenylation reaction followed by the attachment of a Biotin-TEG modified oligo dT.

Polyadenylation reaction was performed using TaqMan® Advanced miRNA cDNA synthesis kit (Thermo Scientific) with some modifications. Briefly, 4 µL of EV-RNA per reaction were reacted with 1 µL of 10X Poly(A) Buffer, 1µL of ATP, 0.6 µL of Poly(A) Enzyme and 3.4 µL of RNase-free water. After vortexing, the polyadenylation reaction was performed at 37°C for 45 min, then stopped at 65°C for 10 min. Half of the polyadenylated product was purified with NORGEN kit (Paragraph 6.10) and used for the Pulldown. The other 5 µL were used to check the correct polyadenylation. For this purpose, we performed the adaptor ligation reaction following the protocol of Kit TaqMan® Advanced miRNA cDNA synthesis kit (Thermo Scientific) with no modifications. Then, the sample was used as a template for the cDNA single strand synthesis using the RevertAid First Strand cDNA Synthesis Kit (Thermo Scientific). The elongation was performed using as a primer the Oligo dT. Finally, the reaction products were then loaded on a 2.5% agarose gel.

6.12 Pull Down (PD)

The Pull Down (PD) assay was optimized on endogenous hnRNPA2B1 from NSC34 cells using the 3 biotinylated probes, and then was applied to evaluate the effect of the compounds on the binding between endogenous hnRNPA2B1 and the probes.

Specifically, an average of 3 millions of cells were lysed in 100 µL buffer R-Lysis (25 mM HEPES pH 7.5, 100 mM NaCl, 1X protease inhibitor) and subjected to a water-bath sonication (35-40 amplitude, 6–7 cycles of 7” on and 45” off). The cellular lysate was

then centrifuged at 14000 rpm for 20 min at 4°C; then, the protein concentration in the supernatant was measured with Pierce™ BCA assay (23228, 1859078 ThermoFisher). Dynabeads™ M-280 Streptavidin (Invitrogen, 11205D) were washed three times with buffer R-Lysis using the magnetic rack DynaMagTM-2. Then, 200 μg of cell lysate was precleared in order to remove proteins that nonspecifically attached to beads. Briefly, 5 μL of washed streptavidin magnetic beads were incubated with the cell lysate in buffer R-Lysis (supplemented with RNAse inhibitors (RI)- 0.5 U/mL) to a final volume of 200 μL, for 15 minutes at 4 °C in rotation. The magnetic rack was used to separate the beads and 10 μL of 100 μM RNA biotinylated probes (RNA EXOmotif: 5'-Biotin-Teg-GGGGAGGUUAGGGAGGAGGGGGGUAGGCGCC; RNA 114: 5'- Biotin-Teg-AAGGACUAGC and RNA 276: 5'-Biotin-Teg- AGGACUGC) were added the pre-cleared lysate. For the RNA EXOmotif a pre-treatment with DTT 1mM and a heating step at 70°C for 2 min were done before its addition to the lysate. The samples were then incubated for 1h at 4 °C in rotation. Then, 5 μL/sample of magnetic beads were added, and the sample were put again in rotation for 20min at 4°C. After the magnetic separation, the recovered solution was kept as Flowthrough (FT) and the beads were washed twice with 300 μL of buffer R-Lysis. 20 μL of 1X Laemmli sample buffer were added to the beads and the samples heated at 95°C for 5 minutes to elute the attached proteins.

The same protocol was applied to select the population of RNA binding proteins able to bind to EV-RNA through Mass Spectrometry and Proteomic analysis. 400ng of biotinylated EV-RNA was used as probe. For this setting, after the magnetic separation, the beads were washed twice with 100 mM ammonium bicarbonate (ABC) and resuspended in 40ul of ABC for mass spectrometry analysis.

6.13 cDNA synthesis and droplet digital PCR (ddPCR)

RNA from EVs, extracted as described in paragraph 6.10, was subjected to cDNA synthesis using the TaqMan™ Advanced miRNA cDNA Synthesis Kit (Applied Biosystems™ - A28007) following the manufacturer's instruction with no modifications. Briefly, 0.5ng of RNA in 2ul of UltraPure™ DNase/RNase-Free Distilled Water (Invitrogen™ - 10977015) were used as input for the first Poly(A) tailing reaction of the

kit for all the samples. The final cDNA product obtained after the miR-Amp reaction was used as a template for digital droplet PCR (ddPCR) analysis.

ddPCR provides high efficiency, specificity, sensitivity, and absolute quantification of the targets. The assay was optimized for the detection of hsa-miR-221-3p in EVs and in cells. For the reactions, the cDNA was firstly diluted 1:200 in UltraPure™ DNase/RNase-Free Distilled Water and then 6µL were used as input. For the assay we exploited the Supermix for probes, which allows the amplification and detection of DNA targets using commercially available probe-based assays. Briefly, 6 µL of diluted cDNA were mixed with 1.15 µL of 20X hsa-miR-221-3p Advanced miRNA Assay (477981_mir- A25576 – ThermoFisher), 11.5 µL of 2X ddPCR Supermix for Probes (Bio-Rad - 1863026) and 4.35 µL of water, to a final volume of 23 µL. Y3 RNA was used, especially for EVs, as a reference. For this reaction the same diluted cDNA was mixed with Y3 primers to a final concentration of 50nM (mouse: mY3 Fw : 5'-GGTTGGTCCGAGAGTAGTGG-3', mY3 Rv : 5'-AAAGGCTGGTCAAGTGAAGC-3'; Human: hY3 Fw : GGCTGGTCCGAGTGCAGTG, hY3 Rv : GAAGCAGTGGGAGTGGAGAA), 11.5 µL of QX200 ddPCR EvaGreen Supermix (Bio-Rad - 1864033) and water to a final volume of 23 µL. Droplet formation and PCR conditions were performed following the manufacturer's instruction with no modifications.

6.14 NF-κB activation

Hek239T cells were co-transfected for 24h with pGL3-basic-NF-κB-RE, containing a consensus NF-κB binding site, and pRL-SV40 plasmid, that is a co-reporter vector for the constitutive expression of wild-type Renilla luciferase and used as internal control for the transfection efficiency. Luciferase activity was measured using Dual-Glo® Luciferase Assay System (E2920, Promega) following the manufacturer's instruction with no modification. Briefly, Dual-Glo® Reagent was added in the wells in a volume equal to the volume of culture medium present in the wells and the sample mixed. After 10 minutes incubation, to allow cell lysis, the firefly luminescence was measured using VarioskanTM LUX Multimode Microplate Reader (ThermoFisher). Then Dual-Glo® Stop & Glo® Reagent was added in the wells in a volume equal to the original culture medium volume, and the samples mixed. After 10min incubation Renilla luminescence was measured at Varioskan™.

The luminescence was then calculated making the ratio between firefly luminescence (experimental reporter) and Renilla luminescence (luminescence from the control reporter).
For co-colture experiments, cells were plated in transwell plates (TC insert, CO 0.4 µm, PET, transparent, 83.3932.041 – Sarstedt, Germany)

6.15 Cell viability assays

Viability of NSC-34 cells was measured using CellTiter-Glo® Luminescent Cell Viability Assay (Promega) following the manufacturer's instruction with no modification. The assay determines the number of viable cells in culture based on quantitation of the ATP present. Briefly, a volume of CellTiter-Glo® Reagent equal to the volume of cell culture medium was added in each well. A two-minute orbital shaking was done to induce cell lysis. Then the plate was incubated at room temperature for 10 minutes to stabilize luminescent signal, and the signal read using VarioskanTM LUX Multimode Microplate Reader (ThermoFisher).
For co-colture experiments, cells were plated in transwell plates (TC insert, CO 0.4 µm, PET, transparent, 83.3932.041 – Sarstedt, Germany)

PrestoBlue reagent was used to check the effects of the compounds on NPC-derived motor neurons. It contains resazurin and a propriety buffering system. When added to media, the PrestoBlue reagent is taken up by cells and resazurin is quickly reduced by metabolically active cells. The non-toxic resazurin is converted in the PrestoBlue reagent to a red-fluorescent dye. This change can be detected by measuring fluorescence or absorbance. The protocol was applied according to the manufacturer's instructions with minor modifications.
Briefly, 10 mL of 10X PrestoBlue™ Cell Viability Reagent (A13261, Invitrogen) were added to 90 mL of cells seeded in 96-well plates. After 1h hour incubation at 37°C, the fluorescence signal was measured with Varioskan LUX Multimode Microplate Reader, setting 560 nm excitation and 590 nm emission. Higher fluorescence signal correlate to greater total metabolic activity.

6.16 Proteomic analysis

Mass Spectrometry analysis was entirely performed at the CIBIO Mass Spectrometry (MS) core facility (UniTN).

After the PD assay, the proteins bound to the beads were subjected to on-bead trypsin digestion. Briefly, samples were reduced and alkylated with DTT 10 mM at 56°C for 45 min and iodoacetamide 20 mM at RT for 30 min in the dark, respectively. One microgram of trypsin (Thermofisher Scientific) was added to each sample and the beads were incubated at 37°C overnight with gentle shaking. Following digestion, beads were collected, and the supernatant was transferred to a fresh Eppendorf tube. Beads were washed with 50 µL of 100 mm ammonium bicarbonate and the supernatants were pooled. Digested peptides were then acidified with 1% TFA to a pH 2.5, desalted on C18 stage-tips and resuspended in 20 µL of 0.1% formic acid buffer for LC-MS/MS analysis.

Digested samples were separated using an Easy-nLC 1200 system (Thermo Scientific). A 28 cm reversed-phase column (inner diameter 75 µm packed in-house with ReproSil-Pur C18-AQ material: 3µm particle size, Dr. Maisch, GmbH), heated at 40°C, was used for separating the peptides, with a two-component mobile phase system of 0.1% formic acid in water (buffer A) and 0.1% formic acid in 80% acetonitrile (buffer B). Peptides were eluted using a gradient of 5% to 25% over 57 minutes, followed by 25% to 40% over 13 minutes and 40% to 98% over 10 minutes, and kept at 98% over 10 minutes, a flow rate of 400 nL/min. Samples were injected in an Orbitrap Fusion Tribrid mass spectrometer (Thermo Scientific, San Jose, CA, USA) and data acquired in data-dependent mode (2100 V). Temperature of the ion transfer tube was set at 275°C. Full scans were performed in the Orbitrap at 120.000 FWHM resolving power (at 200m/z), 50 ms maximum injection time, and an AGC target of 1x10e6. A mass range of 350-1100 m/z was surveyed for precursors, with first mass set at 140 m/z for fragments. Each full scan was followed by a set of MS/MS scans (HCD, collision energy of 30%) over 3 sec cycle time at 150ms maximum injection time (ion trap) and AGC target of 5x10e3. A dynamic exclusion filter was set every 30 sec. Data were acquired using the Thermo software Xcalibur (version 4.3) and Tune (version 3.3). During the project, QCloud was used to control instrument longitudinal performance (C. Chiva, R. Olivella, E. Borràs, G.

Espadas, O. Pastor, A. Solé, E. Sabidó, QCloud: A cloud-based quality control system for mass spectrometry-based proteomics laboratories (Chiva et al. 2018).

Peptides searches were performed in Proteome Discoverer 2.2 software (Thermo Scientific) against the Mus musculus FASTA file (uniprot, downloaded April 2021) and a database containing major common contaminants. Proteins were identified using the MASCOT search engine, with a mass tolerance of 10 ppm for precursors and 0.6 Da for products. Trypsin was chosen as the enzyme with 5 missed cleavages. Static modification of carbamidomethyl (C) and variable modification of oxidation (M) and acetyl (protein N-term) were incorporated in the search. False discovery rate was filtered for <0.01 at PSM, at peptide and protein level. Results were filtered to exclude potential contaminants and proteins with less than two peptides.

MS data analysis was performed using the ProTN proteomics pipeline (manuscript in preparation, www.github.com/TebaldiLab/ProTN and www.rdds.it/ProTN). In summary, peptide intensities were log2 transformed, normalized (median normalization) and summarized into proteins (median sweeping) with functions in the DEqMS Bioconductor package (Zhu et al. 2020). Imputation of the missing intensities was executed by PhosR package (Hani Jieun Kim et al. 2021). Differential analysis was performed with the DEqMS package, proteins with P-value < 0.05 were considered significant. Functional enrichment analysis of differentially expressed proteins was performed with EnrichR (E. Y. Chen et al. 2013). Enriched terms with P-value < 0.05 and Overlap size > 4 were considered significant.

6.17 Statistical analysis

In the relative figure legends are indicated the data and the number of independent experiments.

All the data were calculated using GraphPad Prism Software, using unpaired t-test. The results were considered statistically significant when P value was <0.05 (*), <0.01 (**), <0.001 (***) <0.0001 (****).

Scientific production

Corsi J., Peroni D., Belli R., Lassandro M., Sidarovich V., Adami V., Grosskreutz J., Fabbiano F., Großmann D., Hermann A., Tell G., Basso M., D'Agostino V. G. Biochemical inhibitors of hnRNPA2B1-RNA interactions reveal a predictable sorting of miRNA subsets into extracellular vesicles. (In submission).

Dalle Vedove, A., Cazzanelli, G., **Corsi, J.**, Sedykh, M., D'Agostino, V. G., Caflisch, A., & Lolli, G. (2021). Identification of a BAZ2A Bromodomain Hit Compound by Fragment Joining. *ACS Bio & Med Chem Au*, *1*(1), 5–10. https://doi.org/10.1021/acsbiomedchemau.1c00016

Fabbiano, F., **Corsi, J.**, Gurrieri, E., Trevisan, C., Notarangelo, M., & D'Agostino, V. G. (2020). RNA packaging into extracellular vesicles: An orchestra of RNA-binding proteins? *Journal of Extracellular Vesicles*, *10*(2). https://doi.org/10.1002/jev2.12043

Manganelli, M., Grossi, I., **Corsi, J.**, D'Agostino, V. G., Jurikova, K., Cusanelli, E., … De Petro, G. (2022). Expression of Cellular and Extracellular TERRA, TERC and TERT in Hepatocellular Carcinoma. *International Journal of Molecular Sciences*, *23*(11). https://doi.org/10.3390/ijms23116183

Mangiapane, G., Parolini, I., Conte, K., Malfatti, M. C., **Corsi, J**., Sanchez, M., … Tell, G. (2021). Enzymatically active apurinic/apyrimidinic endodeoxyribonuclease 1 is released by mammalian cells through exosomes. *The Journal of Biological Chemistry*, *296*, 100569. https://doi.org/10.1016/j.jbc.2021.100569

Bibliography

Abels, Erik R., and Xandra O. Breakefield. 2016. “Introduction to Extracellular Vesicles: Biogenesis, RNA Cargo Selection, Content, Release, and Uptake.” *Cellular and Molecular Neurobiology* 36(3): 301–12.

Adamik, Barbara et al. 2008. “An Association between RBMX, a Heterogeneous Nuclear Ribonucleoprotein, and ARTS-1 Regulates Extracellular TNFR1 Release.” *Biochemical and Biophysical Research Communications* 371(3): 505–9.

Ahadi, Alireza et al. 2016. “Long Non-Coding RNAs Harboring MiRNA Seed Regions Are Enriched in Prostate Cancer Exosomes.” *Scientific Reports* 6: 1–14. http://dx.doi.org/10.1038/srep24922.

Aladesuyi Arogundade, Olubankole et al. 2019. “Antisense RNA Foci Are Associated with Nucleoli and TDP-43 Mislocalization in C9orf72-ALS/FTD: A Quantitative Study.” *Acta Neuropathologica* 137(3): 527–30. https://doi.org/10.1007/s00401-018-01955-0.

Alarcón, Claudio R. et al. 2015. “HNRNPA2B1 Is a Mediator of M6A-Dependent Nuclear RNA Processing Events.” *Cell* 162(6): 1299–1308.

Alonso, A., G. Logroscino, S. S. Jick, and M. A. Hernán. 2009. “Incidence and Lifetime Risk of Motor Neuron Disease in the United Kingdom: A Population-Based Study.” *European Journal of Neurology* 16(6): 745–51.

Als, While, and Supplementary Tables. 2021. “Common and Rare Variant Association Analyses in Amyotrophic Lateral Sclerosis Identify 15 Risk Loci with Distinct Genetic Architectures and Neuron-Specific Biology.” 53(December).

Armon, Carmel. 2007. “Sports and Trauma in Amyotrophic Lateral Sclerosis Revisited.” *Journal of the Neurological Sciences* 262(1–2): 45–53.

Ash, Peter E.A. et al. 2013. “Unconventional Translation of C9ORF72 GGGGCC Expansion Generates Insoluble Polypeptides Specific to C9FTD/ALS.” *Neuron* 77(4): 639–46. http://dx.doi.org/10.1016/j.neuron.2013.02.004.

Balaguer, N. et al. 2018. “Heterogeneous Nuclear Ribonucleoprotein C1may Control MiR-30d Levels in Endometrial Exosomes Affecting Early Embryo Implantation.”

Molecular Human Reproduction 24(8): 411–25.

Baradaran-Heravi, Yalda, Christine Van Broeckhoven, and Julie van der Zee. 2020. "Stress Granule Mediated Protein Aggregation and Underlying Gene Defects in the FTD-ALS Spectrum." *Neurobiology of Disease* 134(September 2019): 104639. https://doi.org/10.1016/j.nbd.2019.104639.

Basso, Manuela et al. 2013. "Mutant Copper-Zinc Superoxide Dismutase (SOD1) Induces Protein Secretion Pathway Alterations and Exosome Release in Astrocytes: Implications for Disease Spreading and Motor Neuron Pathology in Amyotrophic Lateral Sclerosis." *Journal of Biological Chemistry* 288(22): 15699–711. http://dx.doi.org/10.1074/jbc.M112.425066.

Berdyński, Mariusz et al. 2022. "SOD1 Mutations Associated with Amyotrophic Lateral Sclerosis Analysis of Variant Severity." *Scientific Reports* 12(1): 1–11. https://doi.org/10.1038/s41598-021-03891-8.

Bériault, Véronique et al. 2004. "A Late Role for the Association of HnRNP A2 with the HIV-1 HnRNP A2 Response Elements in Genomic RNA, Gag, and Vpr Localization." *Journal of Biological Chemistry* 279(42): 44141–53.

Billmeier, Martina et al. 2022. "Mechanistic Insights into Non-Coding Y RNA Processing." *RNA Biology* 19(1): 468–80. https://doi.org/10.1080/15476286.2022.2057725.

Blanc, Lionel, and Michel Vidal. 2018. "New Insights into the Function of Rab GTPases in the Context of Exosomal Secretion." *Small GTPases* 9(1–2): 95–106. https://doi.org/10.1080/21541248.2016.1264352.

Boillée, Séverine et al. 2006. "Onset and Progression in Inherited ALS Determined by Motor Neurons and Microglia." *Science* 312(5778): 1389–92.

Brennan, K. et al. 2020. "A Comparison of Methods for the Isolation and Separation of Extracellular Vesicles from Protein and Lipid Particles in Human Serum." *Scientific Reports* 10(1): 1–13.

Brettschneider, Johannes et al. 2012. "Microglial Activation Correlates with Disease Progression and Upper Motor Neuron Clinical Symptoms in Amyotrophic Lateral Sclerosis." *PLoS ONE* 7(6): 13–15.

Brown, Anna Leigh et al. 2022. "TDP-43 Loss and ALS-Risk SNPs Drive Mis-Splicing and Depletion of UNC13A." *Nature* 603(7899): 131–37.

Burd, C. G., M. S. Swanson, M. Gorlach, and G. Dreyfuss. 1989. “Primary Structures of the Heterogeneous Nuclear Ribonucleoprotein A2, B1, and C2 Proteins: A Diversity of RNA Binding Proteins Is Generated by Small Peptide Inserts.” *Proceedings of the National Academy of Sciences of the United States of America* 86(24): 9788–92.

Chen, Changhao et al. 2020. “Exosomal Long Noncoding RNA LNMAT2 Promotes Lymphatic Metastasis in Bladder Cancer.” *Journal of Clinical Investigation* 130(1): 404–21.

Chen, Chao-Feng et al. 2015. “MicroRNA-221 Regulates Endothelial Nitric Oxide Production and Inflammatory Response by Targeting Adiponectin Receptor 1.” *Gene* 565(2): 246–51.

Chen, Edward Y et al. 2013. “Enrichr: Interactive and Collaborative HTML5 Gene List Enrichment Analysis Tool.” *BMC bioinformatics* 14: 128.

Chen, Hongbo et al. 2018. “Exploring the Genetics and Non-Cell Autonomous Mechanisms Underlying ALS/FTLD.” *Cell Death and Differentiation* 25(4): 646–60. http://dx.doi.org/10.1038/s41418-018-0060-4.

Chiva, Cristina et al. 2018. “QCloud: A Cloud-Based Quality Control System for Mass Spectrometry-Based Proteomics Laboratories.” *PloS one* 13(1): e0189209.

Cho, Kyoung In, Andrew Orry, Se Eun Park, and Paulo A. Ferreira. 2015. “Targeting the Cyclophilin Domain of Ran-Binding Protein 2 (Ranbp2) with Novel Small Molecules to Control the Proteostasis of STAT3, HnRNPA2B1 and M-Opsin.” *ACS Chemical Neuroscience* 6(8): 1476–85.

D’Ambrogio, Andrea et al. 2009. “Functional Mapping of the Interaction between TDP-43 and HnRNP A2 in Vivo.” *Nucleic Acids Research* 37(12): 4116–26.

Datta, Amrita et al. 2017. “Manumycin A Suppresses Exosome Biogenesis and Secretion via Targeted Inhibition of Ras/Raf/ERK1/2 Signaling and HnRNP H1 in Castration-Resistant Prostate Cancer Cells.” *Cancer Letters* 408: 73–81. http://dx.doi.org/10.1016/j.canlet.2017.08.020.

Dellar, Elizabeth R. et al. 2022. “Unpacking Extracellular Vesicles: RNA Cargo Loading and Function.” *Journal of Extracellular Biology* 1(5).

Ding, Xuebing et al. 2015. “Exposure to ALS-FTD-CSF Generates TDP-43 Aggregates in Glioblastoma Cells through Exosomes and TNTs-like Structure.” *Oncotarget* 6(27):

24178–91.

Donoso-Quezada, Javier, Sergio Ayala-Mar, and José González-Valdez. 2021. “The Role of Lipids in Exosome Biology and Intercellular Communication: Function, Analytics and Applications.” *Traffic* 22(7): 204–20.

Dreyfuss, Gideon, V. Narry Kim, and Naoyuki Kataoka. 2002. “Messenger-RNA-Binding Proteins and the Messages They Carry.” *Nature Reviews Molecular Cell Biology* 3(3): 195–205.

Dreyfuss, Gideon, Michael J. Matunis, Serafín Piñol-Roma, and Christopher G. Burd. 1993. “HnRNP Proteins and the Biogenesis of MRNA.” *Annual Review of Biochemistry* 62: 289–321.

Driedonks, Tom A.P. et al. 2020. “Y-RNA Subtype Ratios in Plasma Extracellular Vesicles Are Cell Type- Specific and Are Candidate Biomarkers for Inflammatory Diseases.” *Journal of Extracellular Vesicles* 9(1). https://doi.org/10.1080/20013078.2020.1764213.

Driedonks, Tom A.P., and Esther N.M. Nolte-T’Hoen. 2019. “Circulating Y-RNAs in Extracellular Vesicles and Ribonucleoprotein Complexes; Implications for the Immune System.” *Frontiers in Immunology* 10(JAN): 1–15.

Fabbiano, Fabrizio et al. 2020. “RNA Packaging into Extracellular Vesicles: An Orchestra of RNA-Binding Proteins?” *Journal of Extracellular Vesicles* 10(2).

Fähling, Michael et al. 2006. “Heterogeneous Nuclear Ribonucleoprotein-A2/B1 Modulate Collagen Prolyl 4-Hydroxylase, α (I) MRNA Stability.” *Journal of Biological Chemistry* 281(14): 9279–86.

Fallini, Claudia, Bilal Khalil, Courtney L. Smith, and Wilfried Rossoll. 2020. “Traffic Jam at the Nuclear Pore: All Roads Lead to Nucleocytoplasmic Transport Defects in ALS/FTD.” *Neurobiology of Disease* 140(December 2019).

Fang, Mark Y. et al. 2019. “Small-Molecule Modulation of TDP-43 Recruitment to Stress Granules Prevents Persistent TDP-43 Accumulation in ALS/FTD.” *Neuron* 103(5): 802-819.e11. https://doi.org/10.1016/j.neuron.2019.05.048.

Feiler, Marisa S. et al. 2015. “TDP-43 Is Intercellularly Transmitted across Axon Terminals.” *Journal of Cell Biology* 211(4): 897–911.

Ferrara, Deborah, Laura Pasetto, Valentina Bonetto, and Manuela Basso. 2018. “Role of Extracellular Vesicles in Amyotrophic Lateral Sclerosis.” *Frontiers in*

Neuroscience 12(AUG): 1–9.

Gabrielli, Martina et al. 2022. “Microglial Large Extracellular Vesicles Propagate Early Synaptic Dysfunction in Alzheimer’s Disease.” *Brain* 145(8): 2849–68.

Gagliardi, Delia, Nereo Bresolin, Giacomo Pietro Comi, and Stefania Corti. 2021. “Extracellular Vesicles and Amyotrophic Lateral Sclerosis: From Misfolded Protein Vehicles to Promising Clinical Biomarkers.” *Cellular and Molecular Life Sciences* 78(2): 561–72. https://doi.org/10.1007/s00018-020-03619-3.

Le Gall, Laura et al. 2022. “Muscle Cells of Sporadic Amyotrophic Lateral Sclerosis Patients Secrete Neurotoxic Vesicles.” *Journal of Cachexia, Sarcopenia and Muscle* 13(2): 1385–1402.

Gao, Tianyi et al. 2018. “Exosomal LncRNA 91H Is Associated with Poor Development in Colorectal Cancer by Modifying HNRNPK Expression.” *Cancer Cell International* 18(1): 1–10. https://doi.org/10.1186/s12935-018-0506-2.

Gao, Ying, Junfeng Yin, Youying Tu, and Yi Charlie Chen. 2019. “Theaflavin-3,3’-Digallate Suppresses Human Ovarian Carcinoma OVCAR-3 Cells by Regulating the Checkpoint Kinase 2 and P27 Kip1 Pathways.” *Molecules (Basel, Switzerland)* 24(4).

Garcia-Martin, Ruben et al. 2022. “MicroRNA Sequence Codes for Small Extracellular Vesicle Release and Cellular Retention.” *Nature* 601(7893): 446–51.

Geissler, Rene et al. 2016. “A Widespread Sequence-Specific MRNA Decay Pathway Mediated by HnRNPs A1 and A2/B1.” *Genes and Development* 30(9): 1070–85.

Geissler, Rene, and Andrew Grimson. 2016. “A Position-Specific 3’UTR Sequence That Accelerates MRNA Decay.” *RNA Biology* 13(11): 1075–77. https://doi.org/10.1080/15476286.2016.1225645.

Gerber, Yannick Nicolas et al. 2012. “Early Functional Deficit and Microglial Disturbances in a Mouse Model of Amyotrophic Lateral Sclerosis.” *PloS one* 7(4).

Geuens, Thomas, Delphine Bouhy, and Vincent Timmerman. 2016. “The HnRNP Family: Insights into Their Role in Health and Disease.” *Human Genetics* 135(8): 851–67.

Gomes, Catarina, Sascha Keller, Peter Altevogt, and Júlia Costa. 2007. “Evidence for Secretion of Cu,Zn Superoxide Dismutase via Exosomes from a Cell Model of Amyotrophic Lateral Sclerosis.” *Neuroscience Letters* 428(1): 43–46.

Goodarzi, Hani et al. 2012. “Systematic Discovery of Structural Elements Governing

Stability of Mammalian Messenger RNAs." *Nature* 485(7397): 264–68.

Grad, Leslie I., Edward Pokrishevsky, Judith M. Silverman, and Neil R. Cashman. 2014. "Exosome-Dependent and Independent Mechanisms Are Involved in Prion-like Transmission of Propagated Cu/Zn Superoxide Dismutase Misfolding." *Prion* 8(5): 331–35.

Grant, Charles E., and Timothy L. Bailey. 2021. "XSTREME: Comprehensive Motif Analysis of Biological Sequence Datasets." *bioRxiv*: 458722.

Guil, Sonia, and Javier F. Cáceres. 2007. "The Multifunctional RNA-Binding Protein HnRNP A1 Is Required for Processing of MiR-18a." *Nature Structural and Molecular Biology* 14(7): 591–96.

Hardiman, Orla et al. 2017. "Amyotrophic Lateral Sclerosis." *Nature Reviews Disease Primers* 3.

Harper, Sandra, and David W. Speicher. 2011. "Purification of Proteins Fused to Glutathione S-Transferase." *Methods in Molecular Biology* 681: 259–80.

Van Harten, Alexandra C.M., Hemali Phatnani, and Serge Przedborski. 2021. "Non-Cell-Autonomous Pathogenic Mechanisms in Amyotrophic Lateral Sclerosis." *Trends in Neurosciences* 44(8): 658–68. https://doi.org/10.1016/j.tins.2021.04.008.

He, Yaowu, and Ross Smith. 2009. "Nuclear Functions of Heterogeneous Nuclear Ribonucleoproteins A/B." *Cellular and Molecular Life Sciences* 66(7): 1239–56.

Hill, Andrew F. 2019. "Extracellular Vesicles and Neurodegenerative Diseases." *Journal of Neuroscience* 39(47): 9269–73.

Horbay, Rostyslav et al. 2022. "Role of Ceramides and Lysosomes in Extracellular Vesicle Biogenesis, Cargo Sorting and Release." *International Journal of Molecular Sciences* 23(23).

Hu, Lei et al. 2023. "Identification of a Novel Heterogeneous Nuclear Ribonucleoprotein A2B1 (HnRNPA2B1) Ligand That Disrupts HnRNPA2B1/Nucleic Acid Interactions to Inhibit the MDMX-P53 Axis in Gastric Cancer." *Pharmacological Research* 189(February): 106696. https://doi.org/10.1016/j.phrs.2023.106696.

Huelga, Stephanie C. et al. 2012. "Integrative Genome-Wide Analysis Reveals Cooperative Regulation of Alternative Splicing by HnRNP Proteins." *Cell Reports* 1(2): 167–78. http://dx.doi.org/10.1016/j.celrep.2012.02.001.

Humphries, Fiachra, and Katherine A Fitzgerald. 2019. “HnRNPA2B1: Fueling Antiviral Immunity from the Nucleus.” *Molecular cell* 76(1): 8–10.

Hutchison, Stephen, Catherine LeBel, Marco Blanchette, and Benoit Chabot. 2002. “Distinct Sets of Adjacent Heterogeneous Nuclear Ribonucleoprotein (HnRNP) A1/A2 Binding Sites Control 5’ Splice Site Selection in the HnRNP A1 MRNA Precursor.” *The Journal of biological chemistry* 277(33): 29745–52. http://dx.doi.org/10.1074/jbc.M203633200.

Hutten, Saskia, and Dorothee Dormann. 2016. “HnRNPA2/B1 Function in Neurodegeneration: It’s a Gain, Not a Loss.” *Neuron* 92(4): 672–74. http://dx.doi.org/10.1016/j.neuron.2016.11.014.

Iguchi, Yohei et al. 2016. “Exosome Secretion Is a Key Pathway for Clearance of Pathological TDP-43.” *Brain* 139(12): 3187–3201.

Jackson, Noel A., Marcos J. Guerrero-Muñoz, and Diana L. Castillo-Carranza. 2022. “The Prion-like Transmission of Tau Oligomers via Exosomes.” *Frontiers in Aging Neuroscience* 14(August): 1–9.

Jara, Javier H. et al. 2019. “MCP1-CCR2 and Neuroinflammation in the ALS Motor Cortex with TDP-43 Pathology.” *Journal of neuroinflammation* 16(1): 196.

Jiang, Fengjie et al. 2021. “HNRNPA2B1 Promotes Multiple Myeloma Progression by Increasing AKT3 Expression via M6A-Dependent Stabilization of ILF3 MRNA.” *Journal of Hematology and Oncology* 14(1): 4–8. https://doi.org/10.1186/s13045-021-01066-6.

Johnston, Clare A. et al. 2006. “Amyotrophic Lateral Sclerosis in an Urban Setting: A Population Based Study of Inner City London [2].” *Journal of Neurology* 253(12): 1642–43.

de Jong, Olivier G. et al. 2012. “Cellular Stress Conditions Are Reflected in the Protein and RNA Content of Endothelial Cell-Derived Exosomes.” *Journal of Extracellular Vesicles* 1(1): 1–12.

Julio, Ashley R, and Keriann M Backus. 2021. “New Approaches to Target RNA Binding Proteins.” *Current opinion in chemical biology* 62: 13–23.

Kabashi, Edor et al. 2004. “Focal Dysfunction of the Proteasome: A Pathogenic Factor in a Mouse Model of Amyotrophic Lateral Sclerosis.” *Journal of Neurochemistry* 89(6): 1325–35.

Kamelgarn, Marisa et al. 2016. “Proteomic Analysis of FUS Interacting Proteins Provides Insights into FUS Function and Its Role in ALS.” *Biochimica et Biophysica Acta - Molecular Basis of Disease* 1862(10): 2004–14. http://dx.doi.org/10.1016/j.bbadis.2016.07.015.

Kasim, Mumtaz et al. 2014. “Shutdown of Achaete-Scute Homolog-1 Expression by Heterogeneous Nuclear Ribonucleoprotein (HnRNP)-A2/B1 in Hypoxia.” *Journal of Biological Chemistry* 289(39): 26973–88.

Katsu, Masataka et al. 2019. “MicroRNA Expression Profiles of Neuron-Derived Extracellular Vesicles in Plasma from Patients with Amyotrophic Lateral Sclerosis.” *Neuroscience Letters* 708(January): 134176. https://doi.org/10.1016/j.neulet.2019.03.048.

Kim, Hani Jieun et al. 2021. “PhosR Enables Processing and Functional Analysis of Phosphoproteomic Data.” *Cell reports* 34(8): 108771.

Kim, Hong Joo et al. 2013. “Mutations in Prion-like Domains in HnRNPA2B1 and HnRNPA1 Cause Multisystem Proteinopathy and ALS.” *Nature* 495(7442): 467–73.

Kim, Kyoung Mi et al. 2017. “RNA in Extracellular Vesicles.” *Wiley Interdisciplinary Reviews: RNA* 8(4): 1–14.

Klinge, Carolyn M, Kellianne M Piell, Christine Schaner Tooley, and Eric C Rouchka. 2021. “Author Correction: HNRNPA2/B1 Is Upregulated in Endocrine-Resistant LCC9 Breast Cancer Cells and Alters the MiRNA Transcriptome When Overexpressed in MCF-7 Cells.” *Scientific reports* 11(1): 9235.

Kozu, Tomoko, Birgit Henrich, and Klaus P. Schäfer. 1995. “Structure and Expression of the Gene (HNRPA2B1) Encoding the Human HnRNP Protein A2/B1.” *Genomics* 25(2): 365–71.

Kugeratski, Fernanda G. et al. 2021. 23 Nature Cell Biology *Quantitative Proteomics Identifies the Core Proteome of Exosomes with Syntenin-1 as the Highest Abundant Protein and a Putative Universal Biomarker*. Springer US. http://dx.doi.org/10.1038/s41556-021-00693-y.

Kumar, Manish et al. 2015. “Nuclear Heterogeneous Nuclear Ribonucleoprotein D Is Associated with Poor Prognosis and Interactome Analysis Reveals Its Novel Binding Partners in Oral Cancer.” *Journal of Translational Medicine* 13(1): 1–15.

Kwon, Sunjong, Elisa Barbarese, and John H Carson. 1999. “And Its Cognate Trans-

Acting Ligand HnRNP A2 Enhance Cap-Dependent Translation." 147(2): 247–56.

Lagier-Tourenne, Clotilde et al. 2012. "Divergent Roles of ALS-Linked Proteins FUS/TLS and TDP-43 Intersect in Processing Long Pre-MRNAs." *Nature Neuroscience* 15(11): 1488–97.

Leblond, Claire S., Hannah M. Kaneb, Patrick A. Dion, and Guy A. Rouleau. 2014. "Dissection of Genetic Factors Associated with Amyotrophic Lateral Sclerosis." *Experimental Neurology* 262(Part B): 91–101. http://dx.doi.org/10.1016/j.expneurol.2014.04.013.

Lee, Heedoo et al. 2019. "Caveolin-1 Selectively Regulates MicroRNA Sorting into Microvesicles after Noxious Stimuli." *Journal of Experimental Medicine* 216(9): 2202–20.

Lei, Yi et al. 2018. "Tumor-Released LncRNA H19 Promotes Gefitinib Resistance via Packaging into Exosomes in Non-Small Cell Lung Cancer." *Oncology Reports* 40(6): 3438–46.

Li, Xiaoze et al. 2013. "Suppression of HPV-16 Late L1 5'-Splice Site SD3632 by Binding of HnRNP D Proteins and HnRNP A2/B1 to Upstream AUAGUA RNA Motifs." *Nucleic Acids Research* 41(22): 10488–508.

Li, Yangyang et al. 2021. "Heterogeneous Nuclear Ribonucleoprotein A1 Loads Batched Tumor-Promoting MicroRNAs Into Small Extracellular Vesicles With the Assist of Caveolin-1 in A549 Cells." *Frontiers in cell and developmental biology* 9: 687912.

Liang, Bing et al. 2013. "Characterization and Proteomic Analysis of Ovarian Cancer-Derived Exosomes." *Journal of Proteomics* 80: 171–82. http://dx.doi.org/10.1016/j.jprot.2012.12.029.

Di Liegro, Carlo Maria, Gabriella Schiera, and Italia Di Liegro. 2014. "Regulation of MRNA Transport, Localizationand Translation in the Nervous System of Mammals (Review)." *International Journal of Molecular Medicine* 33(4): 747–62.

Liguori, Maria et al. 2018. "Dysregulation of MicroRNAs and Target Genes Networks in Peripheral Blood of Patients With Sporadic Amyotrophic Lateral Sclerosis." *Frontiers in molecular neuroscience* 11: 288.

Van Lindt, Joris et al. 2022. "F/YGG-Motif Is an Intrinsically Disordered Nucleic-Acid Binding Motif." *RNA biology* 19(1): 622–35.

Liu, Sanhong et al. 2014. "A MicroRNA 221- and 222-Mediated Feedback Loop

Maintains Constitutive Activation of NFκB and STAT3 in Colorectal Cancer Cells." *Gastroenterology* 147(4): 847-859.e11. http://dx.doi.org/10.1053/j.gastro.2014.06.006.

Liu, Yu, and Song Lin Shi. 2021. "The Roles of HnRNP A2/B1 in RNA Biology and Disease." *Wiley Interdisciplinary Reviews: RNA* 12(2): 1–23.

Lööv, Camilla et al. 2016. "α-Synuclein in Extracellular Vesicles: Functional Implications and Diagnostic Opportunities." *Cellular and Molecular Neurobiology* 36(3): 437–48.

Lu, Jiahui et al. 2020. "CryoEM Structure of the Low-Complexity Domain of HnRNPA2 and Its Conversion to Pathogenic Amyloid." *Nature Communications* 11(1): 1–11. http://dx.doi.org/10.1038/s41467-020-17905-y.

Mackenzie, Ian R.A., Rosa Rademakers, and Manuela Neumann. 2010. "TDP-43 and FUS in Amyotrophic Lateral Sclerosis and Frontotemporal Dementia." *The Lancet Neurology* 9(10): 995–1007. http://dx.doi.org/10.1016/S1474-4422(10)70195-2.

Malo, Nathalie et al. 2006. "Statistical Practice in High-Throughput Screening Data Analysis." *Nature biotechnology* 24(2): 167–75.

Marcelo, Adriana et al. 2021. "Stress Granules, RNA-Binding Proteins and Polyglutamine Diseases: Too Much Aggregation?" *Cell Death and Disease* 12(6). http://dx.doi.org/10.1038/s41419-021-03873-8.

Martin, Erik W et al. 2021. "Interplay of Folded Domains and the Disordered Low-Complexity Domain in Mediating HnRNPA1 Phase Separation." *Nucleic acids research* 49(5): 2931–45.

Martinez, Fernando J. et al. 2016. "Protein-RNA Networks Regulated by Normal and ALS-Associated Mutant HNRNPA2B1 in the Nervous System." *Neuron* 92(4): 780–95. http://dx.doi.org/10.1016/j.neuron.2016.09.050.

Massenzio, Francesca et al. 2018. "Microglial Overexpression of FALS-Linked Mutant SOD1 Induces SOD1 Processing Impairment, Activation and Neurotoxicity and Is Counteracted by the Autophagy Inducer Trehalose." *Biochimica et Biophysica Acta - Molecular Basis of Disease* 1864(12): 3771–85. https://doi.org/10.1016/j.bbadis.2018.10.013.

Mayeda, A, S H Munroe, R M Xu, and A R Krainer. 1998. "Distinct Functions of the Closely Related Tandem RNA-Recognition Motifs of HnRNP A1." *RNA (New York,*

N.Y.) 4(9): 1111–23.

McAlary, Luke, Steven S. Plotkin, Justin J. Yerbury, and Neil R. Cashman. 2019. "Prion-Like Propagation of Protein Misfolding and Aggregation in Amyotrophic Lateral Sclerosis." *Frontiers in Molecular Neuroscience* 12(November): 1–21.

McCluskey, Gavin et al. 2022. "Extracellular Vesicles in Amyotrophic Lateral Sclerosis." *Life (Basel, Switzerland)* 13(1).

Mckay, Stewart J., and Howard Cooke. 1992. "HnRNP A2/B1 Binds Specifically to Single Stranded Vertebrate Telomeric Repeat TTAGGGn." *Nucleic Acids Research* 20(24): 6461–64.

Mead, Richard J. et al. 2023. "Amyotrophic Lateral Sclerosis: A Neurodegenerative Disorder Poised for Successful Therapeutic Translation." *Nature Reviews Drug Discovery* 22(3): 185–212.

Mejzini, Rita et al. 2019. "ALS Genetics, Mechanisms, and Therapeutics: Where Are We Now?" *Frontiers in Neuroscience* 13(December): 1–27.

von Mering, Christian et al. 2003. "STRING: A Database of Predicted Functional Associations between Proteins." *Nucleic Acids Research* 31(1): 258–61.

Mitsuhashi, Masato et al. 2013. "Aging Enhances Release of Exosomal Cytokine MRNAs by A1-42-Stimulated Macrophages." *FASEB Journal* 27(12): 5141–50.

Munro, Trent P. et al. 1999. "Mutational Analysis of a Heterogeneous Nuclear Ribonucleoprotein A2 Response Element for RNA Trafficking." *Journal of Biological Chemistry* 274(48): 34389–95. http://dx.doi.org/10.1074/jbc.274.48.34389.

Muslimov, Ilham A. et al. 2014. "Interactions of Noncanonical Motifs with HnRNP A2 Promote Activity-Dependent RNA Transport in Neurons." *Journal of Cell Biology* 205(4): 493–510.

Naujock, Maximilian et al. 2016. "4-Aminopyridine Induced Activity Rescues Hypoexcitable Motor Neurons from Amyotrophic Lateral Sclerosis Patient-Derived Induced Pluripotent Stem Cells." *Stem cells (Dayton, Ohio)* 34(6): 1563–75.

Naumann, Marcel et al. 2018. "Impaired DNA Damage Response Signaling by FUS-NLS Mutations Leads to Neurodegeneration and FUS Aggregate Formation." *Nature Communications* 9(1). http://dx.doi.org/10.1038/s41467-017-02299-1.

Nedelsky, Natalia B., and J. Paul Taylor. 2022. “Pathological Phase Transitions in ALS-FTD Impair Dynamic RNA–Protein Granules.” *Rna* 28(1): 97–113.

van Niel, Guillaume et al. 2022. “Challenges and Directions in Studying Cell–Cell Communication by Extracellular Vesicles.” *Nature Reviews Molecular Cell Biology* 23(5): 369–82.

Van Niel, Guillaume, Gisela D’Angelo, and Graça Raposo. 2018. “Shedding Light on the Cell Biology of Extracellular Vesicles.” *Nature Reviews Molecular Cell Biology* 19(4): 213–28. http://dx.doi.org/10.1038/nrm.2017.125.

Nijssen, Jik, Laura H. Comley, and Eva Hedlund. 2017. “Motor Neuron Vulnerability and Resistance in Amyotrophic Lateral Sclerosis.” *Acta Neuropathologica* 133(6): 863–85.

Nonaka, Takashi et al. 2013. “Prion-like Properties of Pathological TDP-43 Aggregates from Diseased Brains.” *Cell Reports* 4(1): 124–34. http://dx.doi.org/10.1016/j.celrep.2013.06.007.

Notarangelo, Michela et al. 2020. “Rapid Nickel-Based Isolation of Extracellular Vesicles from Different Biological Fluids.” *Bio-Protocol* 10(3): 1–12.

O’Brien, Killian et al. 2020. “RNA Delivery by Extracellular Vesicles in Mammalian Cells and Its Applications.” *Nature Reviews Molecular Cell Biology* 21(10): 585–606. http://dx.doi.org/10.1038/s41580-020-0251-y.

O’Toole, O. et al. 2008. “Epidemiology and Clinical Features of Amyotrophic Lateral Sclerosis in Ireland between 1995 and 2004.” *Journal of Neurology, Neurosurgery and Psychiatry* 79(1): 30–32.

Ouweneel, Amber B., Michael J. Thomas, and Mary G. Sorci-Thomas. 2020. “The Ins and Outs of Lipid Rafts: Functions in Intracellular Cholesterol Homeostasis, Microparticles, and Cell Membranes.” *Journal of Lipid Research* 61(5): 676–86. http://dx.doi.org/10.1194/jlr.TR119000383.

Paul, Kacy R. et al. 2017. “Effects of Mutations on the Aggregation Propensity of the Human Prion-Like Protein HnRNPA2B1.” *Molecular and Cellular Biology* 37(8): 1–15.

Pegoraro, Valentina, Roberta Marozzo, and Corrado Angelini. 2020. “MicroRNAs and HDAC4 Protein Expression in the Skeletal Muscle of ALS Patients.” *Clinical neuropathology* 39(3): 105–14.

Peters, Owen M., Mehdi Ghasemi, and Robert H. Brown. 2015. “Emerging Mechanisms of Molecular Pathology in ALS.” *Journal of Clinical Investigation* 125(5): 1767–79.

Philips, Thomas et al. 2013. “Oligodendrocyte Dysfunction in the Pathogenesis of Amyotrophic Lateral Sclerosis.” *Brain* 136(2): 471–82.

Pinto, Sara et al. 2017. “Exosomes from NSC-34 Cells Transfected with HSOD1-G93A Are Enriched in Mir-124 and Drive Alterations in Microglia Phenotype.” *Frontiers in Neuroscience* 11(MAY).

Polymenidou, Magdalini et al. 2011. “Long Pre-MRNA Depletion and RNA Missplicing Contribute to Neuronal Vulnerability from Loss of TDP-43.” *Nature Neuroscience* 14(4): 459–68.

Purice, Maria D., and J. Paul Taylor. 2018. “Linking HnRNP Function to ALS and FTD Pathology.” *Frontiers in Neuroscience* 12(MAY): 1–12.

Ray, Debashish et al. 2013. “A Compendium of RNA-Binding Motifs for Decoding Gene Regulation.” *Nature* 499(7457): 172–77.

Riemenschneider, Henrick et al. 2022. “Gel-like Inclusions of C-terminal Fragments of TDP-43 Sequester Stalled Proteasomes in Neurons.” *EMBO reports* 23(6): 1–12.

Rosen, Daniel R. et al. 1993. “Mutations in Cu/Zn Superoxide Dismutase Gene Are Associated with Familial Amyotrophic Lateral Sclerosis.” *Nature* 362(6415): 59–62.

Saá, Paula et al. 2014. “First Demonstration of Transmissible Spongiform Encephalopathy-Associated Prion Protein (PrPTSE) in Extracellular Vesicles from Plasma of Mice Infected with Mouse-Adapted Variant Creutzfeldt-Jakob Disease by in Vitro Amplification.” *Journal of Biological Chemistry* 289(42): 29247–60.

Santangelo, Laura et al. 2016. “The RNA-Binding Protein SYNCRIP Is a Component of the Hepatocyte Exosomal Machinery Controlling MicroRNA Sorting.” *Cell Reports* 17(3): 799–808. http://dx.doi.org/10.1016/j.celrep.2016.09.031.

Saucier, Daniel et al. 2019. “Identification of a Circulating MiRNA Signature in Extracellular Vesicles Collected from Amyotrophic Lateral Sclerosis Patients.” *Brain Research* 1708: 100–108. https://doi.org/10.1016/j.brainres.2018.12.016.

Scalabrin, Matteo et al. 2017. “The Cellular Protein HnRNP A2/B1 Enhances HIV-1 Transcription by Unfolding LTR Promoter G-Quadruplexes.” *Scientific Reports* 7(February): 1–13.

Schäfer, Frank et al. 2015. “Purification of GST-Tagged Proteins.” *Methods in*

Enzymology 559: 127–39.

Shan, Jianguo et al. 2003. “A Molecular Mechanism for MRNA Trafficking in Neuronal Dendrites.” *Journal of Neuroscience* 23(26): 8859–66.

Silverman, Judith M. et al. 2019. “CNS-Derived Extracellular Vesicles from Superoxide Dismutase 1 (SOD1)G93A ALS Mice Originate from Astrocytes and Neurons and Carry Misfolded SOD1.” *Journal of Biological Chemistry* 294(10): 3744–59. http://dx.doi.org/10.1074/jbc.RA118.004825.

Singh, Anju, Ritushree Kukreti, Luciano Saso, and Shrikant Kukreti. 2019. “Oxidative Stress: A Key Modulator in Neurodegenerative Diseases.” *Molecules* 24(8): 1–20.

Sofola, Oyinkan A. et al. 2007. “RNA-Binding Proteins HnRNP A2/B1 and CUGBP1 Suppress Fragile X CGG Premutation Repeat-Induced Neurodegeneration in a Drosophila Model of FXTAS.” *Neuron* 55(4): 565–71.

Sork, Helena et al. 2018. “Heterogeneity and Interplay of the Extracellular Vesicle Small RNA Transcriptome and Proteome.” *Scientific Reports* 8(1): 1–12.

Soung, Nak Kyun et al. 2019. “Mechanism of the Natural Product Moracin-O Derived MO-460 and Its Targeting Protein HnRNPA2B1 on HIF-1α Inhibition.” *Experimental and Molecular Medicine* 51(2). http://dx.doi.org/10.1038/s12276-018-0200-4.

Sreedharan, Jemeen, Robert H Brown, and United Kingdom. “Amyotrophic Lateral Sclerosis: Problems and Prospects.” : 1–16.

Statello, Luisa et al. 2018. “Identification of RNA-Binding Proteins in Exosomes Capable of Interacting with Different Types of RNA: RBP-Facilitated Transport of RNAs into Exosomes.” *PLoS ONE* 13(4): 1–30.

Sun, Lingli et al. 2022. “Theaflavin-3,3’-Di-Gallate Represses Prostate Cancer by Activating the PKCδ/ASMase Signaling Pathway through a 67 KDa Laminin Receptor.” *Food & function* 13(8): 4421–31.

Tamaki, Yoshitaka, and Makoto Urushitani. 2022. “Molecular Dissection of TDP-43 as a Leading Cause of ALS/FTLD.” *International Journal of Molecular Sciences* 23(20).

Taylor, J. Paul, Robert H. Brown, and Don W. Cleveland. 2016. “Decoding ALS: From Genes to Mechanism.” *Nature* 539(7628): 197–206.

Teng, Fei, and Martin Fussenegger. 2021. “Shedding Light on Extracellular Vesicle Biogenesis and Bioengineering.” *Advanced Science* 8(1): 1–17.

Thiele, Bernd-Joachim et al. 2004. “RNA-Binding Proteins Heterogeneous Nuclear

Ribonucleoprotein A1, E1, and K Are Involved in Post-Transcriptional Control of Collagen I and III Synthesis." *Circulation research* 95(11): 1058–66.

Vahsen, Björn F. et al. 2021. "Non-Neuronal Cells in Amyotrophic Lateral Sclerosis — from Pathogenesis to Biomarkers." *Nature Reviews Neurology* 17(6): 333–48. http://dx.doi.org/10.1038/s41582-021-00487-8.

Valadi, Hadi et al. 2007. "Exosome-Mediated Transfer of MRNAs and MicroRNAs Is a Novel Mechanism of Genetic Exchange between Cells." *Nature Cell Biology* 9(6): 654–59.

Varcianna, André et al. 2019. "Micro-RNAs Secreted through Astrocyte-Derived Extracellular Vesicles Cause Neuronal Network Degeneration in C9orf72 ALS." *EBioMedicine* 40: 626–35. https://doi.org/10.1016/j.ebiom.2018.11.067.

Veziroglu, Eren M., and George I. Mias. 2020. "Characterizing Extracellular Vesicles and Their Diverse RNA Contents." *Frontiers in Genetics* 11(July): 1–30.

Villarroya-Beltri, Carolina et al. 2013. "Sumoylated HnRNPA2B1 Controls the Sorting of MiRNAs into Exosomes through Binding to Specific Motifs." *Nature Communications* 4: 1–10.

Wang, Dongyang et al. 2022. "FAM76B Regulates NF-KB-Mediated Inflammatory Pathway by Influencing the Translocation of HnRNPA2B1." *bioRxiv*: 2022.12.29.522198. http://biorxiv.org/content/early/2022/12/30/2022.12.29.522198.abstract.

Wang, Hui et al. 2018. "Long Noncoding RNA MiR503HG, a Prognostic Indicator, Inhibits Tumor Metastasis by Regulating the HNRNPA2B1/NF-KB Pathway in Hepatocellular Carcinoma." *Theranostics* 8(10): 2814–29.

Wang, Lei, Mingyue Wen, and Xuetao Cao. 2019. "Nuclear HnRNPA2B1 Initiates and Amplifies the Innate Immune Response to DNA Viruses." *Science (New York, N.Y.)* 365(6454).

Wang, Lijun, David H. Gutmann, and Raymond P. Roos. 2011. "Astrocyte Loss of Mutant SOD1 Delays ALS Disease Onset and Progression in G85R Transgenic Mice." *Human Molecular Genetics* 20(2): 286–93.

Wang, Wenzhang et al. 2016. "The Inhibition of TDP-43 Mitochondrial Localization Blocks Its Neuronal Toxicity." *Nature Medicine* 22(8): 869–78.

Wen, Xinmei et al. 2014. "Antisense Proline-Arginine RAN Dipeptides Linked to

C9ORF72-ALS/FTD Form Toxic Nuclear Aggregates That Initiate Invitro and Invivo Neuronal Death." *Neuron* 84(6): 1213–25. http://dx.doi.org/10.1016/j.neuron.2014.12.010.

Westergard, Thomas et al. 2016. "Cell-to-Cell Transmission of Dipeptide Repeat Proteins Linked to C9orf72-ALS/FTD." *Cell Reports* 17(3): 645–52. http://dx.doi.org/10.1016/j.celrep.2016.09.032.

Weydt, Patrick, Eric C. Yuen, Bruce R. Ransom, and Thomas Möller. 2004. "Increased Cytotoxic Potential of Microglia from ALS-Transgenic Mice." *Glia* 48(2): 179–82.

Wu, Baixing et al. 2018. "Molecular Basis for the Specific and Multivariant Recognitions of RNA Substrates by Human HnRNP A2/B1." *Nature Communications* 9(1). http://dx.doi.org/10.1038/s41467-017-02770-z.

Wu, Xiaoqing et al. 2020. "Targeting the Interaction between RNA-Binding Protein HuR and FOXQ1 Suppresses Breast Cancer Invasion and Metastasis." *Communications biology* 3(1): 193.

Xiao, Qin et al. 2007. "Mutant SOD1G93A Microglia Are More Neurotoxic Relative to Wild-Type Microglia." *Journal of Neurochemistry* 102(6): 2008–19.

Xu, Hong, Xueyan Dong, Yueming Chen, and Xianjun Wang. 2018. "Serum Exosomal HnRNPH1 MRNA as a Novel Marker for Hepatocellular Carcinoma." *Clinical Chemistry and Laboratory Medicine* 56(3): 479–84.

Xu, Qian et al. 2018. "Comparison of the Extraction and Determination of Serum Exosome and MiRNA in Serum and the Detection of MiR-27a-3p in Serum Exosome of ALS Patients." *Intractable and Rare Diseases Research* 7(1): 13–18.

Xue, Yuan Chao et al. 2020. "Dysregulation of RNA-Binding Proteins in Amyotrophic Lateral Sclerosis." *Frontiers in molecular neuroscience* 13: 78.

Yáñez-Mó, María et al. 2015. "Biological Properties of Extracellular Vesicles and Their Physiological Functions." *Journal of Extracellular Vesicles* 4(2015): 1–60.

Yin, Menghui et al. 2021. "HNRNPA2B1 as a Trigger of RNA Switch Modulates the MiRNA-Mediated Regulation of CDK6." *iScience* 24(11): 103345.

Zetterstöm, Per, Peter M. Andersen, Thomas Brännström, and Stefan L. Marklund. 2011. "Misfolded Superoxide Dismutase-1 in CSF from Amyotrophic Lateral Sclerosis Patients." *Journal of Neurochemistry* 117(1): 91–99.

Zhang, J H, T D Chung, and K R Oldenburg. 1999. "A Simple Statistical Parameter for

Use in Evaluation and Validation of High Throughput Screening Assays." *Journal of biomolecular screening* 4(2): 67–73.

Zhang, Ke et al. 2018. "Stress Granule Assembly Disrupts Nucleocytoplasmic Transport." *Cell* 173(4): 958-971.e17. https://doi.org/10.1016/j.cell.2018.03.025.

Zhang, Wenjuan, Bo Huang, Limo Gao, and Cao Huang. 2021. "Impaired 26s Proteasome Assembly Precedes Neuronal Loss in Mutant Ubqln2 Rats." *International Journal of Molecular Sciences* 22(9).

Zhao, Dongjiu et al. 2016. "MiR-221 Activates the NF-KB Pathway by Targeting A20." *Biochemical and biophysical research communications* 472(1): 11–18.

Zhou, Xusha et al. 2020. "HnRNPA2B1 Associated with Recruitment of RNA into Exosomes Plays a Key Role in Herpes Simplex Virus 1 Release from Infected Cells." *Journal of Virology* 94(13).

Zhu, Yafeng et al. 2020. "DEqMS: A Method for Accurate Variance Estimation in Differential Protein Expression Analysis." *Molecular & cellular proteomics : MCP* 19(6): 1047–57.

Acknowledgments

I would like to thank Prof. Vito D'Agostino for giving me the opportunity to join his lab and for giving me the chance to experience the work in a different country. I'd like to thank prof Andreas Hermann for accepting me in his lab and for the kindness he always showed to me.

I thank our collaborators in CIBIO, especially Prof. Manuela Basso for the experiments on primary cultures, and HTS and MS facilities for the help and the technical support on this project. A thanks to all CIBIO people who made CIBIO a young, dynamic and stimulating work place.

A special thanks to Ágata, with whom I started this adventure for her constant care inside and outside CIBIO. I would like to thank all the present and past members of LBN for the scientific support and the constructive discussions. A big thanks to Michelangelo for the help, the desperations and the achievements in the most tricky period of the project.

I would like to thank all the FabLab members, past and present, for the most beautiful playlists ever and for all the AperiPurple. You taught me how important is to have a healthy, positive and supporting work environment. Thank you for all the smiles you gifted me.

Special thanks to Fabrizio, with whom I always shared the best and the worst moments since the beginning of this four years journey. Thanks for all the brainstorming, for your constant professional and personal support. You made the difference.

A big thank to my friends Michela and Silvia who were always there, even from far away.

A final thanks goes to my family, for their patience, for believing in me, and for their constant love.